April 2016

Design of a Flipper Prosthetic for a Kemp's Ridley Sea Turtle

Iok Wong
Worcester Polytechnic Institute

Samantha Stephanie Varela
Worcester Polytechnic Institute

Vivian Liang
Worcester Polytechnic Institute

DESIGN OF A FLIPPER PROSTHETIC FOR A KEMP'S RIDLEY SEA TURTLE

A Major Qualifying Project completed in partial fulfillment of the Bachelor of Science degree at

WORCESTER POLYTECHNIC INSTITUTE

By

Vivian Liang, Samantha Varela, and Iok Wong

2015/2016

Submitted to

Professor Yuxiang Liu, PhD

Professor Brian Savilonis, PhD

Mechanical Engineering Department
Biomedical Engineering Department

Table of Contents

Authorship Page

	Liang	Varela	Wong
Abstract	X	X	
CHAPTER 1 – INTRODUCTION	X		
CHAPTER 2 – LITERARY REVIEW	X	X	X
2.1 Overview	X		
2.1.1 Importance of sea turtles		X	
2.1.2 Causes for flipper amputation		X	
2.1.3 Need for turtle rehabilitation	X	X	
2.1.4 Prostheses assist in rehabilitation	X	X	
2.2 Biology		X	
2.2.1 Flipper anatomy		X	
2.2.2 Muscular system and effect on swimming		X	
2.2.3 Skeletal system		X	
2.2.4 Amputation description		X	
2.3 Sea turtle locomotion			X
2.3.1 Anatomy in relation to locomotion		X	
2.3.2 Lift forces			X
2.3.3 Powerstroke		X	X
2.3.4 Routine swimming		X	X
2.3.5 Vigorous swimming		X	X
2.3.6 Reference coordinate system: global and local			X
2.3.7 Biomimetic turtle hydrofoil AUV			X
2.3.8 Final design of AUV Naro-tartaruga			X
2.4 Turtle prosthetics		X	
2.4.1 Allison and Hofesh, single and dual rudder cases		X	X
2.4.2 Yu, flipper		X	X
CHAPTER 3 – PROJECT STRATEGY	X		
3.1 Initial Client Statement	X		
3.2 Design Requirements	X	X	
3.3 Design Standards	X		
3.4 Revised Client Statement	X		
3.5 Project Approach	X		
CHAPTER 4 – DESIGN PROCESS	X	X	X
4.1 Needs Analysis	X	X	X
4.2 Conceptual Designs		X	X
4.2.1 Design Modules		X	X
4.2.2 Custom Flipper Modeling			X
4.3 Flipper Blade Alternative Designs			X
4.3.1 Mean Aerodynamic Chord			X
4.3.2 Flexible Flipper	X		
4.4 Powerstroke Model			X
4.4.1 Overview			X

4.4.2 Flow Matching			X
4.4.3 Coefficients of Lift, Drag and Quarter Chord Moment			X
4.4.4 Effective Lift and Thrust for Propulsion (TCS)			X
4.4.5 Added Mass	X		X
4.5 Flipper Blade Methodology			X
4.5.1 Fabrication	X		
4.5.2 Wind Tunnel Testing		X	X
4.5.3 Obtaining Resultant Forces			X
4.5.4 Wind Tunnel Limitations			X
4.5.5 Software Coefficient Comparison			X
4.5.6 Flipper Comparisons			X
4.6 Attachment Design		X	
4.6.1Attachment Components		X	
4.7 Prosthetic Predicted Effects and Safety		X	
4.7.1 Stress Analysis		X	
4.7.2 Healthy Flipper Predictions	X		
CHAPTER 5 – DESIGN VERIFICATION	X	X	X
5.1 Flipper Blade Results			X
5.1.1 Experimental Wind Tunnel			X
5.1.2 Theoretical Results			X
5.1.3 Experimental and Software Comparisons			X
5.1.4 Rectangular Wing Omission			X
5.1.5 Lift and Thrust Values throughout Powerstroke			X
5.1.6 Flexible Flipper Blade Fabrication	X		
5.2 Attachment Design		X	
5.2.1 Attachment Manufacturing		X	
5.2.2 Designs Evaluation	X		
5.3 Prosthetic Stress Analysis		X	
5.3.1 Stress at Prosthetic End and Tip of Residual Limb		X	
5.3.2 Stresses within Residual Limb		X	
5.4 Muscle Loadings at Shoulder	X		
5.4.1 Obtaining Human Powerstroke Data	X		
5.4.2 Allometric Scaling	X		
5.4.3 Powerstroke Loadings Using MATLAB	X		
5.4.4 Shoulder Moment Comparison	X		
CHAPTER 6 – Final Design and Validation	X		
6.1 Economics	X		
6.2 Environmental Impact	X		
6.3 Societal Influence	X		
6.4 Political Ramifications	X		
6.5 Ethical Concerns	X		
6.6 Health and Safety Issues	X		

Acknowledgements

The team would like to thank their advisors, Prof. Yuxiang Liu and Prof. Brian J. Savilonis, for their excellent advice and consistent commitment, effort, enthusiasm, and encouragement all year. This project would not be near where it is without them. A special thank you goes out to the generous staff at Lola's aquarium, for providing measurements, videos, x-rays, and allowing us to use Lola as a case study. The team would also like to thank Prof. David Olinger for allowing them to use his wind tunnel for testing and for being every-willing to offer expert advice on aerodynamics. They would also like to thank Prof. Karen Troy for help in understanding musculoskeletal behavior. The team would like to extend their thanks to Siamak Ghorbani Faal for his recommendation to use Javafoil as a computational tool, Adriana Hera for advice with ANSYS, and Erica Stults for help with Solidworks and manufacturing. Lastly, we they would like to thank all their professors, friends and family for their constant support and encouragement throughout the project.

Abstract

Sea turtles often have flipper damage when found. Lola is a sea turtle missing one of her front flippers, causing her to swim improperly and hence unable to survive alone. This project initiated the development of a prosthetic to imitate Lola's healthy flipper to help her swim more effectively. Flipper blades of various shapes were designed using CAD, fabricated with a 3D printing and molding process, and tested in a wind tunnel. The wind tunnel performance was further understood through finite element simulation. The optimal flipper design was identified for superior wind tunnel performance, i.e., high lift and low drag. An attachment mechanism was designed with consideration of fitting Lola's residual limb. Shoulder loadings that Lola can apply were analyzed and compared with the required force for swimming in water. This work paves the way for the development of a biomimetic flipper to help amputated turtles across the world swim with better efficiency and fewer injuries.

Table of Figures

Table of Tables

CHAPTER 1 – INTRODUCTION

Sea turtles have existed for millions of years. However, only seven species of sea turtles exist today, all of which are listed under the Endangered Species Act [1]. Sea turtles are often found with severe tissue damage due to fishing nets, boat collisions, or predatory attacks. Once a sea turtle loses a flipper it can no longer be released back into its natural habitat. Many of these turtles require external help to resurface for air [3]. Turtles with amputated flippers have difficulty maintaining balance and turning while swimming. As a means of rehabilitation, an artificial flipper can greatly improve the daily life of these animals. There have been a few reported cases of sea turtles with prosthetics, but the prosthetics are not ideal. Prosthetics for aquatic animals is a relatively new field, and many issues exist with balance and control in an aquatic environment. The current prosthetics do not effectively replicate a sea turtle's natural movement, the powerstroke. This gap in prosthetic technology indicates room for development. The goal for this project is to create a low-cost, safe prosthetic that improves the turtle's ability to generate propulsive forces.

The team located a Kemp's Ridley sea turtle named Lola that currently lives at an aquarium in Florida. She was the motivation for this project and her rehabilitation would serve as an ideal test for the usability and effectiveness of the designed flipper. The team established contact with employees taking care of the turtle, and they have agreed to collaborate. Lola has a partially amputated flipper due to a shark attack. Her swimming capability has been hindered and her haphazard swimming may cause excessive stress on her injured limb as well as her healthy limbs. Lola also has trouble turning and constantly collides into the walls of her enclosure, sometimes head on.

Dr. Douglas Mader, a veterinarian, provided flipper measurements and X-rays of Lola's two front flippers: the residual limb and the healthy flipper. These reference dimensions guided the design of a viable prosthetic. Literature review provided analytical data about the dimensions of the natural powerstroke. Success of the prosthetic was determined by how closely the artificial flipper imitates a real sea turtle flipper. Assuming the turtle intends to swim forward in a level path, an effective flipper would generate positive thrust and neutral lift after each powerstroke. Experimental and theoretical results were matched to validate the functionality and safety of the prosthetic. After the initial design was complete, it could be sent to Florida for live testing with support from Lola's caregivers.

Creating a prosthetic in this case study can be the start of further research and development towards a universal design for sea turtle amputees. This project can also be used in aiding the design of hydrofoils for underwater vehicles and robotics.

CHAPTER 2 – LITERARY REVIEW

A thorough literary review was conducted prior to the design phase of the project. Section 2.1 encompasses a review of the importance of sea turtles, causes of amputation, and the need for prosthetics. Section 2.2 explores the biology of sea turtles to further the team's anatomical understanding of the problem. Sea turtle locomotion was researched in Section 2.3 to aid in the design of a biomimetic flipper. Finally, the current state-of-the-art of turtle prosthetics was reviewed in Section 2.4.

2.1 Overview

An understanding of the importance of sea turtles and the environmental problems that can cause severe injuries and amputation provided inspiration for this project. Designing an effective prosthetic required knowledge of basic rehabilitation and the anatomy and the locomotion of sea turtles, so these subjects were studied and analyzed. Evaluations of prior underwater robotic vehicle designs and sea turtle prosthetic cases showed areas for improvement of the swimming mechanism. The design goal is to of recreate the natural swimming pattern of sea turtles to ameliorate the overall health and potentially extend the life of a sea turtle.

2.1.1 Importance of sea turtles

Sea turtles all over the world are endangered. While the extinctions of species have occurred since life first began on Earth, those extinctions were mainly due to natural processes and major climate changes. In recent decades, sea turtle populations have severely decreased due to human interference, primarily habitat destruction and ocean pollution. It is important that sea turtles are preserved, as sea turtle extinction could lead to major ecological changes. Only a few animals consume seagrass, with sea turtles being the most prominent species [2]. Seagrass is used as a breeding ground for many crustaceans, fish, and other underwater animals. It requires maintenance to keep the grass short and spread over the ocean floor. However, there has been a decline in the amount of seagrass beds over the past decades, directly linked to the decline in sea turtles and other animals whose diet contains the plant [4]. If sea turtles become extinct, then seagrass will continue to dwindle, affecting dependent species. This loss will affect species higher up on the food chain and eventually reach humans [5].

Sea turtles are also responsible for the composition of coral reefs. Specifically, the Hawksbill sea turtle diet consists of sponges, which compete with coral for space. By eliminating some of the sponge growth in coral reef communities, sea turtles allow for other species to grow. If these turtles no longer maintain the coral reefs, the structure and ecology in the reefs will change as sponges grow rampantly [6]. Sponges have chemical and physical defense mechanisms that prevent most fish from preying on them [6]. It is due to the selective foraging of the Hawksbill that allows for the sponge population to be kept in check. Without the turtles, the structure and composition of coral reefs would change. Another major component of sea turtle diet is jellyfish. Leatherbacks play an important role in maintaining the jellyfish population, as they are a top jellyfish predator consuming up to 440 pounds of jellyfish per day [7]. However, due to declining sea turtle numbers and other predators, the jellyfish population is proliferating worldwide, replacing fish stocks that feed other species, including humans [8].

Sea turtles not only have an impact on marine ecology, but beach systems as well. Beach dunes are popular nesting environments for sea turtles. When the time comes to lay eggs, female sea turtles come ashore and construct nests. The eggs and hatchlings which do not survive distribute nutrients to the sparse vegetation, which not only feeds certain species, but also stabilizes the shoreline [9]. If sea turtles were to become extinct, a key source of nutrients would disappear from the beach ecosystem. This would cause for faster erosion affecting the environment negatively. Sea turtles play an important role in maintaining the delicate balance of our ecosystem. Therefore, feasible solutions for the aid and preservation of sea turtles are important. Raising awareness for the plight of sea turtles is another crucial way to help slow the regression of sea turtle populations.

2.1.2 Causes for flipper amputation

Many times, because of various environmental causes or human interference, severely injured or sick sea turtles are found at sea or washed up on beaches. Serious sea turtle flipper injuries can impair the circulatory system of the turtle due to severe trauma to blood vessels and surrounding tissues. Severe injuries from predator attacks or from getting caught in fishing nets are common and can cause wounds that will not heal [10]. Open wounds and cuts that take too long to heal can cause infection anywhere in the limb or to surrounding tissue and lead to further inflammation if they are not properly treated [10]. Blood clotting from wounds can also result in reduced blood circulation that leads to a lack of oxygenation and transportation of vital nutrients to the flipper's tissues, which leads to live tissue death [11]. When this happens, physicians will generally decide to amputate the injured limb [10].

2.1.3 Need for turtle rehabilitation

Amputated sea turtles without their front flippers cannot resurface to breathe. Turtles can drown within minutes when they are stressed or in pain due to faster oxygen consumption [12]. Organizations, like Sea Turtle Inc., rescue injured sea turtles and then prescribe treatments and monitor their progress. According to the director of Sea Turtle Inc., the organization may return three-flippered turtles into the wild or transfer two-flippered turtles for care at a zoo. However, one-flippered turtles may need to be put down [13]. Rehabilitation via prosthetics can help amputees live longer, healthier lives [14]. If sea turtles are given a better chance at life, they are more likely to live well beyond maturity and help their species grow [14].

2.1.4 Prostheses assist in rehabilitation

One of the primary goals of medicine and what medical professionals strive for is to restore, sustain, and improve the quality of life of patients [15]. Their mission is not only to prevent or treat a disease and find a cure, but also to deliver palliative and rehabilitative care when necessary [15]. In the case of amputations, patients no longer have a part of their body, which can be detrimental to their everyday way of life. Rehabilitation with a dynamic prosthetic enables patients to regain control of movement [16]. A prosthetic is an external or internal artificial device which supplements a missing or damaged part of a body. The ideal prosthetic would essentially replace the functionality and capability of the user's missing body part. Prosthetics can help patients (with a disabling injury or illness) heal and return to their normal lifestyle [17]. Use of prosthetics can

alleviate some of the physical and mental stress patients face after amputation surgery, during recovery, and later throughout their lives [14].

The degree of how well a sea turtle will respond to changes in its environment and stressful situations depends on the type of injury sustained and the turtle's species [18]. In general, sea turtles have very advanced nervous and immune systems which allow them to recuperate and adapt remarkably fast, finding ways to heal and redistribute activity to still be able to carry out daily tasks [19]. When an injured turtle no longer has the muscles and bones it once used to swim, it will naturally try to use another part of its body to make up for this loss [19]. However, using other parts of the body to make up for the loss may not necessarily be beneficial in the long-run, as other muscles will need to work harder and mechanical stresses will be distributed differently. The extra work throughout the turtle's life can put a strain on its health.

2.2 Biology

Knowledge of the essential anatomy of a sea turtle's flipper allowed for assessment of the degree of damage and repair required for a functional prosthetic. Sea turtle limbs are a complex network of bones, skin and muscle tissue, and blood vessels. All these separate features work together to enable the turtle to swim. Understanding the anatomy of an amputation site would allow for a more comprehensive outlook of the project goal.

2.2.1 Flipper anatomy

Sea turtle flippers are elongated and semi-rigid. Their hydrodynamic flipper is formed with elongated digits that are fused under stiff layers of fibrous tissue and scaled skin [23]. Compared to terrestrial turtles, sea turtles have strengthened muscle groups to retract, abduct and rotate their forelimbs with greater power [23]. The muscles and bones both play a role in moving and rotating the flipper.

2.2.2 Muscular system and effect on swimming

Marine turtles are streamlined to allow them to move easily through water. This project will focus specifically on trying to recreate the form and functions of the skeletal muscles in the turtle's forelimb. Two main functions of skeletal muscles are to contract to allow the animal to move and to provide stability and structure in the body [24]. Their forelimbs or front flippers are hypertrophied, with constantly increasing in muscle mass and cross-sectional area to meet the demands of a vigorous exercise such as swimming [24].

Muscles are the best force attenuators in the body. Skeletal muscles, in particular, control the movement of bones and are efficient shock absorbers [25]. During prolonged activities, muscles are subjected to fatigue and can become damaged, unable to absorb stresses as well as they would normally. Damaged muscles are weaker, less flexible, and have insufficient endurance [25]. Any kind of stress or injury to muscle fibers will cause new cells to move to the traumatic site in the muscle and fuse with the muscle fibers there. The cell proliferation process increases the size of the muscle fibers that experienced the extra load [24]. In general, this is how muscles respond to added stress and external loads of swimming.

Transmission of motion between skeletal muscles happen via tendons, which attach to bones. Sea turtles have mineralized or ossified tendons and ligaments that give them a slender,

elongated shape [26]. Trochleae are pulley-shaped, bony, fibrous structures through which tendons pass through or with which other structures overlap. The large pectoralis major is part of a powerful muscle group that retracts and adducts the front flipper. The deltoideus and supracoracoideus work together to protract and abduct the humerus. Underneath the pectoralis major, there are the deep pectoral muscles which include the biceps brachii superficialis and the coracobrachialis magnus which retract the turtle's front flipper. The posterior part of the supracoracoideus is a bigger part of the muscle that both adducts and retracts the flipper. Major rotational movement of the shoulder is controlled by the pectoralis muscles. These muscles can be seen in Fig. 1. Lola still has her shoulder completely intact on the side with the partial flipper, so she is still able to rotate her shoulder to some extent.

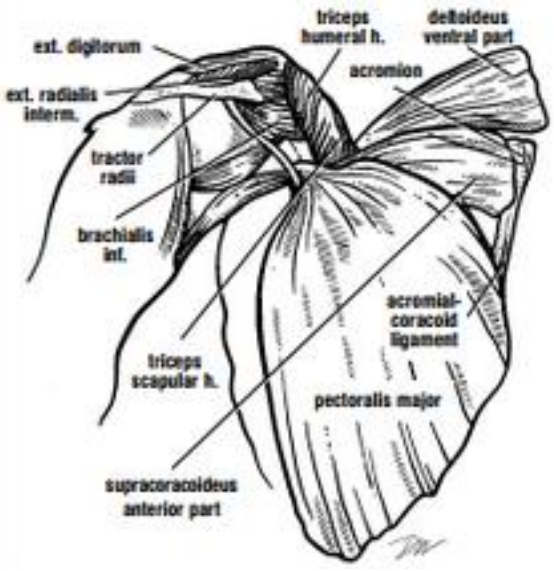

Figure 1: Muscles that control flipper movement in a sea turtle [27][1]

In Fig. 2, the turtle's flipper blade muscles are shown in more detail. The coracobrachialis, coracoideus, scapularis, biceps, and triceps groups all extend over the humerus, radius, and ulna bones. The flexor and extensor muscles extend over and around the carpals, metacarpals, and phalanges. These in particular are the muscles that rotate the tip of the sea turtle's flippers, and Lola is missing all of them in her partial flipper.

[1] [27] Wyneken, J. (2001). Muscle Anatomy. The Anatomy of Sea Turtles: 59-67.

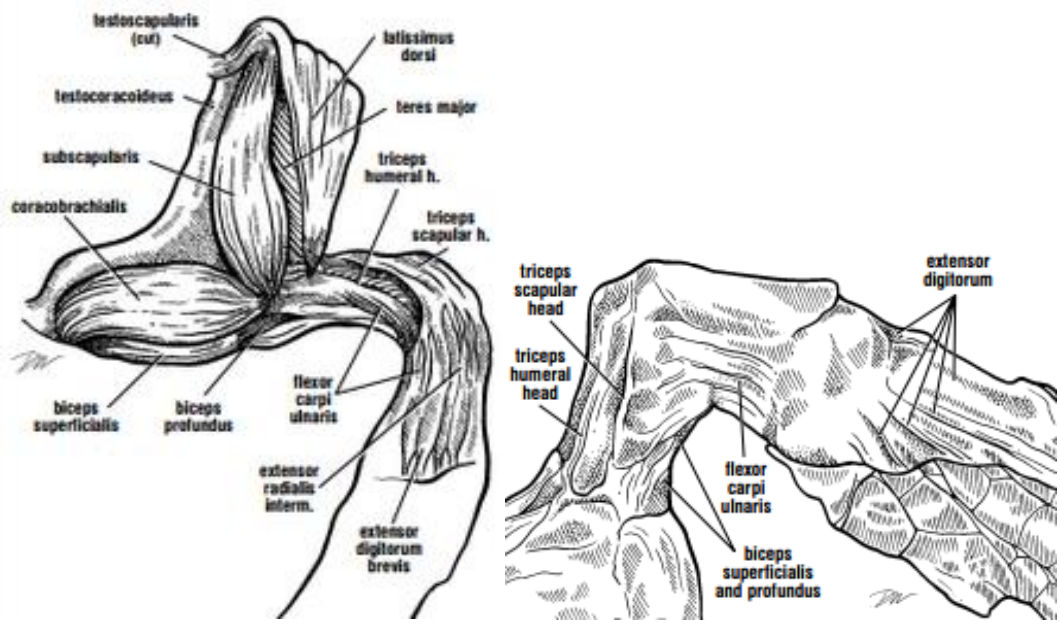

Figure 2: A detailed schematic of muscles in a sea turtle flipper [27]

2.2.3 Skeletal system

The skeletal system provides the turtle with a protective, supporting structure. Just like muscle, bone is a dynamic structure that remodels in response to changing forces. The forelimb of sea turtles is composed of the humerus, radius, ulna, carpals, metacarpals, and five phalanges. The humerus is the biggest (but not necessarily the longest) bone in the flipper and moves the shoulder. The bones of the wrist (carpals) are wide and flat and the elongated forelimb and finger bones (metacarpals and phalanges) form the flipper blade. These bones along with the radius and ulna are fused together by fibrous, connective tissue, as shown in Fig. 3.

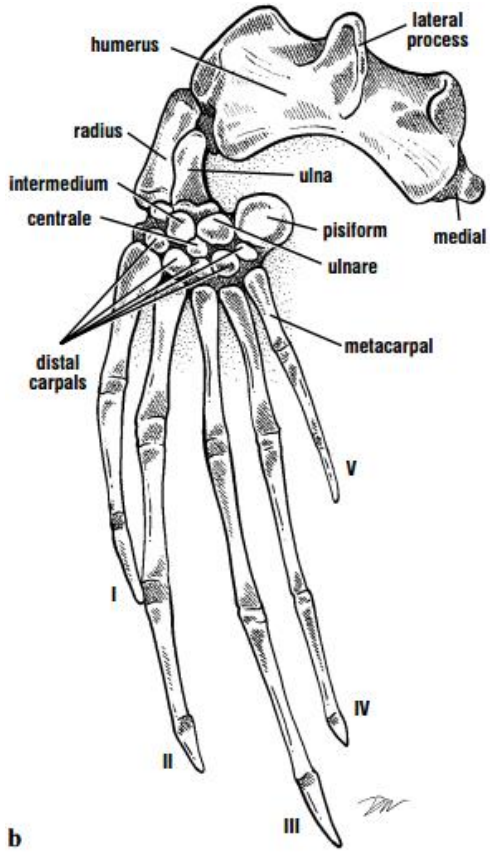

Figure 3: Bones in a sea turtle flipper [28]

The medial process which extends after the head of the humerus is where the flipper's abductor and extensor muscles attach. The U-shaped lateral process (deltoid crest bone) attaches to the major ventral swimming (protractor) muscles such as the deltoideus and supracoracideus. The scapula, acromion process, and coracoid form wide, flat, triangular bones to which the main swimming muscles (like the pectoralis) near the shoulder attach to, as seen in Fig. 4.

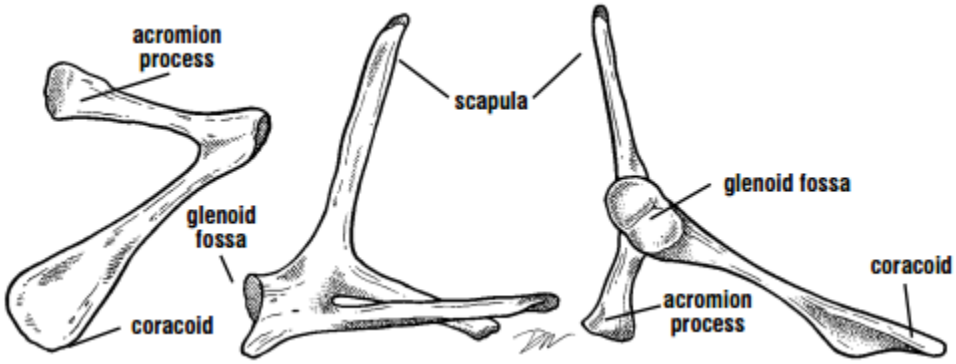

Figure 4: Bones that maintain the swimming muscles [28][2]

[2] [28] Wyneken, J. (2001). Skeletal Anatomy. The Anatomy of Sea Turtles: 51-54.

The main muscles doing the work of the powerstroke are the supracoracoideus, pectoralis, and deltoideus. Other smaller muscles and bones in the flipper are in the digits and phalanges, that go outwards to the tip of the flipper blade and rotate it. The nerves in these small muscles are made for finer motor control.

2.2.4 Amputation description

Surgeons who perform amputation surgeries will commonly choose an anatomical site to cut the limb and still save as much healthy skin, muscle, nerve tissue and blood vessel mesh as possible [11]. For this reason, surgical cuts are made after the nerve endings that control the movement of the turtle's flipper. This common practice helps to heal and preserve as much feeling and muscular control in that part of the limb after surgery. It also prevents scar tissue from forming around the nerves as well as losses in range of motion in the joint immediately next to the amputation site that could cause further damage [19]. A patient will be more likely to effectively use a prosthetic later on if there is sensory adaptation to the artificial limb and if the amputated site is able to fully heal before fitting the prosthetic.

After the amputation is completed, the surgeon will tightly wrap a tourniquet around the surgical site to stop bleeding [11]. Turtle patients take as little as 6 weeks and as much as 3-4 months to completely recover from the amputation surgery [19]. Once the wound has completely healed, a prosthetic can be fitted in place of the original limb [11]. Lola's partial flipper was amputated at her radioulnar joint; the cut was made just after her radius and ulna and before her carpals, leaving her without the entire blade of the flipper from the carpals down. She can still extend the partial flipper and rotate her shoulder with the remaining bones and muscles.

2.3 Sea turtle locomotion

The natural movement of a sea turtle must be understood in order for the team to design a more biomimetic flipper. Like all mobile organisms, sea turtles have multiple means of locomotion. There are two general classes of movement, terrestrial and aquatic locomotion. Sea turtles primarily remain in water, surfacing only to breathe. However, when laying eggs, sea turtles will drag themselves onto beaches to deposit their eggs in the sand [20]. For the purpose of this project, only aquatic locomotion will be considered. The bodies of marine turtles differ from their terrestrial cousins in that their body design is more tailored for an aquatic environment. A sea turtle is more streamlined to minimize drag, allowing for a more efficient locomotion [21]. Because of this, sea turtles are able to swim at velocities up to six times that of land turtles [22].

Most sea turtle aquatic locomotion analyses use juvenile sea turtles to produce kinematic analyses. Young turtles can use a drag-dominating mechanism like dog-paddling or use their back flippers as paddles, but adult sea turtles use a lift and propulsion-based mechanism which is more efficient and can be used to travel longer distances while migrating [29]. A sea turtle's front flippers serve as hydrodynamic wings that generate thrust. When swimming in a straight direction, sea turtles sweep their frontal limbs synchronously [29]. In steering, the right and left front flippers move asynchronously, with the duration of limb stroke shorter on the turning side. The hind flippers may assist in turning, though turning can be accomplished by frontal flippers alone. In order to turn, one flipper paddles less frequently relative to the other flipper [23]. For example for a left turn, the turtle would paddle the left flipper fewer times.

2.3.1 Anatomy in relation to locomotion

The radius and ulna in the front flipper are fused functionally by dense connective tissue so the bones can move as a unit [29]. The phalanges of the frontal flippers are elongated and held together by fibrous connective tissue which allows the front flippers to act as semi-rigid wings. Sea turtles also have large pectoral muscles that allow the turtle to retract, abduct, and rotate the frontal flippers [29]. The hind flippers essentially act as paddles, providing some thrust and acting as a rudder. In Davenport, Munks, and Oxford's study comparing the swimming of marine and freshwater turtles, green sea turtles' wing-like fins were found to have a maximum chord length halfway between the humerus and the fin tip [22]. Sea turtles alternate using their front limbs as wings and paddles throughout the powerstroke, with lift generated from the convex surfaces of the flippers [29].

2.3.2 Lift forces

The orientation of the turtle's "wing" with respect to flow dictates movement [29]. At lower angles of attack, lift is produced by the force from the pressure differential in the water surrounding the wing, which can serve as thrust. At higher angles to the current (more perpendicular to the flow), the wing can stall to counter forward propulsion, producing higher drag. Regardless of orientation of the wing with respect to gravity, lift forces are always perpendicular to the local fluid flow and drag [29]. These lift forces can serve as thrust for movement, especially in the sea turtles' main swimming behavior, the powerstroke. Fig. 5 shows the directions of lift and drag forces on the cross-section of the flipper with respect to the flow of the water.

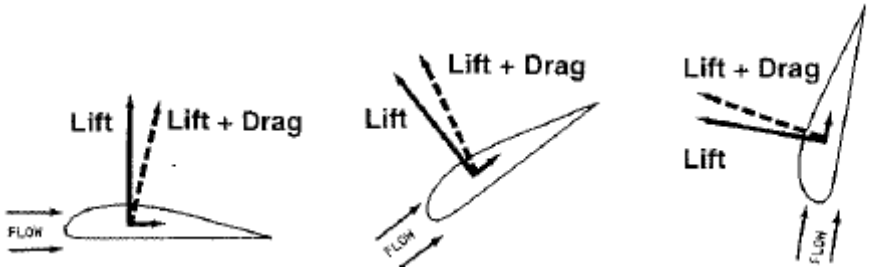

Figure 5: Lift and drag relative to flow [29][3]

2.3.3 Powerstroke

Compared to other swimming methods, the powerstroke produces the highest propulsion vectors [29]. Fig. 6 illustrates the movement of a frontal flipper during the powerstroke. The sea turtle sweeps both of its forelimbs roughly up and down. The powerstroke produces propulsion throughout most phases of the movement. Wyneken theorizes that the powerstroke is both lift and drag based. The first part of the powerstroke is the protraction of the flipper, with the turtle sweeping its limb upwards. Protraction and retraction are part of the recovery strokes [29]. Little forward thrust is produced during the initial protraction. Meanwhile more thrust is produced at the end of the protraction phase on the downstroke, when the flipper blade rotates in preparation for the retraction phase of the powerstroke. The retraction generates propulsion.

[3] [29] Lutz, P. L., Musick, J. A., Wyneken, J. (2002). The Biology of Sea Turtles Vol. 2. CRC press.

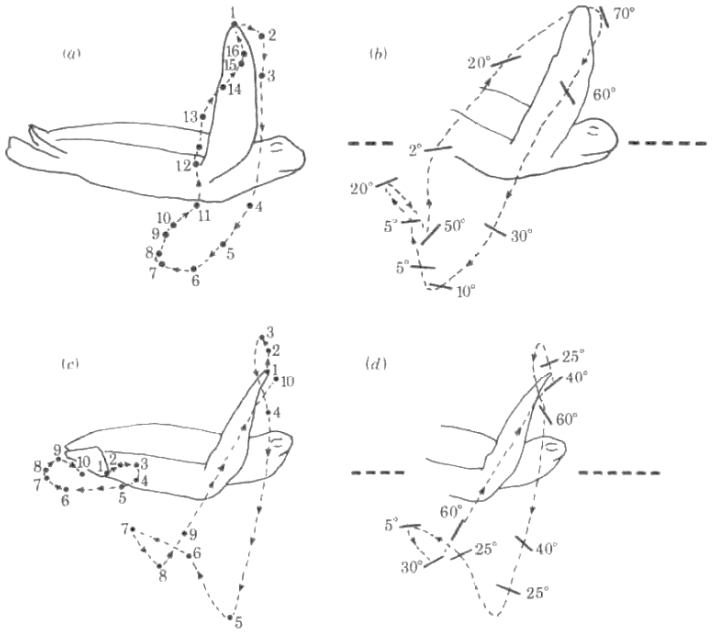

Figure 6: Flipper angles during routine and frenzied powerstroke. [22][4]

During the first half of retraction, the blade twists and begins the ventral sweep. The flipper blade acts as a paddle during the second half of the ventral sweep, producing thrust from drag-based propulsion. It also "feathers" while it rotates during the recovery stroke to minimize drag [29]. The feathering minimizes drag by reducing the surface area of the flipper blade that is pushing the water (perpendicular to flow) [29]. Kinematic analyses suggest that during early protraction, no thrust is actively produced, and the sea turtle is carried forward by momentum [30].

In another study, Davenport, Munks and Oxford, observed small, juvenile green sea turtles (Chelonia mydas) that grew from 200g to 1200g between 1982 and 1983 [22]. To calculate the aerodynamics of a turtle, Davenport et al. measured different aspects of the turtle, such as the surface areas of the front flippers and the center of gravity. The center of gravity varied but was generally near the center of the shell. The front and hind flippers have a 2:1 surface area ratio, resulting in considerable frictional drag [22]. Sections of the flipper were distinguished as the blade and the distal (outwards, farthest away from the turtle's body in the middle) tip [22]. During the powerstroke, the blade and the distal tip rotate to different angles with respect to the horizontal (WRTH) to correlate with the different free-stream velocities along the leading edge [22].

Davenport et al. analyzed two types of swimming in sea turtles: routine (every day, slower) and vigorous (panicked state, much faster) swimming. Like Wyneken, Davenport et al. observed that the cambered hydrofoil cross-section of the flipper is "[slightly concave] beneath the trailing edge" [22]. The flipper is shaped to contribute to low drag, low turbulence, and high thrust and lift.

[4] [22] Davenport, J., Munks, S. A., Oxford, P. J. (1984). A comparison of the swimming of marine and freshwater turtles. Proceedings of the Royal Society of London B: Biological Sciences 220 (1221): 447-475.

When the leading edge is perpendicular with the freestream, pressure drag becomes minimal [22]. Davenport, Munks and Oxford used an aspect ratio of 7 and a Reynold's number of 1.8 x 103 to analyze the lift and drag forces generated by the flipper [22].

The next section explains both routine and vigorous swimming in more detail. Each of t type of sea turtle swimming was divided and analyzed in four main parts: downstroke, recovery, upstroke, and recovery. In the angle blade orientation pictures, the motion of the wing tip is what is being traced.

2.3.4 Routine swimming

Routine swimming is how sea turtles spend most of their lives swimming. One complete pectoral wing flapping, routine swimming cycle takes 1.13 sec (this is the time it takes for one cycle) at a swimming rate or speed of 9-14 cm/sec [22]. The sea turtles are usually slightly tilted forward when they swim, downwards at a 10 degree angle [22]. On average, the duration of each part of the routine cycle is as follows:

19 % downstroke (0.2147 sec)

38 % recovery after the downstroke (0.4294 sec)

19 % upstroke (0.2147 sec)

23 % recovery after upstroke (0.2599 sec)

Let the downstroke be the first stage of the routine cycle. While the flipper is above the horizontal , the blade downstrokes and the flipper moves backwards (posteriorly) at approximately -70 to -80 degrees with respect to the horizontal (WRTH) with the tip at -60 degrees (WRTH) [22]. As the downstroke progresses below the horizontal, the blade reduces to -30 degrees [22]. The tip angle (WRTH) was not specified. Then, the turtle prepares for the upstroke by gradually rotating the blade in the opposite direction to +20 to +30 degrees (WRTH) and the tip to +50 degrees (WRTH) [22]. On the upstroke (the third stage), the flipper moves forward (anteriorly).

In the study, speeds of 42 cm/s and 34cm/s were measured at the tip for the downstroke and the upstroke respectively. The downstroke is faster. During the upstroke, the tip remains twisted on the way up with more pitch/curved at the very end (distal). The tip traces a path closer to body than on the downstroke [22]. Fig. 7 helps visualize each phase in the powerstroke during routine swimming, with angles of attack (AOA's) labeled.

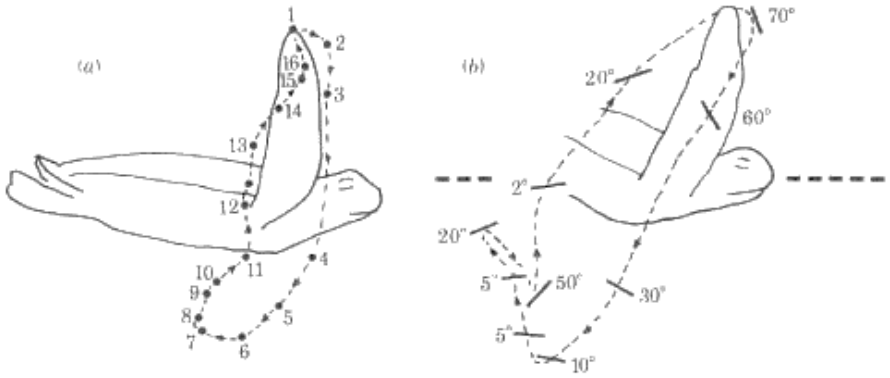

Figure 7: Powerstroke curve and AOA during routine swimming [22]

2.3.5 Vigorous swimming

Davenport, Munks and Oxford observed vigorous swimming as a reaction to restraint or fright [22]. One cycle of the vigorous powerstroke takes 0.87 sec at a velocity of 10 – 50 cm/sec. Compared to routine swimming, vigorous swimming sets the angles of attack at much higher amplitudes. The powerstroke increased in vertical and horizontal amplitude to reach swimming speeds of 50 cm/s [22]. The maximum speed of 44-143.0 cm/s was reached by a green sea turtle whose carapace measured 11cm x 8cm [22]. The amplitude of the power stroke contributes more to acceleration than frequency does. On average, the duration of each part of the vigorous cycle is as follows:

20 % downstroke (0.174 sec)

40 % recovery after the downstroke (0.348 sec)

10 % upstroke (0.087 sec)

30 % recovery after upstroke (0.261 sec)

Fig. 9 represents a version of the vigorous powerstroke. During the vigorous downstroke, the blade tip pushes downward a near -90 degrees trajectory while inclined downwards at -60 degrees (WRTH) [22]. Propulsive resultant force increases to a maximum (1-4). Then, the blade travels in a minor loop to readjust for the upstroke, during which little propulsive force is produced (4-7). The flipper twists in the opposite direction and glides a +60 degree (WRTH) upward trajectory while inclined at +40 to +60 (WRTH) [22]. Compared to the downstroke, the upstroke generates 20 to 40% of the maximum propulsion value (8-9). Finally, to prepare for the next cycle, the blade reorients to -60 (WRTH) through another loop, producing zero to slightly negative thrust in the process (9-10) [22]. Speeds of 80 cm/s and 66cm/s were measured at the tip for the downstroke and the upstroke respectively. In vigorous swimming, the back flippers may contribute to propulsion.

While the downstroke produces most of the thrust, the upstroke has some contributions. Meanwhile the recovery stages produce no thrust or even a small amount of negative thrust. Fig. 8 shows vigorous swimming with the position of the flipper traced and AOA's labelled. Adult green turtles can produce thrust magnitudes between 66.7 to 364.8 N, an average of 91 N [23].

Wyneken calculates that adult loggerheads can produce thrusts between 89 to 200 N. Furthermore, she reports loggerhead turtles can swim at 10 to 30 strokes per minute [23].

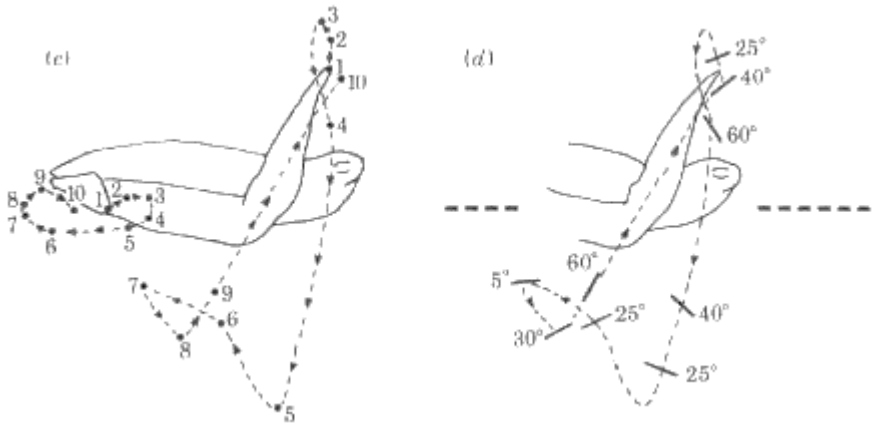

Figure 8: Powerstroke curve and AOA during vigorous swimming [22]

In the study, Davenport, Munks, and Oxford did not always observe the figure-of-eight pattern described by other researchers [22]. As shown by Fig. 9, the figure-of-eight powerstroke did occur at times with a cycle period that matched vigorous swimming (0.87s) [22]. Thus, the figure-of- eight form may be an abbreviated version of vigorous swimming.

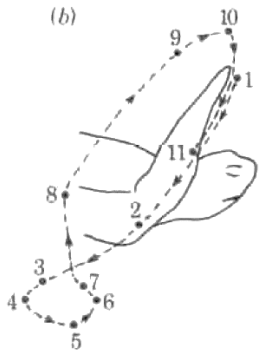

Figure 9: Occasional occurrence of figure-of-eight curve [22]

2.3.6 Reference coordinate system: global and local

Angle of attack (AOA) is the angle between the chord of the hydrofoil cross-section and the direction of the relative fluid flow. It may be important to note that the induced water velocity always reduces the effective/true AOA. In Figure 10, the horizontal vector (labeled swimming speed) is the turtle's general direction of travel. It will represent the positive x-direction in the Global Coordinate System (GCS) [22, 59]. With respect to the horizontal (GCS), the flipper is oriented at a positive angle during the upstroke, and at a negative angle during the downstroke [22]. In Fig. 10, the diagonal vector is the flipper's trajectory, representing the positive x direction in the Local Coordinate System (LCS) for the upstroke. Similarly, the diagonal vector represents the positive x' direction (LCS) for the downstroke.

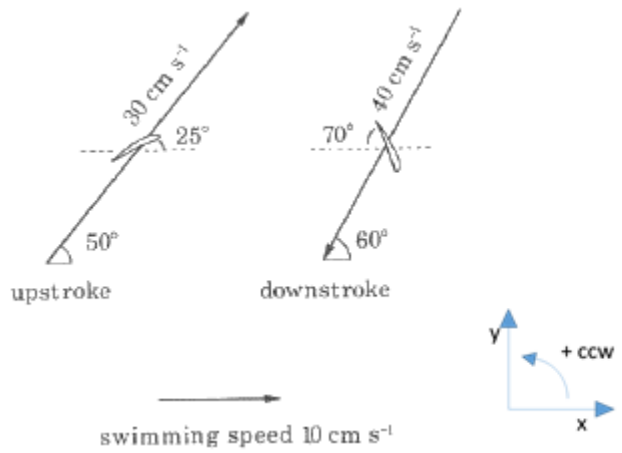

Figure 10: Upstroke and downstroke angles GCS, adapted from [22]

During the downstroke, the flipper faces a resultant freestream velocity of 36 cm/s [22]. The flipper is at +36 degrees with respect to freestream, or commonly referred to as angle of attack (AOA) [22]. As a result, the downstroke generates the majority of the powerstroke's forward thrust, with positive horizontal contributions from lift and drag. During the upstroke, the flipper travels at a resultant velocity of 37 cm/s with an AOA of -14 degrees [22]. The upstroke produces less forward propulsion. The drag has a negative x- component that reduces forward thrust [22]. Fig. 11 illustrates the routine upstroke and routine downstroke.

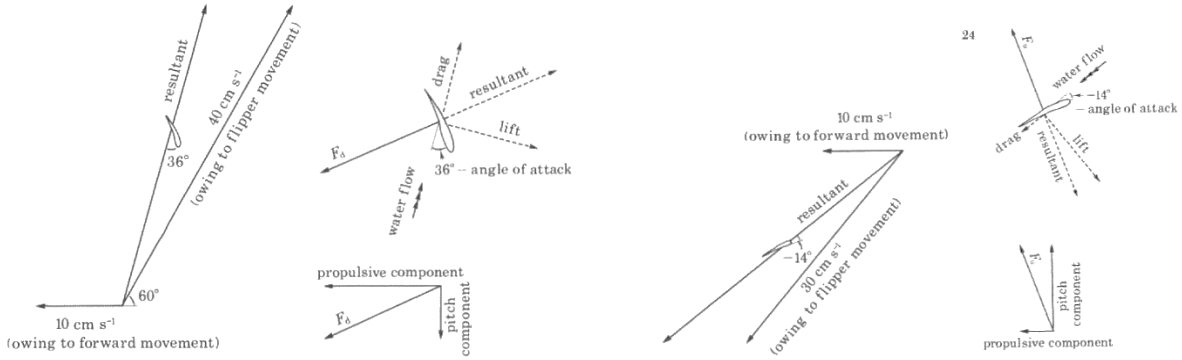

Figure 11: Routine downstroke (left) and routine upstroke (right) [22]

According to the Davenport team, the angle of attack is lower for vigorous swimming than routine swimming to avoid stall and excessive forces on the blade. During the vigorous downstroke, the flipper has a resultant velocity of 83 cm/s and is oriented at +24 degrees [22]. At a higher velocity, the lift generates the maximum forward thrust. Nevertheless, drag slightly reduces the forward thrust from the downstroke. During the vigorous upstroke, the freestream is 89 cm/s and the flipper's AOA is +7 degrees [22]. As a result of the orientation and the small angle of attack, the upstroke generates minimal negative thrust. Davenport, Munks and Oxford describes this phenomena as the flipper being "feathered". All of this is illustrated in Fig. 12.

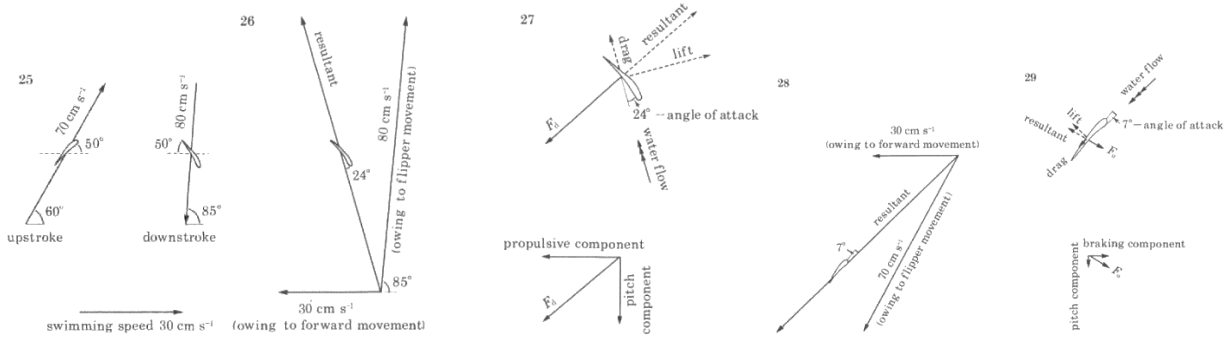

Figure 12: Vigorous downstroke (left) and vigorous upstroke (right) [22]

2.3.7 Biomimetic turtle hydrofoil AUV

In 2011, Font and his team designed a hydrofoil mechanism to automate a sea turtle's powerstroke [31]. The goal was to support the development of an Autonomous Underwater Vehicle (AUV), designed to dive up to 100 m [32]. The design consisted of a hydrofoil and a ball and socket mechanism. Using AUV operational specifications, the team compared airfoils at a constant freestream velocity of 1 m/s and a constant Reynold's number of 112,359 [31]. For juvenile sea turtles, Davenport et al. reported a Reynold's number of 1,800 for much lower swimming speeds on the magnitude of cm/s [22]. After analyzing lift and drag ratios for various airfoils, Font et al. determined that the NACA0014 airfoil best matched the hydrodynamics of a sea turtle's front flipper, as shown in Fig. 13.

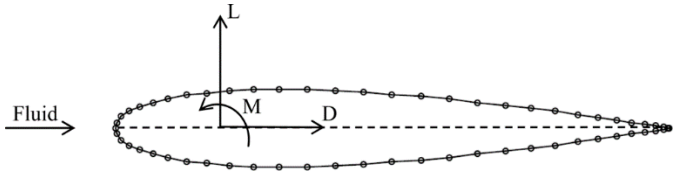

Figure 13: NACA0014 airfoil [31][5]

The same results were achieved although the airfoil shape was not identical to the shape of a natural turtle flipper, described as "[slightly concave] beneath the trailing edge," [22, 31]. The hydrofoil was made using rapid prototyping with the material Full Cure 720, and had a linear dimension of 100 mm and a profile length of 307 mm. Interestingly, the aspect ratio of the hydrofoil used in the AUV was to be 3.07 [31], but Davenport et al. reported an aspect ratio of 7.0 for juvenile sea turtles.

For the study, Font et al. designed a mechanism to produce the powerstroke motion, which was simplified into four phases: the downstroke, pronation (recovery), upstroke, and supination

[5] [31] Font, D., Tresanchez, M., Siegentahler, C., Palleja, T., Teixido, M., Pradalier, C., & Palacin, J. (2011). Design and Implementation of a Biomimetic Turtle Hydrofoil for an Autonomous Underwater Vehicle. Sensors, volume number 11, Issue 12. Retrieved from http://www.mdpi.com/1424-8220/11/12/11168/htm.

(recovery) [31]. In reality, a turtle's powerstroke has a more complex motion and does not usually form a perfect "figure eight" curve, as seen in Fig. 14.

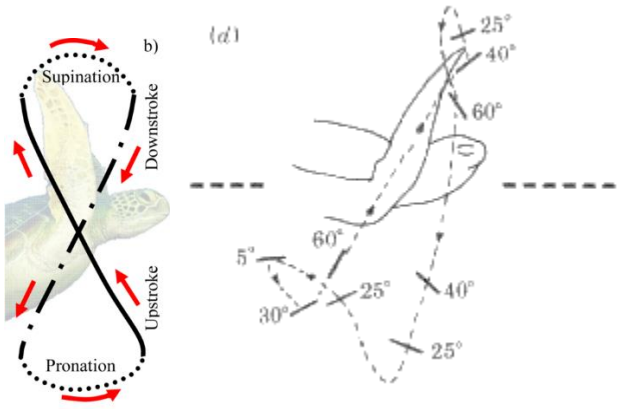

Figure 14: (Left) Figure-of-eight powerstroke [31], (Right) Vigorous powerstroke [22]

The geared differential mechanism shown in Fig. 15 depends on a central vertical bevel gear that rotates around two horizontal bevel gears [31]. Motor M3 in the central gear rotates the hydrofoil, while motors M1 and M2 rotate the central gear to generate the desired coupler curve. However, the geared differential concept was not favorable in terms of sealing and compactness.

Figure 15: Geared differential mechanism [31]

The ball and socket mechanism shown in Fig. 16 was chosen to simulate the powerstroke, meeting the requirements for sealing, compactness, propulsion path, and input torque. The ball and socket mechanism has three degrees of freedom. Motors M1 and M2 control translational movements, while M3 actuates rotation. The team explained the main challenge was synchronizing the rotation of the motors [31]. However, the hydrofoil was rigid and did not account for the twisting of the blade along the span of the flipper. Davenport et. al and Wyneken observed the significance of the twisting distal tip [22, 29].

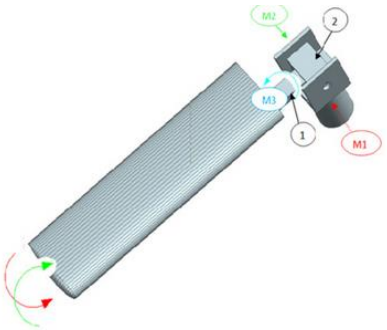

Figure 16: Ball and socket mechanism [31]

2.3.8 Final design of AUV Naro-tartaruga

The final design of the aforementioned project was the Naro-tartaruga AUV design. Foam blocks were incorporated into a hollow aluminum body to control buoyancy. A NACA0015 airfoil was used instead of Ryan BQM-34 Firebee (as in the study) to create a flipper with twenty varying chord lengths [32]. NACA0015 and Ryan BQM-34 Firebee share similar symmetries, however NACA0015 has a smaller aspect ratio [33]. A comparison of the airfoils can be seen in Fig. 17.

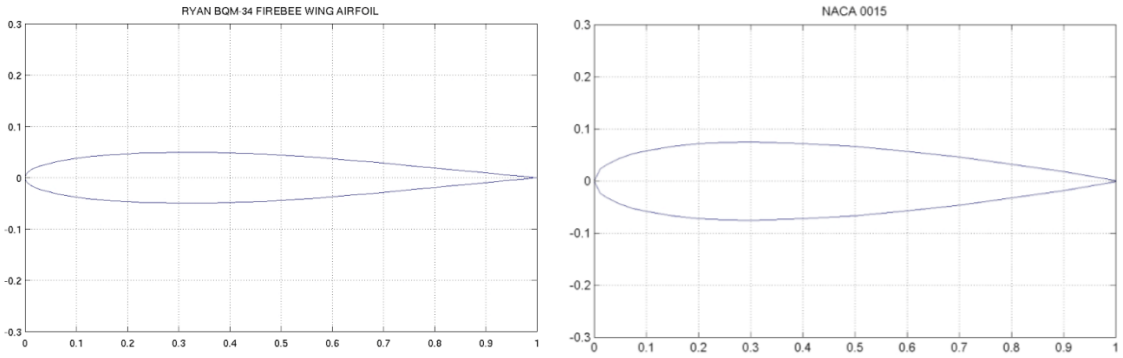

Ryan BQM-34 Firebee NACA0015

Figure 17: Comparison of airfoils used [33][6]

The design incorporates bevel gears as the actuators for the ball and socket mechanism, a combination of the ball socket (Fig. 16) and geared differential (Fig. 15) concepts illustrated in the previous study [31, 32]. Fig. 18 shows the prototype used in the study.

[6] [33] Index of /ads/afplots. Retrieved from http://m-selig.ae.illinois.edu/ads/afplots/.

Figure 18: Ball and socket mechanism prototype [32][7]

The motion of the flipper was generalized into three degrees of freedom (DOF). For each degree of freedom, sine waves were used to model the locomotion (Figure 19). Flapping describes the up-down motion (a range of 190 degrees). Pitching describes the rotation of the fin (a range of 90 degrees). Finally, feathering describes the forward-backward paddling motion (a range of 90 degrees) [32]. The mechanism imitates the routine swimming described by Davenport et al. [22].

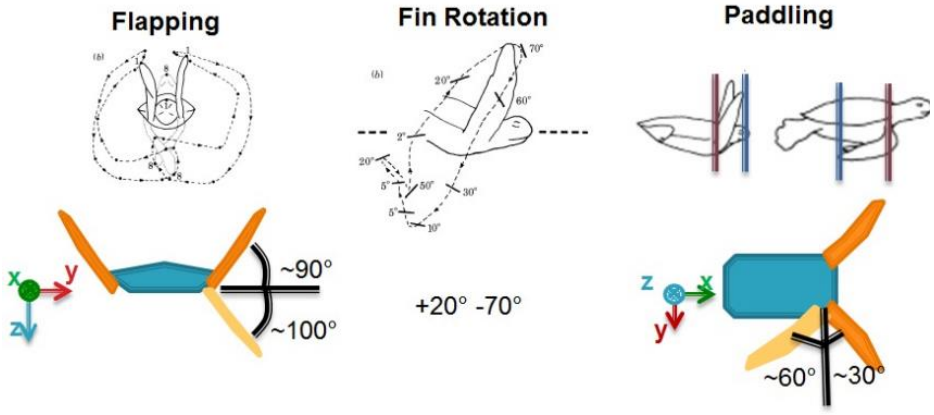

Figure 19: Locomotion approximations shown in [32] based on diagrams from [22]

2.4 Turtle prosthetics

Sea turtle prosthetics are a relatively new field. Not many cases exist where a prosthetic is designed for a sea turtle that has lost one or more flippers. At the moment, only three sea turtle amputees in the world are publicly known for obtaining prosthetics. Understanding the current state-of-the-art of sea turtle prosthetics provides a baseline for the team to start off of.

2.4.1 Allison and Hofesh, single and dual rudder cases

Allison, a green sea turtle, lost three of her flippers due to a shark attack. Without prosthetics, Allison could neither resurface for air nor feed and could only swim in circles. A rudder-like prosthetic was designed to help her better maneuver and control movement with her one right forelimb [3]. An intern at Allison's rehabilitation center conceptualized the rudder by

[7] [32] Siegenthaler, C. (2012). System Integration and Fin-Trajectory Optimization for a Robotic Turtle (Master Thesis). Retrieved from Swiss Federal Institute of Technology Zurich. (386) http://students.asl.ethz.ch/upl_pdf/386-report.pdf.

relating Allison's one sided swimming to a canoe paddling technique [3]. A canoe can be propelled forward by rowing one paddle and trailing the opposite paddle to create drag. Similarly, by using her one flipper and the trailing prosthetic rudder to create drag, Allison can swim forward and regain balance [3].

In a preliminary rudder design, Allison wore a wetsuit with a plywood rudder, stabilized on a black neoprene wetsuit covering three-quarters of the shell, shown in Fig. 20 and Fig. 21 [3][34]. To minimize buoyancy effects and maintain a lightweight structure, newer iterations of the prosthetic were made of carbon fiber as shown in a 2014 PBS Nature webisode (Fig. 20) [3]. The carbon fiber rudder is attached on the turtle's shell via a clamp mechanism (Fig. 21). At both the front and back of Allison's shell, two prongs are bent to fit the curvature and a clamp is tightened for stability via a ratchet mechanism. Both the wetsuit and the clamp secure the rudder, but the clamp requires less effort to put into place [13]. The carbon fiber rudder remains stationary when Allison is swimming. With no moving parts except for the clamp, the carbon fiber rudder requires little maintenance but does not help produce more thrust.

Figure 20: Allison's plywood prosthetic [3][8]

Figure 21: (Left to Right) Carbon fiber prosthetic, ratchet clamp, neoprene wetsuit [3, 34][9]

Hofesh is another sea turtle with a similar problem. This green sea turtle from Israel suffered severe injuries after getting caught in a fishing net that required the amputation of both front and hind left flippers [35]. A plastic dual tailfin prosthetic also gave Hofesh more hydrodynamic stability [35] and enabled him to resurface [36], as seen in Fig. 22. Similar to Allison's

[8] [3] "Allison's Prosthesis." Allison's Prosthesis. Sea Turtle Inc., Retrieved from http://www.seaturtleinc.org/rehabilitation/allison/.

[9] [34] Liz Hazelton. (2009, Apr 9). "Saved from Swimming in Circles: Allison the One-finned Turtle Gets a New Prosthetic." Daily Mail. Retrieved from http://www.dailymail.co.uk/news/article-1168707/Saved-swimming-circles-Allison-finned-turtle-gets-new-prosthetic.html.

rudder, the back dorsal fin significantly improved his balance and ability to control movement, but did not contribute to thrust [35, 36]. The prosthetic design for this project will aim to produce thrusts proportional to those of real sea turtles. The design attachment can possibly be made from a wetsuit material like what was used for Allison and Hofesh.

Figure 22: Hofesh's dual flipper helps him balance more [35][10]

2.4.2 Yu, flipper

In Japan, a loggerhead turtle, Yu, received a pair of prosthetic limbs to enable her to swim again. Yu had lost ⅓ of her right front flipper and a half of her left front flipper to a shark attack. After 26 design iterations, the most recent prosthetic flipper consisted of two artificial fins attached to a soft vest that fitted over her shell [37].

The flipper component in Yu's prosthetic protects the amputation sites. They are more biomimetic than stationary rudders. The flippers are both secured by a wetsuit and additional adjustable straps that improve fitting, shown in Fig. 23. The prosthetics have the potential to increase thrust generated by each powerstroke because they expand the span of each flipper.

[10] [35] Iacurci, Jenna. (2014, May 17). "Sea Turtle Amputee Swims Again with Jet-Like Prosthetic Fin." Nature World News. Retrieved from http://www.natureworldnews.com/articles/7110/20140517/sea-turtle-amputee-swims-again-with-jet-like-prosthetic-fin.htm.

Figure 23: Yu's prosthetic [37][11]

However, the larger span may also increase the risk of the turtle accidentally hitting herself. Also, the locomotion does not utilize a turtle's natural lift-based mechanism; Yu's prosthetic functions more like a rowing paddle than a moving limb, which reduces control and increases drag. Although it consists of a more flexible material, the prosthetic flipper will remain rigid without rotating to more favorable angles of attack.

Yu's prosthetic design was simple to design for locomotion because she was missing both front flippers. The design was not attempting to replicate the motion of one side because they did not need to balance with remaining healthy flipper. By attaching the same prosthetics for both flippers, it improves balance by accounting for the uneven amputations. In Lola's case, designing an aerodynamic prosthetic that can match the size and shape, as well as the locomotion of the fully intact front flipper will be crucial in keeping her balanced. This can be achieved by following the natural lift-based mechanism of sea turtles.

However, the larger span may also hinder the turtle's movement through seaweed, for example. Also, the locomotion does not utilize a turtle's natural lift-based mechanism; Yu's prosthetic functions more like a rowing paddle than a moving limb, which reduces control and increases drag. The prosthetic flipper will remain rigid without rotating to more favorable angles of attack.

Yu's prosthetic design was simple to design for locomotion because she was missing both front flippers. The design was not attempting to replicate the motion of one side because they did not need to balance with remaining healthy flipper. By attaching the same prosthetics for both flippers, it improves balance by accounting for the uneven amputations. In Lola's case, designing an aerodynamic prosthetic that can match the size and shape, as well as the locomotion of the fully intact front flipper will be crucial in keeping her balanced. This can be achieved by following the natural lift-based mechanism of sea turtles.

To summarize, there is a need to create a patient-specific prosthetic that a sea turtle can use to produce more thrust during each powerstroke. Currently, the patient exerts excessive effort to

[11] [37] Wang, Yue. (2013). Disabled Sea Turtle Gets 27th Pair of Artificial Fins. Time. Retrieved from http://newsfeed.time.com/2013/02/22/disabled-sea-turtle-gets-27th-pair-of-artificial-fins/.

generate minimal thrust with her shortened residual limb. The artificial limb would serve as extension to her residual limb, aiming to make swimming more efficient.

CHAPTER 3 – PROJECT STRATEGY

Chapter 3 discusses the design approach of this project. A client statement from Lola's aquarium was established in Section 3.1. The prosthetic design requirements were then organized in Section 3.2 based on the client statement. Design standards were researched and listed in Section 3.3. In Section 3.4, the client statement was revised to better fit the scope of the project. The project approach and Gantt chart can be found in Section 3.5.

3.1 Initial Client Statement

The inspiration for this project comes from a Kemp's Ridley sea turtle named Lola. Lola is an adult female turtle that is missing a critical part of a frontal right flipper due to a shark attack. Her veterinarian amputated the flipper at the radioulnar joint to prevent infections and closed the wound, leaving her without the majority of the limb. Lola cannot be released into the wild and must stay at the aquarium for the remainder of her life. Her swimming capabilities are hindered due to the amputation. She has trouble balancing, turning, and avoiding collisions with her tank. Lola's swimming patterns likely cause excess stress on her remaining healthy limbs. For this design project, the team collaborated with Lola's caretakers. Dr. Douglas Mader (veterinarian) and aquarium staff provided X-rays, measurements, videos, and pictures of Lola. Materials from the aquarium are provided in Appendix A. The initial client statement is to develop a prosthetic that can help Lola swim more efficiently.

3.2 Design Requirements

The first step of the design process was specifying the objectives and from there, the functional needs of the prosthetic. The main function of the prosthesis was to improve the amputated flipper's efficiency in generating propulsive forces. The objectives tree shown below in Figure 24 organized overarching design parameters.

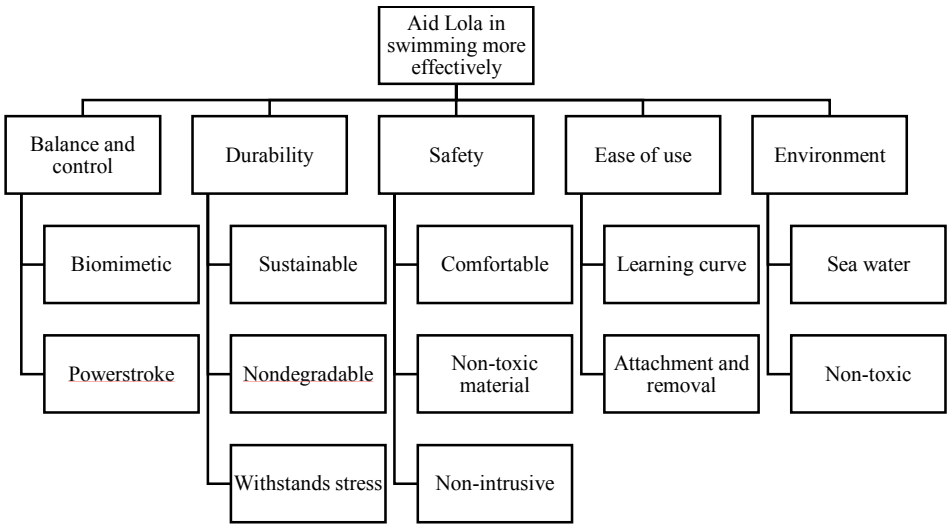

Figure 24: General objectives tree

Safety for the patient as well as the care takers was the first priority. A safe design would be biocompatible, non-toxic, and ensured freedom of movement for the turtle. The design would also be safe for the caregiver handling the prosthetic. It should be non-degradable and durable so

that it could be used daily without deteriorating. The manufacturing process should be simple and also inexpensive. In general, the prosthetic should be easy to maintain, attach and detach. If it was too complicated to use or took too long to attach, the aquarium may not be inclined to use the product at all. The material chosen should not corrode in salt water.

Functionally, the prosthetic should aid Lola in producing higher propulsive forces during the powerstroke without impeding her swimming habits. To serve this function, the prosthetic was modeled based on the geometry of the healthy flipper. Literature described the powerstroke in terms of thrust, flipper orientation and angle of attack as a function of time. In simulations, lift and thrust forces were observed to evaluate performance. To correct Lola's balancing issue, the flipper should be designed so that it can generate sufficient forces when used synchronously with the fully intact flipper.

3.3 Design Standards

Adhering to design standards in industry is important in engineering. For this project, the team found the following standards to follow in the design process.

SolidWorks software is approved to support industry drafting standards, such as Military-Standard-31000A, ASME Y14.41, ISO 16792, and DIN ISO 16792 [56]. This standard allows for the universality of models created in SolidWorks, reducing the amount of errors and allowing for more robust production. ANSYS software qualifies for ISO 26262 automotive safety standard, indicating the reliability of the software [57].

In regards to ethical standards, no foreseeable component to this project is ethically questionable. Safety of all personnel involved will be prioritized, and any chemical wastes will be disposed of in accordance to U.S. Environmental Protection Agency in accordance with the Resource Conservation and Recovery Act (RCRA) [58].

3.4 Revised Client Statement

The team decided to design a prototype of the flipper prosthetic that could be used for live testing and serve as the baseline for future iterations. The initial design would fit Lola specifically and come as close to producing biomimetic loadings as possible given the time constraints and lack of access to the turtle. The model would be sent to the aquarium to test on Lola once the project was completed, to begin a new generation of the flipper prosthetic.

3.5 Project Approach

The project was a year-long design capstone, beginning with research and literature review on sea turtles and turtle locomotion. The preliminary designs for the prosthetic flipper were discussed and feasibility studies conducted to eliminate unfeasible designs. Once a primary design was settled, the testing method and measures of success were determined. At the halfway point, the stages of literature review, conceptual design, and testing procedures were prepared. The following half-year consisted of testing the conceptual designs and alternative designs, collecting data, data analysis, and verification and validation of a final design. Once the prosthetic was deemed safe and effective, it would be sent for live testing. Live testing would be completed by Lola's caretakers in Florida for validation on a living specimen. Fig. 25 shows the Gantt chart for this project.

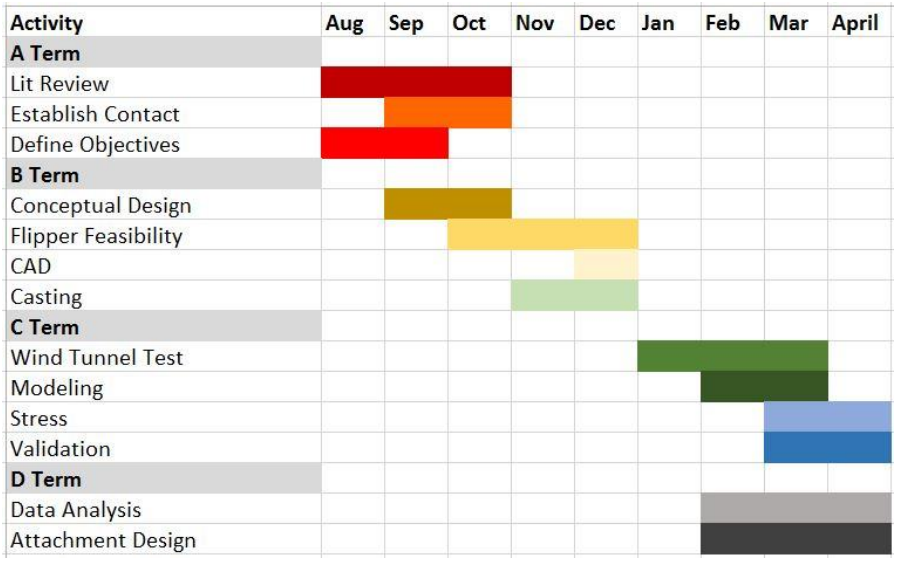

Figure 25: Gantt chart of the year-long project

CHAPTER 4 – DESIGN PROCESS

Chapter 4 presents the methodology and design process. The needs analysis is discussed in Section 4.1, to reiterate the project objectives. Section 4.2 highlights the conceptual design of the prosthetic and its components: the flipper blade and attachment system. The various flipper blade options that were explored can be found in Section 4.3. The biomimetic powerstroke model used for finding important values such as lift and thrust is introduced in Section 4.4. Section 4.5 highlights the methods for obtaining values to quantify the best flipper blade option, such as wind tunnel testing and software simulations. Alternative attachment designs are shown in Section 4.6, which would be fitted to the chosen flipper blade shape. Finally, Section 4.7 emphasizes the safety of the assembled prosthetic with stress analysis and comparison of healthy flipper loadings.

4.1 Needs Analysis

In order to create a more biomimetic flipper, the concepts behind steady sea turtle locomotion were analyzed. For the prosthetic to be successful, the flipper blade should yield positive thrust and minimal lift from each powerstroke cycle. The turtle would benefit from swimming more efficiently. However, thrust and lift magnitudes will vary depending on the turtle's input. To predict the prosthetic's performance, the powerstroke was modeled as a sinusoidal function using constants retrieved from literature [44]. Constants included amplitude, frequency, angle of attack and swimming speed. In order to ensure operation safety and to understand the failure criteria for the prosthetic, stress concentrations from the highest force loads were observed. Furthermore, resultant moments at the shoulder were predicted to ensure that the turtle could generate sufficient forces without over-exertion. The end goal was to create a replacement limb to aid Lola in swimming.

Unfortunately, no studies provided the flipper force values of adult sea turtles throughout the powerstroke. This lack of data might be due to the difficulty of performing tests on the endangered population. Forces also vary depending on the animal's input. Nevertheless, studies have been conducted on hatchling turtles to understand the mechanics of the powerstroke as shown in Fig 26. To compensate, the team made the assumption that powerstrokes performed by hatchling turtles and adult turtles mainly differ in velocity and force magnitudes. Hatchlings and adult turtles were assumed to follow similar locomotions with the same angles of attack. Their muscle forces were also assumed to be scalable.

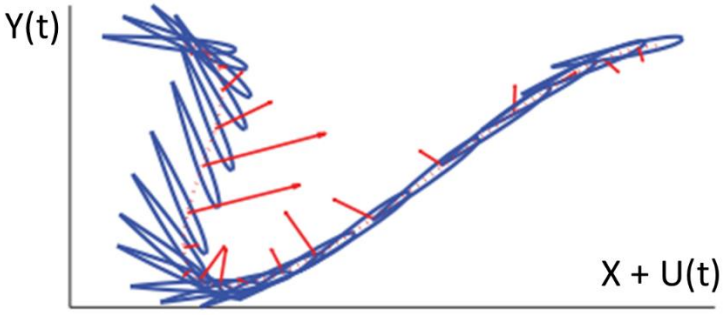

Figure 26: Position graph of the powerstroke with superimposed foil, AOA, and thrust (red arrows) [38][12]

4.2 Conceptual Designs

The goal of this project was to develop a baseline design that could help Lola generate greater forces during each powerstroke. It was a passive design that could be further iterated to include a control mechanism with linkages and motors. Airfoils and wing geometries were compared in terms of aerodynamics and practicality for the patient. Due to time limitations, the wings were modeled as rigid structures to predict optimal performance. Different attachment methods were considered to secure the prosthetic to the residual limb. Stress analysis focused on the strength of the attachment and making sure it was safe to use. The final product was manufactured using flexible materials for durability and safety.

4.2.1 Design Modules

The prosthetic was separated into distinct modules, the flipper blade and the cast. The prosthetic mimicked the lift and drag trends described in literature. The cast was designed to protect the amputation from injury when using the prosthetic, but aimed to not interfere with natural movement.

4.2.2 Custom Flipper Modeling

The flipper blade should propel Lola forward when she performs the powerstroke. The flipper blade was modeled after her healthy flipper to take advantage of its hydrodynamic geometry. Lola's caretakers provided pictures with scales and measurements of the healthy and residual flippers. The team analyzed the images through the ImageJ program to obtain approximate dimensions of the length and width of Lola's healthy flipper, which were then used to create a single flipper outline in SolidWorks. To create the flipper blade, the airfoils NACA0015 and Ryan BQM-34 Firebee were extruded following the outline (Figure 27). The shape of Lola's actual healthy flipper determined the dimensions of the rigid flipper blade including: chord length, flipper length (span), and varying camber thickness.

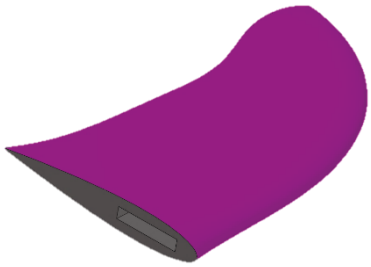

Figure 27: SolidWorks model of flipper blade using Lola's healthy flipper and the NACA0015 airfoil

[12] [38] Licht, S. C., Wibawa, M. S., Hover, F. S., & Triantafyllou, M. S. (2010). In-line motion causes high thrust and efficiency in flapping foils that use power downstroke. The Journal of experimental biology, 213(1), 63-71.

To ensure dimensional similarity, the dimensions of the artificial flipper were compared with measurements provided by Lola's caretakers, seen in Figure 28.

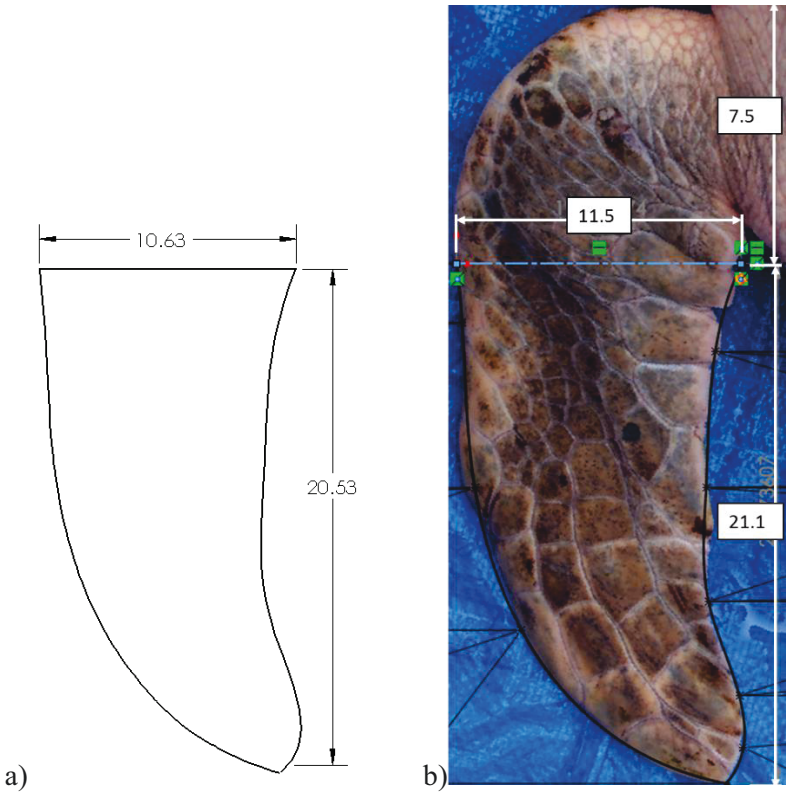

Figure 28: Dimensions [cm] of a) SolidWorks Flipper b) Lola's Healthy Flipper

Table 1 lists the dimensions of the artificial flipper and the healthy flipper. The prosthetic's root chord was 10.6 ± 0.1cm at the base of the flipper component. This resembled the widest part of Lola's flipper, which measured 11.5 cm. The artificial flipper's span was 20.8 ± 0.2cm from root to tip, not including the attachment to the residual limb. Lola's caretakers measured the length of 28.5 cm for the entire limb including the humerus. Thus, the attachment module should have the length of 7.5 ± 0.3cm to account for the difference.

Table 1: Comparison of digital model dimensions and healthy flipper

Dimension	SolidWorks	Healthy Flipper
Root Chord	10.6 ± 0.1 cm	11.5 cm
Span	20.8 ± 0.2 cm for flipper	28.5 cm for entire length
	7.5 ± 0.3cm for attachment	

The flipper blade design is a critical piece for the prosthetic because it generates the majority of the lift and thrust forces during the powerstroke. If the flipper blade is effective, it would enable Lola to swim more efficiently without overexerting her shortened limb. For completeness, various potential flipper shapes were compared to determine the optimal shape for the prosthetic.

4.3 Flipper Blade Alternative Designs

Multiple flipper blade shapes were tested to determine which produced the most beneficial aerodynamic forces. Higher lift and thrust from the prosthetic might allow Lola to better synchronize the locomotion of the shortened limb with the healthy flipper. To enhance the biomimetic design, measurements of Lola's healthy flipper were used as reference dimensions. Furthermore, the AUV Naro-tartaruga case studies showed that symmetric airfoils, such as NACA0014 and NACA0015, were viable airfoils to imitate the natural flipper's performance during the powerstroke. Because NACA0014 was too similar to 0015, a modified version of the NACA0014 called the Ryan BQM-34 Firebee airfoil was used instead. The Ryan BQM-34 Firebee airfoil is much a much thinner, symmetric airfoil. Fig. 29 shows the flipper blades that were tested. In total, there were 2x2 permutations (4 flipper blade types) tested.

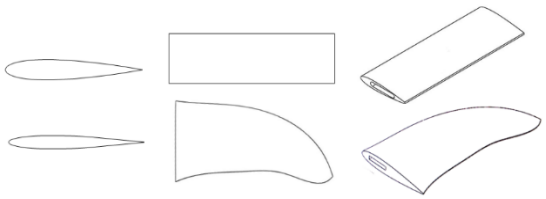

Figure 29: Flipper blade comparison. a) Airfoils NACA0015 (top) and Ryan BQM-34 Firebee (bottom) b) Rectangular and customized planar shapes c) isometric view

The flipper design with the most biomimetic performance (i.e., high thrust), would be chosen and used in the prosthetic prototype.

4.3.1 Mean Aerodynamic Chord

In order to quantify the aerodynamic force production of the flippers, the mean aerodynamic chord (MAC) was found first. All force calculations would be based on this parameter. For each airfoil, the root chords at the base were equal for rectangular and flipper wings. The mean aerodynamic chord is the weighted average chord length that can be used to represent the wing [60, 68]. Having a constant chord along the span, the rectangular wing's MAC was equal to the root chord. On the other hand, the flipper blade had a curved leading edge with a varying sweep angle (the angle between the horizontal and the leading edge) (Figure 28). Eq. 1 is a general equation for calculating MAC for swept wings could be calculated using

$$MAC = \frac{2}{S}\int_0^{b/2} c(y)^2 dy \qquad (1) \quad [60]^{13}$$

$S = Planform\ area\ of\ 2\ wings$

$b = Wing\ span\ of\ 2\ wings$

$c(y) = Chord\ at\ distance\ y\ from\ root\ of\ 1\ wing$

[13] [60] Wing Geometry Definitions. Retrieved from http://adg.stanford.edu/aa241/wingdesign/winggeometry.html.

Because these equations are generally used for aircraft, two wings are assumed. The planform area (S) is the projected area of two wings and the wing span (b) is the length between the tips of two wings. The chord (c(y)) is a function of the distance between the root chord and the incremental chord. Trapezoidal approximation was used to estimate the MAC based on ten increments along the span (Eq 2).

$$MAC = \frac{\Delta y}{2}\frac{2}{S}\sum_{i=1}^{10} c_i^2$$

$$MAC = \frac{\Delta y}{2}\frac{2}{s}[c_1^2 + 2c_2^2 + 2c_3^2 + \cdots + 2c_{n-1}^2 + c_n^2] \qquad (2)\ [61]^{14}$$

In aerodynamics studies, the resultant lift, drag and moment vectors are often placed at the quarter chord point [68]. This critical point will be referred to as 1/4MAC in later calculations.

To estimate the location of the MAC along the span, the wing was simplified into a rectangular trapezoid (outlined in gray in Figure 30 below). The trailing edge was treated as a horizontal base and the tip and root chords were perpendicular lines. The leading edge was a diagonal at a constant 24.8° sweep angle (avg.). Consequently, the MAC turned out to be 8.7 cm (Ryan BQM-34 Firebee) and 8 cm (NACA0015) from the root. This distance will be referred to as $\bar{Y}$. To ensure trapezoidal wings were similar to the flippers, the wing areas were compared and only deviated by ± 0.12 m^2.

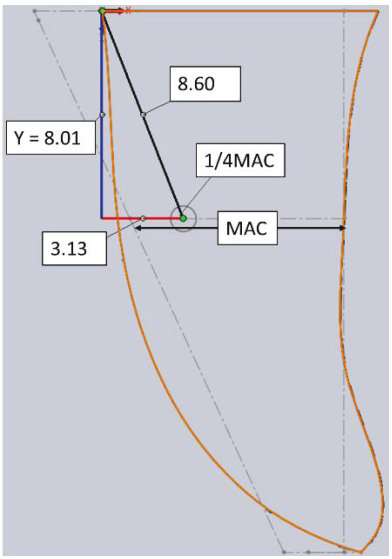

Figure 30: Diagram indicating MAC for NACA0015 [dimensions in cm]

Finding the MAC of each flipper allowed the team to represent the flipper shape as a single parameter rather than an extrusion with varying chord lengths. Overall, the chosen flipper shape for the final design would be fabricated as a full-sized flexible flipper blade. The blade would be

[14] [61] Dawkins, Paul. (2016). Approximating Definite Integrals. Retrieved from http://tutorial.math.lamar.edu/Classes/CalcII/ApproximatingDefIntegrals.aspx.

incorporated into an attachment system. Furthermore, it would be made of a flexible material for durability and safety reasons.

4.3.2 Flexible Flipper

The final chosen flipper blade shape for Lola's prosthetic would ideally be made of a flexible material. Previous studies indicated that oscillating foils have a higher propulsion efficiency than rigid foils for marine-based systems [46]. It was speculated that this advantage was due to the increase in span of the foil during upstroke and downstroke, demonstrated in Fig. 31.

Figure 31: Extended span of flexible foils (solid) compared to rigid foils (dotted), adapted from [45][15]

From this information and further research into turtle locomotion, the team decided to pursue a flexible flipper approach for a final flipper blade product. A flexible flipper would also better to model the flexibility and/or stiffness of turtle flesh. In addition to producing more thrust and similarities in material stiffness [99, 101, 105], a flexible material is safer than a rigid material for swimming. If Lola were to hit her enclosure, a rigid material would either break or refuse to yield; both cases are non-ideal. A broken rigid blade could have rough or sharp edges that could harm Lola. An unyielding flipper would mean that an impact would affect Lola directly, either causing a large torque on her shoulder or concentrating the impact onto her amputated area. Compared to a rigid flipper, a flexible flipper would disperse the impact energy, reducing the likelihood of material failure and harming Lola.

4.4 Powerstroke Model

A sea turtle's primary form of locomotion is the powerstroke. In order to create a more biomimetic flipper, the team analyzed Lola's natural course of swimming and based estimations and calculations off of the powerstroke model. An overview of a powerstroke mathematical model is introduced in Section 4.4.1, which includes the position and derived velocities and accelerations of a sea turtle flipper. Flow matching methods were described in Section 4.4.2 to tie together air flow and "true" water flow that the prosthetic would experience. Using the flipper's dimensions, flow characteristics, and airfoil coefficients, lift, drag and moment can be calculated as described in Section 4.4.3. In Section 4.4.4, the forces were then translated to effective lift and thrust vectors that would actually propel the turtle forward. Because the flipper would be moving in water, added mass effects from fluid acceleration were added to the effective forces in Section 4.4.5.

4.4.1 Overview

The forces generated during each powerstroke were calculated in order to understand how the prosthetic may affect the turtle's swimming. As mentioned previously, to the best knowledge

[15] [45] University of Illinois at Urbana-Champaign Applied Aerodynamics Group. (n/a). UIUC Airfoil Coordinates Database [Data file]. Retrieved from http://m-selig.ae.illinois.edu/ads/coord_database.html.

of the authors, no existing literature provided resultant force values generated by adult sea turtles. However, the powerstroke has been studied extensively using hatchling sea turtles. Zhou and his team modeled the trajectory of the flipper through a series of equations (Eq. 3 – 8) [44]. The two recovery loops between the downstroke and upstroke shown in Fig. 8 (Section 2.3.5) were not included in order to simplify the model. The flipper's position with respect to the turtle was modeled using

$$y(t) = hcos(2\pi ft) \quad (3),$$

$$x(t) = -\frac{h}{tan\beta}\cos(2\pi ft) \quad (4),$$

where t was the time variable (0 to 0.588 sec), h was the heaving amplitude (8.27 cm), f was the flapping frequency (1.7 1/s) and β was the stroke angle, (125 degrees), "determin[ing] the shape of the trajectory" [44]. Position equations were differentiated with respect to time for the flipper's vertical and horizontal velocities:

$$\dot{y}(t) = -hsin(2\pi ft) * 2\pi f \quad (5),$$

$$\dot{x}(t) = \frac{h}{tan\beta}\sin(2\pi ft) * 2\pi f \quad (6).$$

Velocity equations were then differentiated again for acceleration:

$$\ddot{y}(t) = -hcos(2\pi ft) * (2\pi f)^2 \quad (7),$$

$$\ddot{x}(t) = \frac{h}{tan\beta}\cos(2\pi ft) * (2\pi f)^2 \quad (8).$$

Wing position was plotted as a function of time to illustrate the powerstroke (Figure 32). The turtle was centered on the horizontal axis (x(t) + Ut). The horizontal axis represents the turtle's straight and level swimming path at a velocity U. The vertical axis (y(t)) represents flipper's position relative to the turtle's shoulder. More specifically, the flipper is represented by the Quarter Chord point (1/4MAC) as discussed in Section 4.4.3. The 1/4MAC was superimposed to trace the position curve.

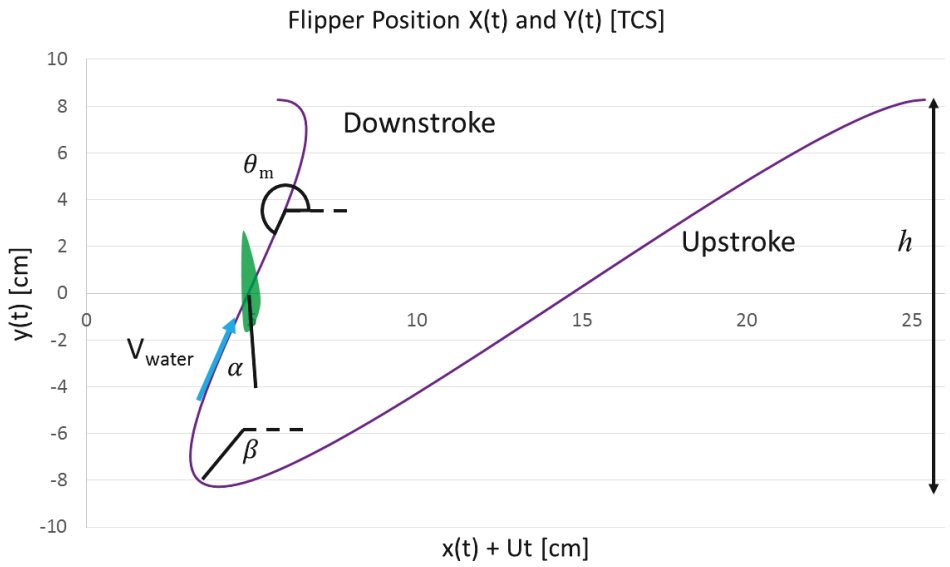

Figure 32: Flipper Position Graph, adapted from [38,44]16,17

In order to make the powerstroke model more relevant to the turtle, constants were modified to reflect the behavior of adult sea turtles. These constants include: flapping frequency (f), swimming speed (U), heaving amplitude (h), and stroke angle (β). The frequency ($f = 1.7\ s^{-1}$) was estimated from recordings of the patient swimming. The actual forward speed was estimated based on shell size. Based on the curved carapace length (CCL = 56 cm), the straight carapace length (SCL) was 53.3 cm based on:

$$SCL = 0.4449 + 0.9433(CCL) \qquad (9)\ [62]18$$

With a SCL greater than 50 cm, Lola could be treated as an adult that swims at a migratory speed of U = 33.32 cm/s [63]. The heaving amplitude (h = 8.27 to 8.76 cm) represents the 1/4MAC's peak position before starting each cycle. It was calculated as the projected vertical length between the shoulder joint and the 1/4MAC shown in Figure 33. With the set constants U, h, and f; the stroke angle (β = 125 degrees) was modified until the position graph matched literature [44, 62].

[16] [38] Licht, S. C., Wibawa, M. S., Hover, F. S., & Triantafyllou, M. S. (2010). In-line motion causes high thrust and efficiency in flapping foils that use power downstroke. The Journal of experimental biology, 213(1), 63-71.

[17] [44] Zhou, K., Liu, J., Chen, W. (2015). Proceedings from 2015 IEEE: International Conference on Information and Automation. Lijiang, China.

[18] [62] Gallaway, Benny J. and Caillouet, Jr., Charles W. (2013, Jun). Kemp's Ridley Stock Assessment Project. Retrieved from http://www.gsmfc.org/publications/Miscellaneous/Kemp%20Ridley%20Stock%20Assessment%20Report%20Final%20June%2027%202013.pdf.

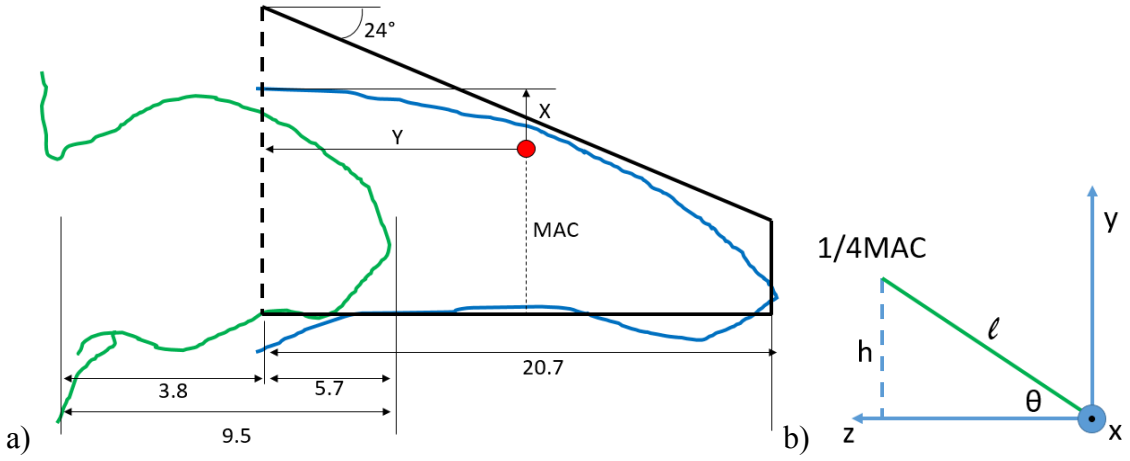

Figure 33: a) Flipper diagram b) Heaving amplitude

Up until this point, the discussion was about modeling the position of the flipper at each point during the powerstroke. Angles describing the flipper's locomotion are also important. The direction of the force vectors depended on the flipper's orientation. The angle of foil motion $\theta_m(t)$ was the angle between the swimming speed U and lines tangent to the trajectory (Eq. 10). Depending on $\theta_m(t)$, lift and drag may have positive or negative contributions to overall propulsion. The angle of foil motion was modeled as:

$$\theta_m(t) = \arctan\left(\frac{\dot{y}(t)}{\dot{x}(t)+U}\right) \qquad (10)^{[44]19}$$

The angle of attack $\alpha_{eff}(t)$ was the angle between the chord and the freestream velocity [68]. The flipper was assumed to rotate about the 1/4MAC. Zhou provided $\alpha_{eff}(t)$ as a piecewise function:

$$\alpha_{eff}(t) = \begin{cases} \alpha_{max}\sin(2\pi f) & 0 \le t < T/2 \\ 0 & T/2 \le t < T \end{cases} \qquad (11)^{[44]}$$

where α_{max} was the highest angle of attack at mid-downstroke, $0 \le t < T/2$ was the downstroke and $T/2 \le t < T$ was the upstroke [44]. The maximum angle of attack (α_{max}) for the downstroke was 24 degrees corresponding with the vigorous powerstroke observed by Davenport et al. [22]. The upstroke was reported to have an angle of attack of 7 degrees, but was assumed zero to minimize negative propulsive forces [22, 44]. The total time (T) was 0.6 seconds, the time needed to complete one powerstroke cycle.

Using the model described above, the flipper's position and orientation could be predicted. The following sections explain how the aerodynamic forces and moments were then calculated at each position. These forces and moments were dependent on the effective freestream velocity. At a forward speed U, the flipper faces a local freestream as it concurrently treads through salt water. The flipper experiences a resultant velocity (ex. V_{water} = 83 cm/s) of the two freestreams, illustrated in Fig. 34 [22].

[19] [44] Zhou, K., Liu, J., Chen, W. (2015). Proceedings from 2015 IEEE: International Conference on Information and Automation. Lijiang, China.

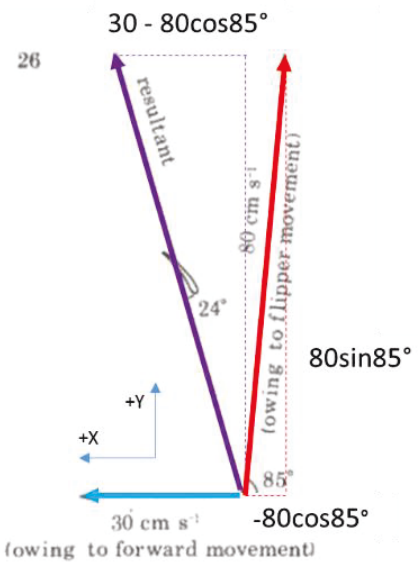

Figure 34: Vigorous downstroke, adapted from [22][20]

The effective angle of attack (α_{eff} = 24°) describes the flipper's angle relative to V_{water}. In this project, V_{water} was calculated as the magnitude of the x and y velocities at each flipper position:

$$V_{water} = \sqrt{(\dot{x} + U)^2 + \dot{y}^2} \qquad (12)$$

4.4.2 Flow Matching

Naturally, the turtle's powerstroke is performed in water. To predict flipper performance using results from wind tunnel testing, Reynolds numbers (Re) of water and air flows needed to be matched. Flows with similar Reynolds numbers exhibit similar characteristics [68]. The resultant velocity in salt water (V_{water}) was used to calculate an equivalent airspeed (V_{air}) by matching the Reynolds Numbers:

$$R_e = \frac{\rho_{air} V_{air} C_{model}}{\mu_{air}} = \frac{\rho_{water} V_{water} C_{turtle}}{\mu_{water}} \qquad (13)$$[68][21]

Based on the position model above, the flipper would reach peak velocities between 0.9 and 1.4 m/s in water. As a safety factor, 1.7 m/s was used as the upper limit. This resulted in a Reynolds number around 176,000. Since the highest Reynolds number was below 200,000, it validated the laminar flow assumption for the duration of the powerstroke. 1.7 m/s windspeeds also produced the most reliable results as will be discussed in Section 5.1.1.

Flow matching accounted for the difference in fluid densities (ρ_{air} ; ρ_{water}), dynamic viscosities (μ_{air} ; μ_{water}) as well as the difference in the chord lengths (C_{model} ; C_{turtle}). Table 2 below

[20] [22] Davenport, J., Munks, S. A., Oxford, P. J. (1984). A comparison of the swimming of marine and freshwater turtles. Proceedings of the Royal Society of London B: Biological Sciences 220 (1221): 447-475.

[21] [68] Anderson, Jr., John D. (2011). Fundamentals of Aerodynamics, 5th ed. New York, NY: McGraw-Hill.

lists constants used in flow matching. Air was assumed to be 20°C at sea level; with corresponding air density (ρ_{air}) of 1.204 kg/m^3 and dynamic viscosity (μ_{air}) of 1.84E-5 kg/m-s [40, 41]. Sea water was assumed to be 20°C with a salinity of 20g/kg; with corresponding density (ρ_{water}) of 1013.4 kg/m^3 and dynamic viscosity (μ_{water}) of 1.04E-3 kg/m-s [39]. The mean aerodynamic chords (MAC) were used for flow matching because they effectively represent the wings.

Table 2: Flow matching parameters

Wind Tunnel	Value	Prosthetic	Value
ρ_{air}	1.204 kg/m^3 [41][22]	ρ_{water}	1013.4 kg/m^3 [39][23]
V_{air}	11.86 – 25.2 m/s	V_{water}	0.8 – 1.7 m/s
C_{model}	2.84 - 3.99 cm	C_{turtle}	7.58 - 10.63 cm
μ_{air}	1.84e-5 kg/m*s [40][24]	μ_{water}	1.04e-3 kg/m*s [39][25]

By matching Reynolds numbers, the characteristics of equivalent water and air freestreams were determined. These characteristics could be used to calculate lift, drag and quarter chord moment coefficients that represent the wings' aerodynamic performance.

4.4.3 Coefficients of Lift, Drag and Quarter Chord Moment

In general, wings generate lift, drag, and moments corresponding to the angle of attack. Lift curves show parabolic trends and drag curves are exponential. On the other hand, moment varies depending on the reference point. The Quarter Chord point (1/4MAC) is often used as a reference because it experiences a consistent moment at all angles of attack [68, 44]. It effectively represents the aerodynamic center [68]. Symmetric airfoils like the Ryan BQM-34 Firebee and NACA0015 have small quarter chord moments. Force and moment magnitudes retrieved from experimental data are often translated into non-dimensional coefficients in order to compare aerodynamic performance:

$$C_L = \frac{L}{0.5\,\rho_{water} V_{water}^2 S} \qquad (14)^{[68]}$$

[22] [41] The Engineering Toolbox. (n/a). Air Density and Specific Weight [Data file]. Retrieved from http://www.engineeringtoolbox.com/air-density-specific-weight-d_600.html.

[23] [39] Sharqawy, M. H., Lienhard V, J. H., Zubair, S.M. (2010). Thermophysical Properties of Sea Water: A Review of Existing Correlations and Data. Desalination and Water Treatment, 16, 354-380.

[24] [40] Edwards, K. (2015). LMNO Engineering, Research, and Software, Ltd.: Gas Viscosity Calculator [Software]. Available at http://www.lmnoeng.com/Flow/GasViscosity.php.

[25] [39] Sharqawy, M. H., Lienhard V, J. H., Zubair, S.M. (2010). Thermophysical Properties of Sea Water: A Review of Existing Correlations and Data. Desalination and Water Treatment, 16, 354-380.

$$C_D = \frac{D}{0.5\,\rho_{water} V_{water}^2 S} \qquad (15)^{[68]}$$

$$C_{M_{c/4}} = \frac{M_{c/4}}{0.5\,\rho_{water} V_{water}^2 SC} \qquad (16)^{[68]26}$$

Inversely, the coefficients can also be used to predict the performance of wings with the same airfoil.

4.4.4 Effective Lift and Thrust for Propulsion (TCS)

The position, velocity, and acceleration of the flipper as well as the angle of attack were predicted using a sinusoidal model retrieved from Zhou et al.'s locomotion study [44]. The flipper's lift, drag and moment coefficients were then obtained from wind tunnel testing, and software including Javafoil and ANSYS Fluent (Section 4.5.2 - 4.5.6). At each flipper position, the coefficients were matched with the closest angle of attack (α_{eff}) at time t. Eq 14 to 16 were manipulated to solve for lift, drag and moment values using the coefficients and freestream characteristics.

The Turtle Coordinate System (TCS) was designated to describe forces with respect to the turtle's position (X_{Turtle} +Ut) as shown in Fig. 35. The corrected pitch angle (θ_{mc}) accounts for the direction of the lift and drag in this new coordinate system:

$$\theta_{mc} = \begin{cases} \theta_m & 0° \le \theta_m < 90° \\ 180° - \theta_m & 90° \le \theta_m < 180° \\ \theta_m - 180° & 180° \le \theta_m < 270° \\ 360° - \theta_m & 270° \le \theta_m < 360° \end{cases} \qquad (17)$$

Figure 35 shows the relative orientations of forces in their respective coordinate systems: the Local Coordinate System (LCS), Global Coordinate System (GCS) and the Turtle Coordinate System (TCS).

[26] [68] [Aero] Anderson, Jr., John D. (2011). Fundamentals of Aerodynamics, 5th ed. New York, NY: McGraw-Hill.

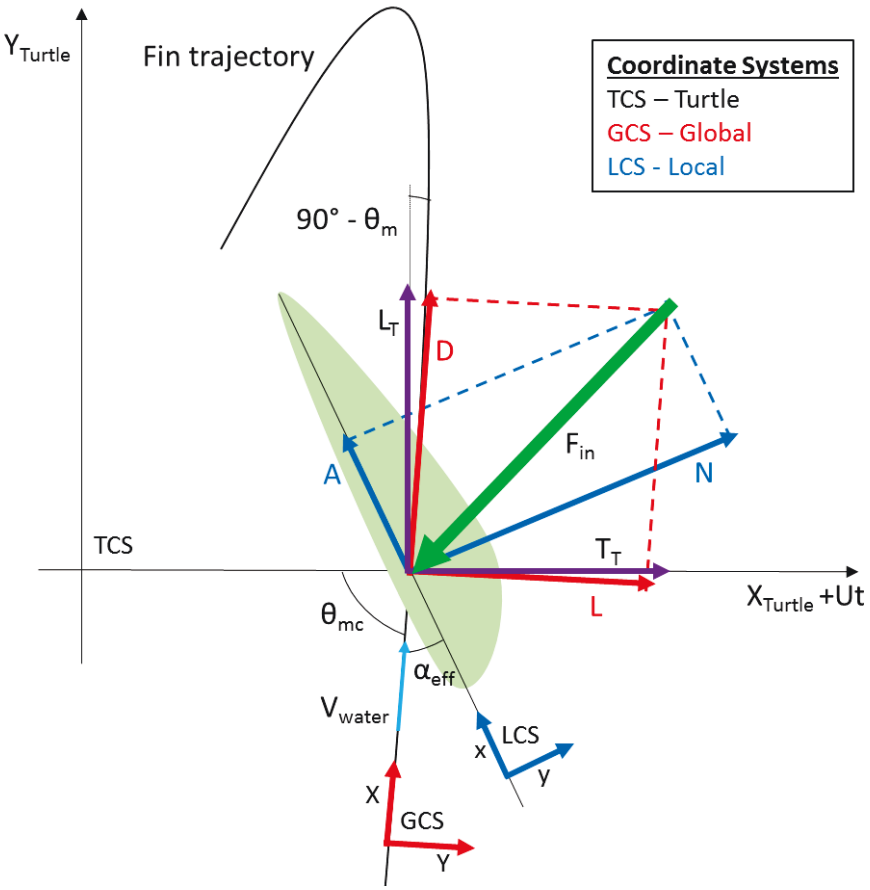

Figure 35: Free Body Diagram of Aerodynamic Forces acting on Flipper, adapted from [22, 32, 44, and 52][27]

The lift and drag forces previously calculated in Global Coordinate System (GCS) were translated to effective lift (L_T) and thrust (T_T) in TCS to understand how much the flipper will propel the turtle in water:

[27] [22] Davenport, J., Munks, S. A., Oxford, P. J. (1984). A comparison of the swimming of marine and freshwater turtles. Proceedings of the Royal Society of London B: Biological Sciences 220 (1221): 447-475.

[32] Siegenthaler, C. (2012). System Integration and Fin-Trajectory Optimization for a Robotic Turtle (Master Thesis). Retrieved from Swiss Federal Institute of Technology Zurich. (386) http://students.asl.ethz.ch/upl_pdf/386-report.pdf.

[44] Zhou, K., Liu, J., Chen, W. (2015). Proceedings from 2015 IEEE: International Conference on Information and Automation. Lijiang, China.

[52] [Image] Retrieved from http://baike.baidu.com/pic/%E5%8D%87%E5%8A%9B%E7%B3%BB%E6%95%B0/6221003/0/faf2b2119313b07efc8a4a630dd7912397dd8ca1?fr=newalbum#aid=0&pic=faf2b2119313b07efc8a4a630dd7912397dd8ca1.

$$L_T = \begin{cases} L\cos(\theta_{mc}) - D\sin(\theta_{mc}) & 0° \le \theta_m < 90° \\ -L\cos(\theta_{mc}) - D\sin(\theta_{mc}) & 90° \le \theta_m < 180° \\ -L\cos(\theta_{mc}) + D\sin(\theta_{mc}) & 180° \le \theta_m < 270° \\ L\cos(\theta_{mc}) + D\sin(\theta_{mc}) & 270° \le \theta_m < 360° \end{cases} \quad (18)\ [22, 23]$$

$$T_T = \begin{cases} -L\sin(\theta_{mc}) - D\cos(\theta_{mc}) & 0° \le \theta_m < 90° \\ -L\sin(\theta_{mc}) + D\cos(\theta_{mc}) & 90° \le \theta_m < 180° \\ L\sin(\theta_{mc}) + D\cos(\theta_{mc}) & 180° \le \theta_m < 270° \\ L\sin(\theta_{mc}) - D\cos(\theta_{mc}) & 270° \le \theta_m < 360° \end{cases} \quad (19)\ [22, 23]28$$

where L was lift, D was drag, and θ_{mc} was the corrected angle of foil motion. The input force (F_{in}) required from the turtle is the negative of the resultant force given by:

$$-F_{in} = R = T_T\,\hat{\imath} + L_T\,\hat{\jmath} \quad (20).$$

Weight and buoyancy were ignored for simplicity because turtles are known to regulate their lung volume for neutral buoyancy [64]. To summarize, Axial (A) and Normal (N) forces in LCS were translated to Lift (L) and Drag (D) in GCS. Lift and Drag were then translated to effective Lift (L_T) and Thrust (T_T) in TCS. Lift and Thrust were the forces propelling the turtle forward during the powerstroke.

4.4.5 Added Mass

The previous section explained how to obtain effective lift and thrust values without added mass effects. Added mass (or virtual mass) describes the mass of the fluid being accelerated and should be considered for dense fluid mediums like water [65]. Eq. 21 was derived to calculate the added mass (or virtual mass) for water turbine hydrofoils [65].

$$M_{VM} = \frac{\pi}{4}(MAC)^2 \rho_{water} L_{flipper} \quad (21)^{[65]}$$

The blades were assumed to be flat plates [65]. The virtual mass force was calculated by multiplying the total mass (flipper mass and virtual mass) by the flipper's acceleration [66]:

$$F_{VM} = (M_{flipper} + M_{VM})a_{flipper} \quad (22)\ [66]$$

---

[28] [22] Davenport, J., Munks, S. A., Oxford, P. J. (1984). A comparison of the swimming of marine and freshwater turtles. Proceedings of the Royal Society of London B: Biological Sciences 220 (1221): 447-475.

[23] Wyneken, J. (1997). Sea turtle locomotion: mechanisms, behavior, and energetics. The biology of sea turtles Vol. 1. CRC Press.

[65] Maniaci, David C., Li, Ye. (2012). "Investigating the Influence of the Added Mass Effect to Marine Hydrokinetic Horizontal-Axis Turbines Using a General Dynamic Wake Wind Turbine Code." NREL. Journal Article-5000-54403. Retrieved from http://www.nrel.gov/docs/fy12osti/54403.pdf.

[66] White, Frank M. (2011). Fluid Mechanics, 7th ed. New York, NY: McGraw-Hill.

Since the virtual mass force (F_{VM}) is in the direction of acceleration (TCS), its components can be added directly to the effective Turtle lift (L_T) and thrust (T_T) vectors [66]. The resultant force (F_{IN}) is the input force needed from Lola. Figure 36 below is a final free body diagram showing the directions of L_T and T_T and F_{VM}, which are generated by the input force F_{IN}.

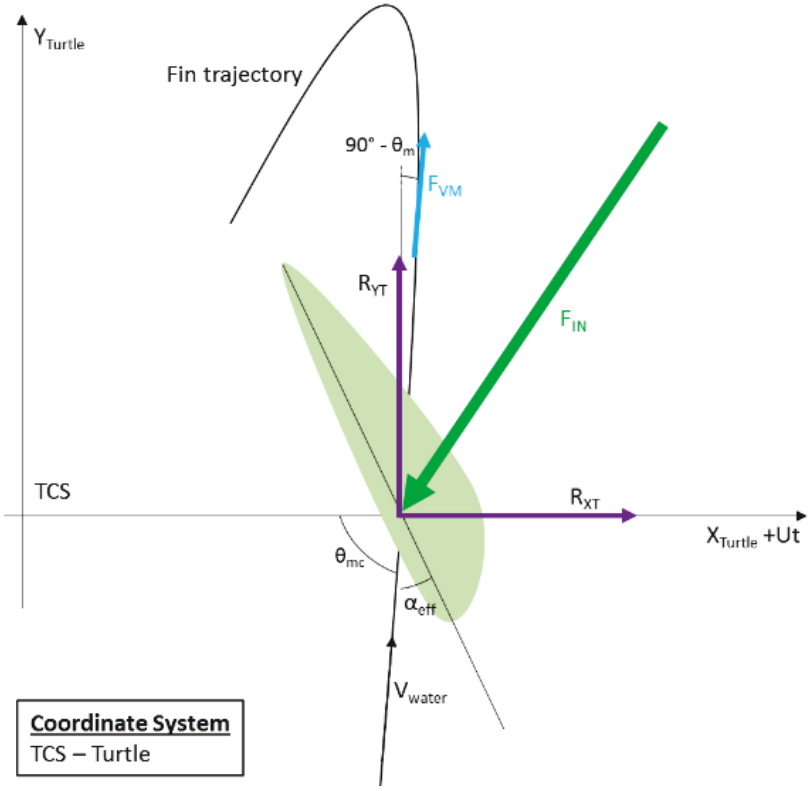

Figure 36: Final Free Body Diagram including Virtual Mass Effects, adapted from [22, 32, 44, 52, 66 and 67][29]

4.5 Flipper Blade Methodology

The flipper blades created in SolidWorks were fabricated and subjected to wind tunnel testing. They were then compared based on lift and drag results from wind tunnel testing, Javafoil, and ANSYS FLUENT. The lift and drag values of the flippers at varying freestream velocities and angles of attack were recorded. The accuracy of the experimental wind tunnel results was limited because part of the wind tunnel's force stinger was unreliable. The team used the best-fit theoretical software results to find lift and thrust values for full-size flippers. Section 4.5.1 describes the manufacturing process for the wind tunnel test assembly. Section 4.5.2 provides the procedure for the wind tunnel experiment. Section 4.5.3 explains how to interpret results and Section 4.5.4 discusses the experimental limitations. Section 4.5.5 describes the software simulations used to

[29] [67] Hepperle, Martin. (2007, Jan 27). JavaFoil- Analysis of Airfoils. Retrieved from http://www.mh-aerotools.de/airfoils/javafoil.htm.

collect 2D airfoil data and Section 4.5.6 explains how the airfoil data was corrected for 3D finite wings.

4.5.1 Fabrication

The rectangular and customized flipper wings were designed in SolidWorks and 3D printed as rigid PLA (polylactide or polylactic acid) models (Figure 37). The dimensions of the actual sized wings and their wind tunnel models are listed in Table 3. The models were scaled down by 0.375 to fit into a small wind tunnel, as mentioned previously.

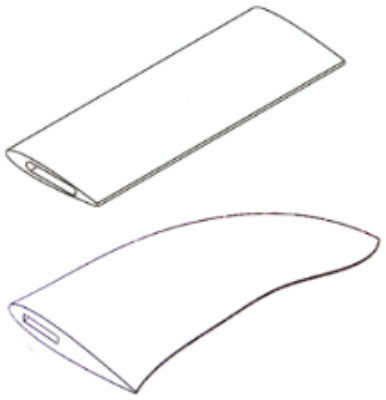

Figure 37: Rectangular and Customized Flipper wings

Table 3: Dimensions of Rectangular and Customized Flipper wings

airfoil	shape	size	Root Chord [mm]	Tip Chord [mm]	Half Span [mm]	Mean Aerodynamic Chord (MAC) [mm]	Mass [g]	Swing [mm^2]	AR
Ryan BQM-34 Firebee	rect	big	98.580	98.580	206.341	98.580	376.870	40682.062	4.186
Ryan BQM-34 Firebee	flip	big	98.580	0.010	206.341	75.787	203.710	29046.940	5.863
NACA0015	rect	big	106.336	106.336	208.662	106.336	622.870	44376.304	3.925
NACA0015	flip	big	106.336	0.010	208.662	82.500	345.180	32101.066	5.425
Ryan BQM-34 Firebee	rect	small	36.967	36.967	77.378	36.967	19.870	5720.914	4.186
Ryan BQM-34 Firebee	flip	small	36.967	0.010	77.378	28.420	10.740	4084.726	5.863
NACA0015	rect	small	39.876	39.876	78.248	39.876	32.830	6240.418	3.925
NACA0015	flip	small	39.876	0.010	78.248	30.938	18.200	4514.212	5.425

4.5.2 Wind Tunnel Testing

Wind tunnel testing provided experimental results that illustrated how the flipper might perform in a real environment. Wind tunnel testing required angles of attack and airspeed (V_{air}) to yield outputs of normal force, and axial force; which could then be used to calculate lift and drag. These experimental results were corroborated to validate results from Javafoil and ANSYS FLUENT. Assumptions made for wind tunnel testing included: laminar flow, constant freestream velocity in test section, and rigid wing [68].

Wind Tunnel Description

The 8” Open Circuit Wind Tunnel by Engineering Laboratory Design, Inc. was used for wind tunnel testing. Fig. 38 shows the wind tunnel used. It had an 8in x 8in test section and a sting that measured forces and moments. It had a velocity range of 0 - 50 m/s and an angle of attack

range of 0 - 24 degrees. The owner of the wind tunnel offered resources and guidance for wind tunnel testing.

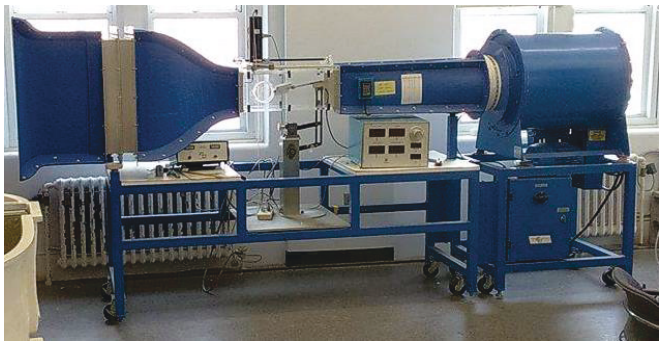

Figure 38: 8" Open Circuit Wind Tunnel used in experimentation

Wind Tunnel Experiment Setup

The actual-size flippers were scaled down to mitigate wall effects in the wind tunnel. For the 8in x 8in test section, the model to prototype scale was 0.375 to 1. It was recommended that the clearance be greater than half the MAC (Clearance > MAC/2). This clearance was not met in order to avoid decreasing the already small wing areas. Nevertheless, the wings did have some clearance to avoid touching the wall.

Because the wind tunnel was designed to simulate both wings of an aircraft, a dual-flipper assembly was attached to a sting (Figure 39). Solidworks drawings for flipper assembly are provided in the Appendix F.

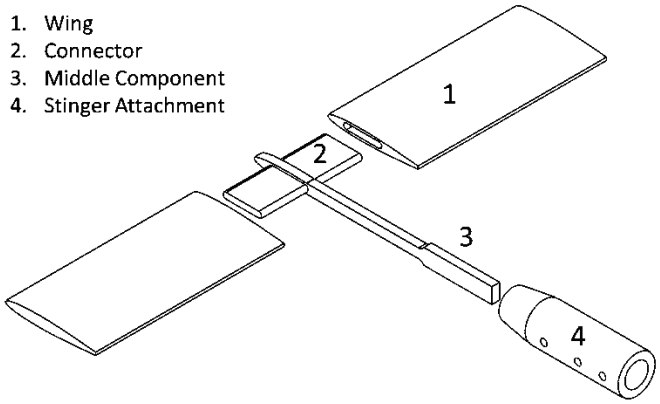

Figure 39: Components for wind tunnel testing

The wind tunnel assembly consisted of two wings (1) attached to a middle component (3) via a connector (2) (Figure 39 above). Wood served as the connector to minimize vibrations. To avoid added interference from test stand parts, the middle component was thin and matched the flipper's airfoil in the front. The sting attachment (4) was secured to the end of the middle component through a key slot. The sting attachment was slide fitted onto the sting rod, following the standards for a close sliding fit class RC1 [51]. Screws were inserted on both sides of the sting

attachment to secure the position of the assembly onto the sting (Fig. 40). The middle component and sting attachment were machined aluminum parts. Wind Tunnel Test Setup is shown in Fig. 40 below.

Figure 40: Wind Tunnel Test Setup

Wind Tunnel Experiment Procedure

The wind tunnel required airspeed (V_{air}) and effective angle of attack (α_{eff}) inputs. To accommodate for the sting's sensitivity, the airspeed was set at 1.7 m/s (See Section 5.1.1 for details). The airspeed controller was set to the corresponding frequency of 33.82 s^{-1}. The sting's angle of attack was rotated counterclockwise from zero to -24 degrees due to physical constraints. The sting would only reach +10 degrees before colliding with wind tunnel wall. Since the airfoils were symmetric, the negative angles did not affect the magnitudes of the forces and moments. Before each wing was tested, the wings were leveled and the sensor box was zeroed to improve accuracy. The same angles of attack (α_{eff}) and airspeed (V_{air}) were inputted into the wind tunnel, Javafoil, and ANSYS FLUENT.

The procedure for experiments in the wind tunnel was as follows:

1. Remove the top of the wind tunnel's test section. Ensure the sting's tip rotator is secured to the right most position. If the tip rotator is not secured, the sting will rotate during testing and invalidate results. The sting's components are shown in Figure 41 below.

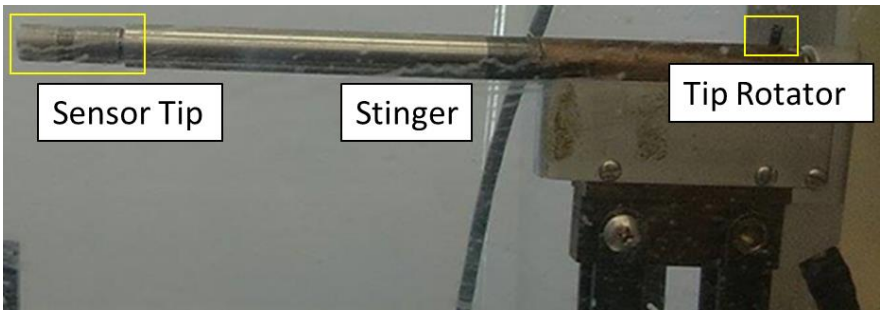

Figure 41: Sting components

2. Slide the wing assembly onto the sting. Insert screws on opposite sides to secure the sting attachment. Tighten screws until the wing assembly cannot rotate easily. Use a bubble level to level the wing assembly. The secured wing assembly on the sting is shown in Fig. 42.

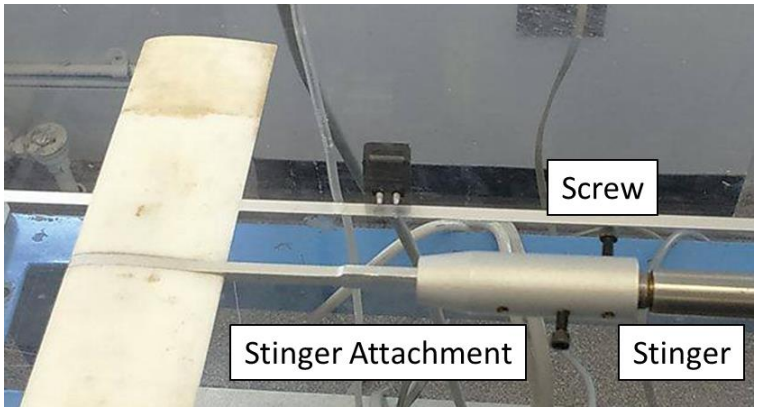

Figure 42: Secured wing assembly

3. Replace the top onto the test section and secure. The sting is attached to a parallel bar linkage. Turn the angle of attack (AOA) knob to level the sting. The wing is now at zero angle of attack as shown in Fig. 43.

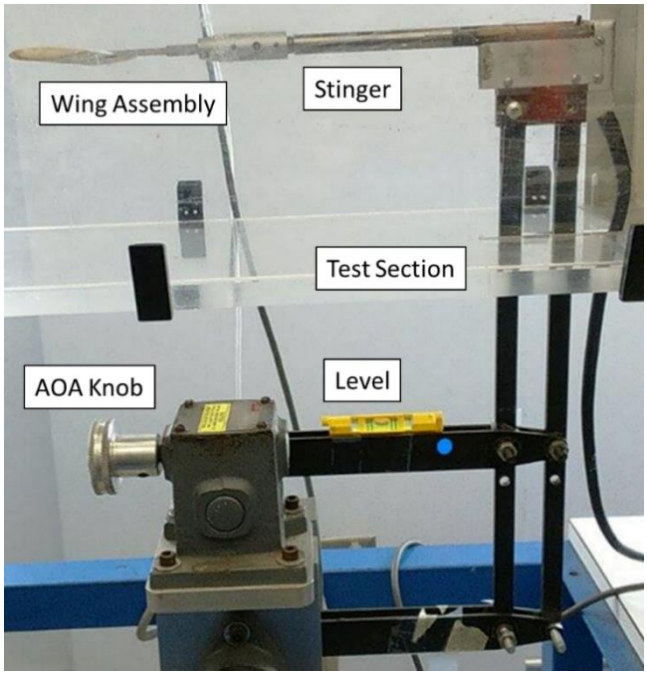

Figure 43: Leveled sting

4. Use a screw driver to zero the normal force, axial force, pitching moment, and angle of attack readings on the sensor box (Figure 44). Note that the readings will not be exactly zero and will oscillate.

Figure 44: Sensor box

5. Push "Panel/Remote" on the wind speed controller (Figure 45). Use the arrow keys to adjust the frequency to 33.8 Hz, which corresponds with V_{air} = 1.7 m/s. Hit "Run".

Figure 45: Wind speed controller

6. Wait until the wind tunnel reaches full power and the coefficients settle. Record the normal force, axial force and pitching moment for the set angle of attack.
7. Hit "Stop" to turn off the airflow. When the airflow is completely off, record the zeroes for each reading (numbers each monitor finally stops at).
8. Turn the AOA knob to decrease the angle by -1 degrees. Repeat steps #5 to #8 until -24 degrees.

4.5.3 Obtaining Resultant Forces

Wind tunnel testing yielded experimental data on axial force (A), normal force (N) and pitching moment (M_P). The forces were described in the airfoil's local coordinate system (LCS) [68, 50]. The directions of the forces and moments acting on the wing assembly is shown in Fig. 46 below. Axial force is the local drag parallel to the chord and normal force is the local lift perpendicular to the chord. The pitching moment was measured at the base of the sting tip. The directions of the normal force and moment were reversed to account for the negative angle. The direction of the axial force did not change. Because the sensor zero shifted, the final zero reading was subtracted from the reading after each test.

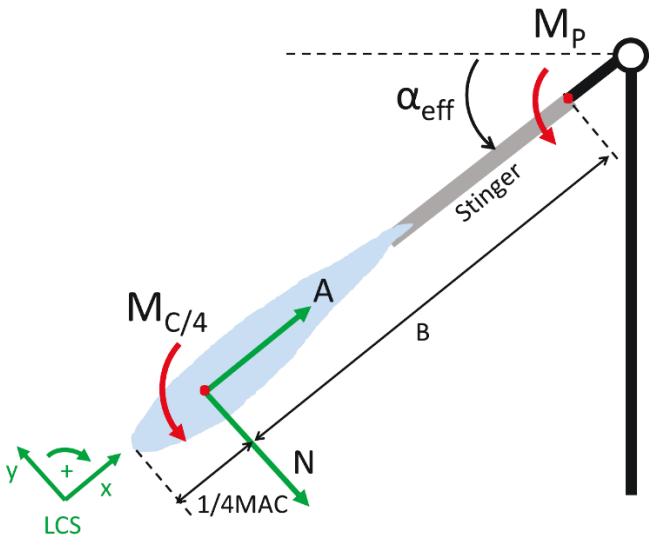

Figure 46: Wind Tunnel Force Diagram

Figure 47 illustrates the orientation of the normal and axial forces with respect to the lift and drag forces. Normal and axial forces were translated in terms of the global coordinate system (GCS) to yield lift (L) and drag (D):

$$L = N\cos\alpha_{eff} - A\sin\alpha_{eff} \qquad (23)$$

$$D = N\sin\alpha_{eff} + A\cos\alpha_{eff} \qquad (24)$$ [50, 52, 68][30]

Lift and drag were then used to calculate a resultant force magnitude:

$$R = \sqrt{L^2 + D^2} \qquad (25).$$

[30] [68] Anderson, Jr., John D. (2011). Fundamentals of Aerodynamics, 5th ed. New York, NY: McGraw-Hill.

[50] Lift coefficient atlas. Retrieved from http://baike.baidu.com/pic/%E5%8D%87%E5%8A%9B%E7%B3%BB%E6%95%B0/6221003/0/faf2b2119313b07efc8a4a630dd7912397dd8ca1?fr=newalbum#aid=0&pic=faf2b2119313b07efc8a4a630dd7912397dd8ca1.

[52] [Image] Retrieved from http://baike.baidu.com/pic/%E5%8D%87%E5%8A%9B%E7%B3%BB%E6%95%B0/6221003/0/faf2b2119313b07efc8a4a630dd7912397dd8ca1?fr=newalbum#aid=0&pic=faf2b2119313b07efc8a4a630dd7912397dd8ca1.

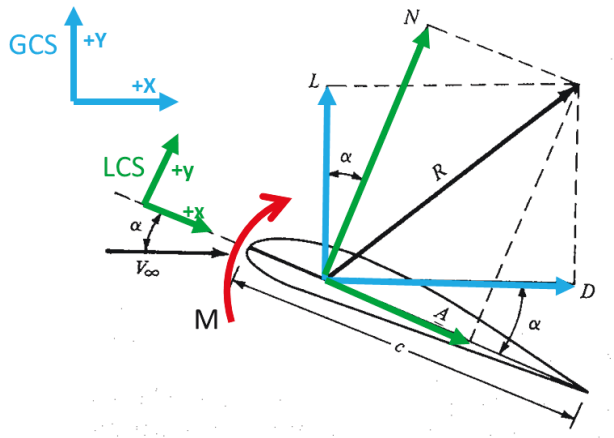

Figure 47: Free Body Diagram [adapted from 52, 68]

The pitching moment (M_P) was translated to the quarter chord moment ($M_{c/4}$) by subtracting the moment produced by the normal force on the moment arm B between the sting and the 1/4MAC (refer to Fig. 47 above).

$$M_{c/4} = M_P - BN \qquad (26)^{[68]}$$

4.5.4 Wind Tunnel Limitations

Because the wind tunnel's force sensors were designed for bigger geometries, the accuracy of results for the small wings needed to be investigated further. To better understand the readings on the sensor box, additional tests were conducted from 0 to +10 degrees. Following the same procedure as described in Section 4.5.2, readings were recorded when the wind tunnel was at full power. Full power will be referred to as "1.ON". A few seconds after hitting the "Stop" button to turn off the airflow, another set of readings was recorded at "2.DOWN". When the airflow stopped completely, the last set of readings was recorded at "3.OFF". In the Figure 48 below, each colored line represents results from one angle of attack. The normal force readings were as expected: highest at full power (1.ON), lower at power down (2.DOWN), and lowest at power off (3.OFF) (Figure 48a). The pitching moment sensor behaved similarly, but sometimes read negative values at 2.DOWN and returned to near zero at 3.OFF (Figure 48c). In contrast, the axial forces were near zero at 1.ON, became more negative at 2.DOWN and were the highest at 3.OFF (Figure 48b). Consequently, if the values at 3.OFF are subtracted, the corrected axial forces would be negative. Negative axial forces point towards the leading edge instead of the trailing edge, going against conventional results where axial forces contribute to drag. As a result, drag cannot be accurately calculated. As discussed in Section 5.1.3, the quarter chord moments were also too high for symmetric airfoils. Since normal force is the main component of lift, lift results were accurate to an extent. Therefore, lift could be used to validate the results from Javafoil and ANSYS Fluent.

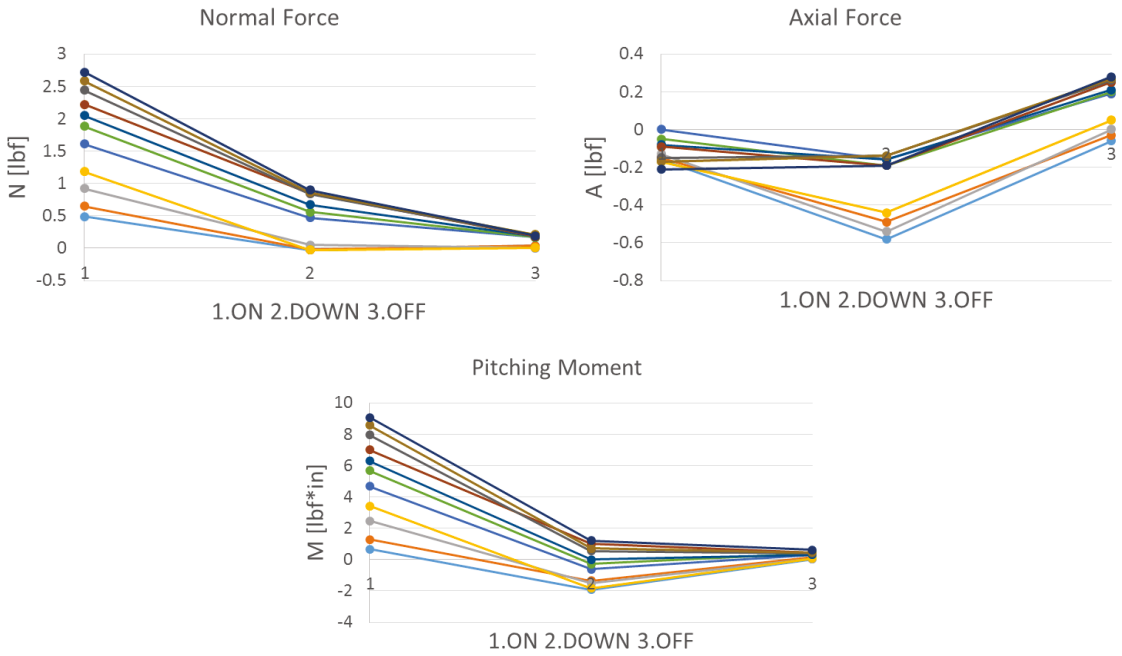

Figure 48: Sensor Behavior during Power On, Power Down and Power Off a) Normal b) Axial Force c) Pitching Moment

4.5.5 Software Simulations: Javafoil and Ansys

Experimental data collected from wind tunnel testing provided real world results for finite wings. This data was necessary to validate results from software simulations. Due to time limitations, finite wings were not modeled in simulations. Instead, 2D airfoil results were corrected for finite wings and compared to wind tunnel data. Using Lola's healthy flipper and residual limb as a guide, the prosthetic flipper was modeled in Javafoil and ANSYS. Javafoil predicts the performance of 2D airfoils at various Reynolds Numbers. ANSYS is a finite element analysis software. Specifically, the team used the FLUENT module of ANSYS for computational fluid dynamics to model testing within a wind tunnel.

Javafoil

Airfoil coordinates were retrieved from the University of Illinois Airfoil Database [45]. The tested Reynolds numbers represent both the airflow in wind tunnel testing and the water flow in prosthetic application. The input constants were similar to those used in flow matching. For example, to model the saltwater freestream that the prosthetic would experience, saltwater properties including density (ρ), kinematic viscosity (v) and speed of sound (a) were set under the "Options" tab (Figure 49 Top) [83]. The kinematic viscosity was calculated based on dynamic viscosity (μ) and density (ρ):

$$v = \frac{\mu}{\rho} \qquad (27)^{[79]31}$$

[31] [79] Absolute, Dynamic, and Kinematic Viscosity. Retrieved from http://www.engineeringtoolbox.com/dynamic-absolute-kinematic-viscosity-d_412.html.

Speed of sound was 1504.68 m/s for saltwater and 343.11 m/s for air [83, 84]. Mach number is calculated as the freestream velocity (V) divided by the speed of sound [68]. Because the highest Mach numbers (M) did not exceed 0.074, the Mach number was assumed to be zero to simplify simulations. Since the M << 0.25, the freestream was subsonic and can be treated as incompressible fluid flow. In the "Polar" tab, the first and last Reynolds Numbers were set corresponding to the freestream velocities (ex. 0.8 and 1.7 m/s) (Figure 49 Bottom). The angles of attack were 0 to 24 degrees like for wind tunnel testing. The "Surface Finish" was set to smooth finish to minimize viscous effects. The program then generates results for each Reynolds Number, starting from the first at increments set by the "Reynolds number step" (ex. Re step = 3005).

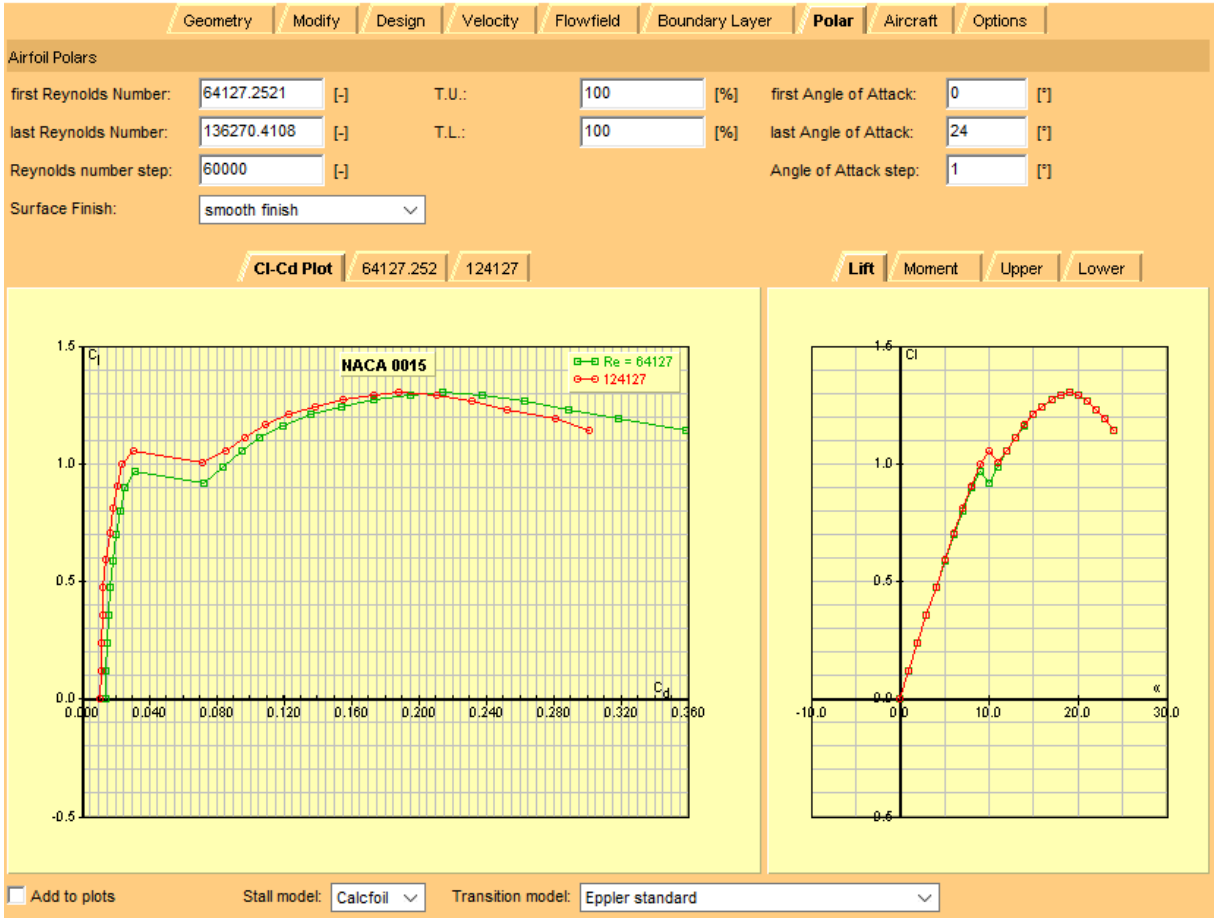

Figure 49: Javafoil Options (Top), Polar (Bottom)

Nevertheless, software limitations should be addressed. Javafoil does not predict laminar separation bubbles or flow separation. To compensate, the program uses empirical corrections to provide some estimations for coefficients after stall. The programmer acknowledges that flow separation cannot be modelled without considering the 3D dimensions of a wing such as aspect ratio, span and sweep angle. These dimensions were set to zero for 2D airfoil analysis. After the coefficients for 2D airfoils were obtained, the coefficients were corrected for finite wings and then used to calculate forces generated during the powerstroke.

2-D ANSYS FLUENT

2D airfoil simulations were ran in ANSYS FLUENT, a computational fluid dynamics program which uses finite element analysis for further verification and understanding. The flippers were modeled as stationary airfoils facing uniform, constant, and laminar flow. For flow similarity in wind tunnel testing, the freestream velocity in sea water was converted to a velocity in air. Flow matching was discussed in Section 4.4.2. Table 4 displays the properties inputted into Ansys to simulate saltwater and air at room temperature.

Table 4: Seawater and air properties

Seawater			
Property	Value	Unit	Source
Salinity	20	g/kg	[39][32]
Density	1013.4	kg/m^3	[39]
Dyn. Viscosity	1.043E-03	kg/(m*s)	[39]
Air			
Density	1.204	kg/m^3	[41]
Dyn. Viscosity	1.837E-05	kg/(m*s)	[40]

The coordinates of the NACA0015 and the Ryan BQM-34 Firebee airfoils were uploaded into FLUENT. Both airfoil geometries were finely meshed, following procedures outlined in the Cornell tutorials and additional video tutorials by Pavan Mehta for flow over an airfoil [85,86,87]. Figure 50 shows the airfoil setup a) with the reference coordinate system, b) with a zoomed in view of the fine mesh, and c) the full mesh shown in the solver.

[32] [39] Sharqawy, M. H., Lienhard V, J. H., Zubair, S.M. (2010). Thermophysical Properties of Sea Water: A Review of Existing Correlations and Data. Desalination and Water Treatment, 16, 354-380.

[40] Edwards, K. (2015). LMNO Engineering, Research, and Software, Ltd.: Gas Viscosity Calculator [Software]. Available at http://www.lmnoeng.com/Flow/GasViscosity.php.

[41] The Engineering Toolbox. (n/a). Air Density and Specific Weight [Data file]. Retrieved from http://www.engineeringtoolbox.com/air-density-specific-weight-d_600.html.

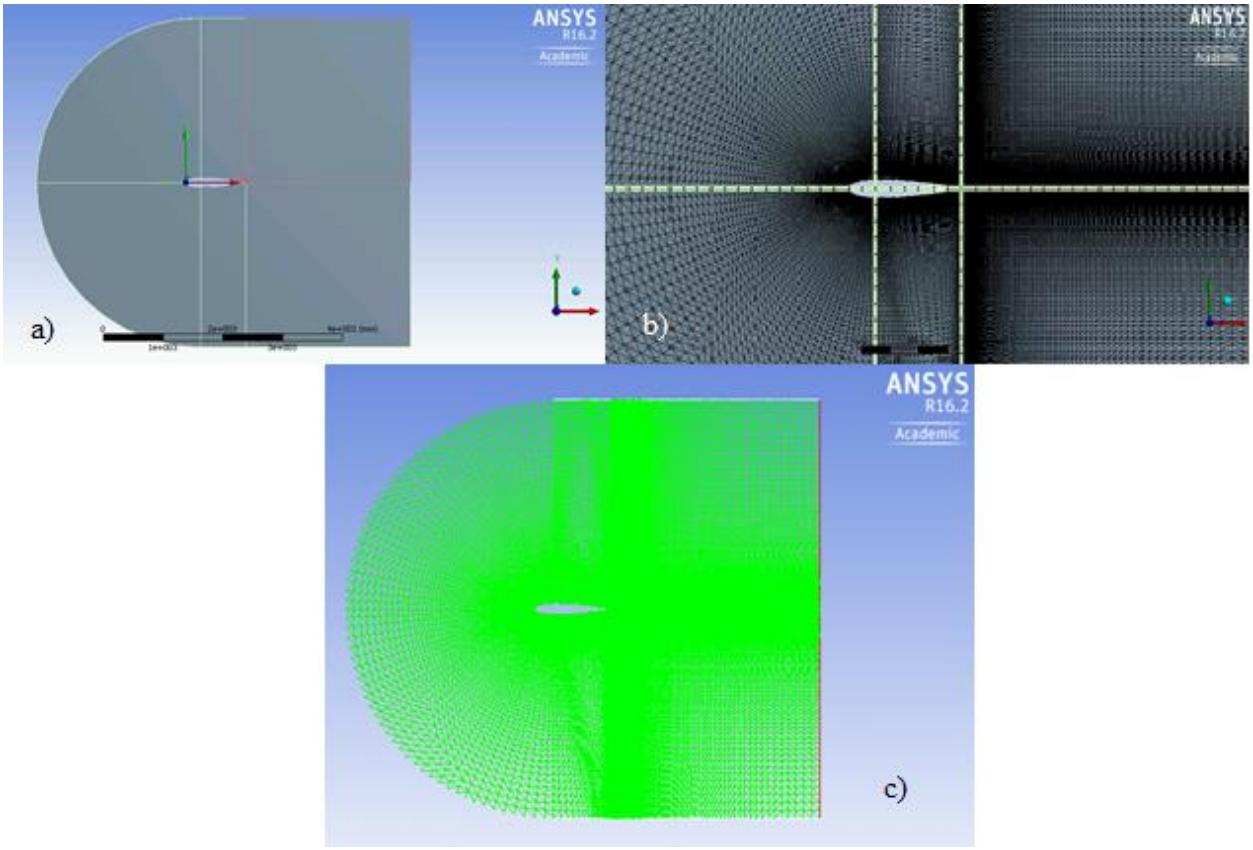

Figure 50: 2D Airfoil Geometry in ANSYS FLUENT

Following the tutorials, the flow inlet was an arc with the global and local coordinate systems set at the leading edge of the airfoil. Because the reference coordinate system was not set at the aerodynamic 1/4MAC point, the distance from the 1/4MAC to the leading edge was noted and accounted in settings for the moment coefficients. The boundaries of the mesh were set as named selections (inlet of flow, walls of enclosure, outlet, and airfoil wall) shown in Fig. 51 below.

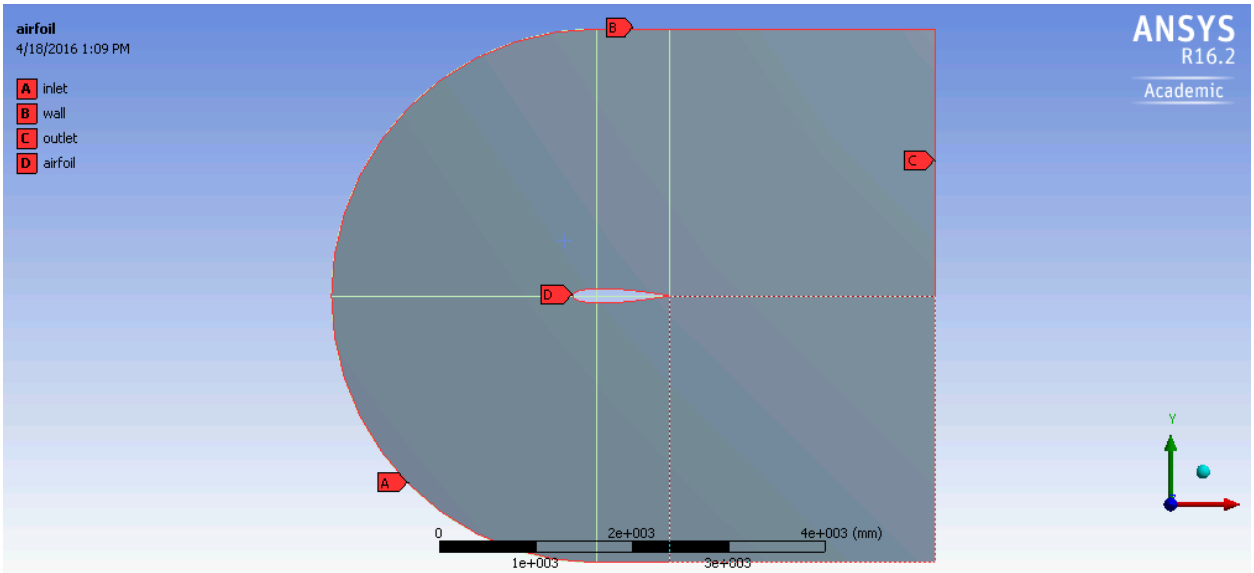

Figure 51: Setting boundary conditions

A density-based solver was used in FLUENT. The type of flow was set to inviscid. Instead of the Reynolds number, the density and dynamic viscosity of air were input as constant parameters. Unlike the wind tunnel where the airfoil could be adjusted to different angles of attack, the direction of the freestream was adjusted instead: (v_x = v*cos (AOA) and v_y = v*sin (AOA)). In addition, the directions of axial and normal forces needed to be corrected to match the conventional orientations shown in Figure 47.

With the input parameters set at the appropriate values, the next step was to conduct the simulations. Simulations at each AOA were run until the values of the lift, drag, and leading edge moment coefficients converged. For example, the coefficient of drag converged for an AOA of 0° as shown in Figure 52a. In some simulations, the solutions did not converge completely and seemed to oscillate around the correct value as observed for 13° (Figure 52b). Oscillating coefficients were averaged to settle at a single coefficient according to an acceptable procedure used in computational fluid dynamics [88].

a)

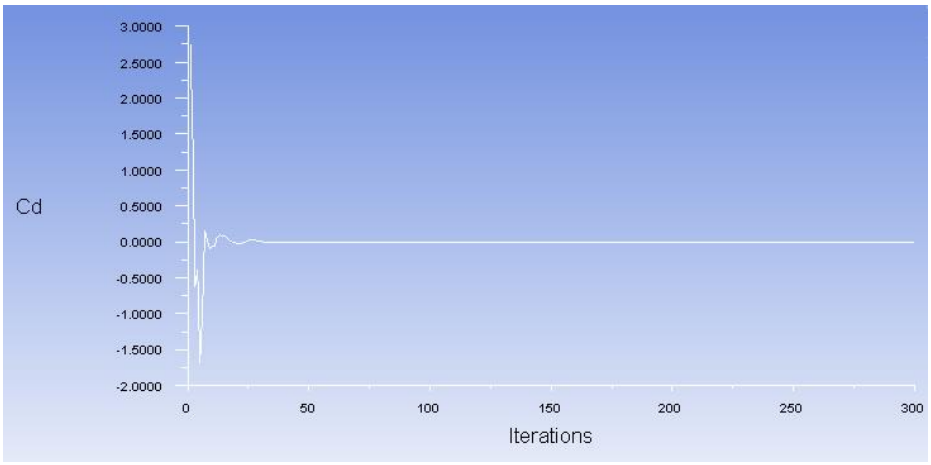

b)

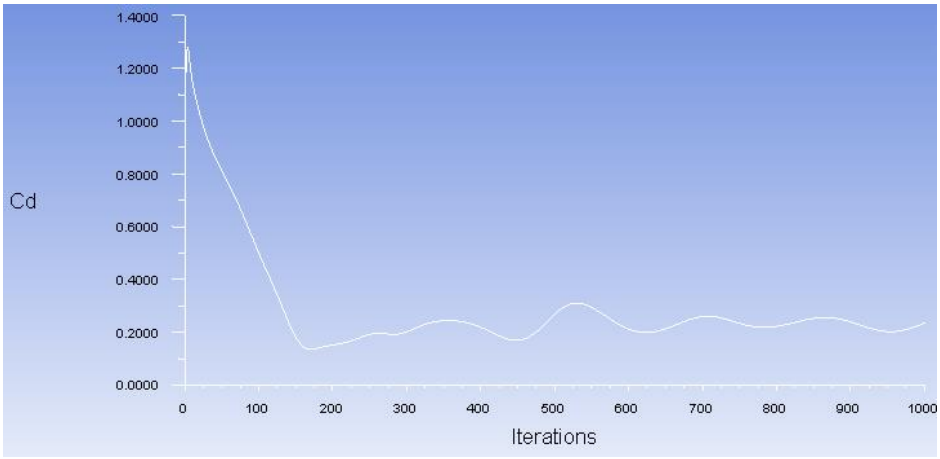

Figure 52: Coefficient convergence, a) values obtained directly b) solutions found after averaging values at a steady oscillation interval

This section discussed how the force and moment coefficients were obtained from wind tunnel testing and software simulations. Recall that software simulations yielded coefficients for 2D airfoils. In the following section, methods for correcting the 2D airfoil results for finite wings are discussed.

4.5.6 Finite Wing Correction

For finite wings, wing tip vortex effects must be considered. Air will circulate from the higher pressure on the lower surface to the lower pressure on the upper surface [90, 92]. As a result, the finite wings experience wing tip vortices and local freestreams at smaller effective angles of attack [90, 92]. Figure 53a shows a frontal view of two wings experiencing wing tip vortices. Furthermore, the lift vector is tilted, resulting in reduced lift and an induced drag as shown in Figure 53b [90, 92]. Assumptions included incompressible fluid (Mach < 0.25) and elliptical lift loading (Oswald efficiency factor, e = 1) [90], as seen in Figure 53c below. Induced angle of attack was ignored for simplicity.

a)

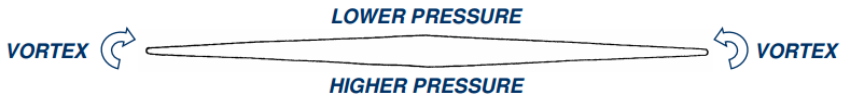

b)

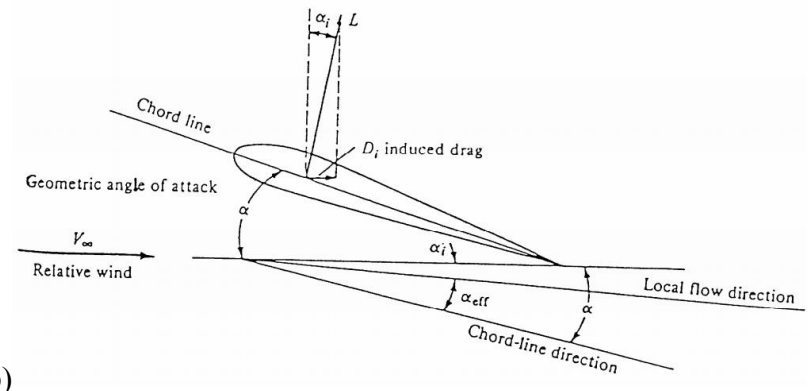

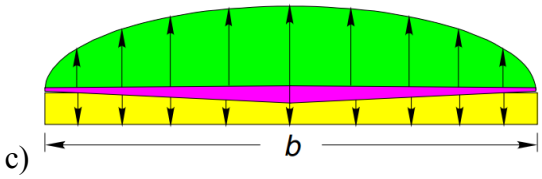

Figure 53: a) Wing tip vortices b) Induced drag and reduced angle of attack c) Elliptical lift loading [90][33]

Lift Coefficient

The airfoils' lift curve slopes (denoted by a_o) were corrected between each angle of attack (α_n) to calculate the new lift coefficient for finite wings ($C_{L\,n}$).

$$C_{L\,n} = a(\alpha_n - \alpha_{n-1}) + C_{L\,n-1} \qquad (28)^{[68]}$$

Aspect ratio is the span length squared (b^2) over the area (S). Because aspect ratios were all approximately 4, both rectangular and flipper blades were treated as high aspect ratio wings. For rectangular wings, the lift curve slope was corrected using:

$$a_{rect} = \frac{a_o}{1 + a_o/(\pi e AR)} \qquad (29)^{[72,\ 90]}$$

As described in Section 4.3.1, the flipper was simplified into a trapezoidal wing with a similar projected area (Figure 54).

[33] [90] Finite Wings. Retrieved from http://people.clarkson.edu/~pmarzocc/AE429/AE-429-4.pdf.

[68] Anderson, Jr., John D. (2011). Fundamentals of Aerodynamics, 5th ed. New York, NY: McGraw-Hill.

[72] Lift for a Finite Wing. Retrieved from http://www.srmuniv.ac.in/sites/default/files/downloads/class4-2012.pdf.

[80] Air Properties. Retrieved from http://www.engineeringtoolbox.com/air-properties-d_156.html.

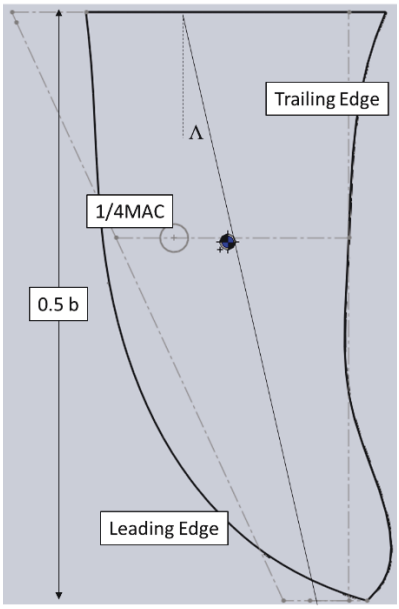

Figure 54: Simplified trapezoidal with half chord sweep angle (Λ) [80]

The leading edge sweep angle was 24.8°, the average of incremental angles along the span. Its half chord sweep angle (Λ) was 12.4°, the average between the leading edge and the trailing edge (assumed 0°). Taking into account half chord sweep angle and aspect ratio of the flipper blade, the corrected lift curve slope was calculated using:

Equation 2: Corrected lift curve slope for swept finite wing [80, 90][34]

$$a_{flip} = \frac{a_o cos\Lambda}{\sqrt{1+[(a_o cos\Lambda)/(\pi AR)]^2}+(a_o cos\Lambda)/(\pi AR)} \qquad (30).$$

In subsonic applications (Mach < 0.25), swept wings often have higher induced drag, but also stall at higher angles. However, these characteristics are advantageous for this application because the turtle rotates the flipper to 24 degrees and orients the drag vector to contribute thrust.

Drag Coefficient

Induced drag was calculated using the corrected lift coefficient:

$$C_{D,induced} = \frac{C_L^2}{\pi e AR} \qquad (31)^{[91]}$$

The total drag coefficient was the sum of the airfoil and induced drag coefficients.

$$C_D = C_{Dairfoil} + C_{D,induced} \qquad (32)^{[91]}$$

[34] [90] Finite Wings. Retrieved from http://people.clarkson.edu/~pmarzocc/AE429/AE-429-4.pdf.

[91] Spedding, G.R. and McArthur, J. (2010). Span Efficiencies of Wings at Low Reynolds Numbers. Journal of Aircraft, Vol. 47, No. 1. Retrieved from http://drydenwt.usc.edu/documents/LowReAero/SMac_JA_10.pdf.

This is the effective drag coefficient that swept finite wings generate. The corrected lift and drag coefficients were used to calculate the lift and drag forces. This section described how the flipper blades were validated in terms of aerodynamic performance. The optimal flipper blade design was chosen based on results yielded from these procedures. The flipper blade would then be integrated with the attachment module.

4.6 Attachment Design

The attachment system was designed to integrate the chosen flipper blade shape with Lola's residual limb, allowing her to move the prosthetic flipper to swim more effectively. To create alternative designs for an attachment onto Lola's limb, the team reviewed the objective tree presented in Fig 24 (Section 3.2). An attachment system would secure the flipper blade onto Lola's residual limb without harming her. The design was divided into two pieces: the residual limb cast and a fixing mechanism to adhere the flipper blade to the cast. Section 4.6.1 introduces two alternative designs for the residual limb cast. Section 4.6.2 discusses conceptual designs for fixing a fabricated flipper blade onto the residual limb cast, as well as how the SolidWorks model of the residual limb was created in order to make the cast.

4.6.1 Residual Limb Cast

The residual limb cast would go around Lola's limb comfortably, while still allowing her to move the flipper blade for thrust production. Unlike common methods for creating a prosthetic cast, the cast that would fit over Lola's residual limb was designed in SolidWorks because of lack of access to Lola. First, the team created two alternative designs for the part of the prosthetic that would serve as the protective cast on the inside of the flipper blade. Figure 55 shows a design that follows the contour of the sea turtle's residual limb. A silicone gel would be used inside the cast to make sure that the material would not be abrasive to marine amputees [110, 111, 112, 113, 114].[35] Silicone gel was used in marine animal prosthetics for comfort as well as a better adherence to the amputation site. In either of the two designs, this material would hug the patient's residual limb to reduce stresses and friction which can lead to problems and discomfort.

---

[35] [110] (2015). *Winter the Dolphin*. Hanger, Inc. Retrieved from http://www.hangerclinic.com/success-stories/winter-the-dolphin/Pages/prosthesis.aspx.

[111] (2016) *Winter.* Clearwater Marine Aquarium. Retrieved from http://www.seewinter.com/winter.

[112] n.a. (2010, Mar 12). *The 'Prosthetic Tale' of a Dolphin Tail*. WB Engineering. Retrieved from http://www.seewinter.com/web-cam-angle-3.

[113] n.a. (2007, Aug 26). *Dolphin's new tail can help human amputees*. NBC News. Retrieved from http://www.nbcnews.com/id/20415964/ns/health-health_care/t/dolphins-new-tail-can-help-human-amputees/#.VyHFzvkrLIV.

[114] Morris, Don. (2011, Oct 13). *Don Morris meets Winter, the star of Dolphin Tale*. Retrieved from http://alexanderpollard.typepad.com/the_pimento_files/2011/10/don-morris-meets-winter-the-star-of-a-dolphin-tale.html.

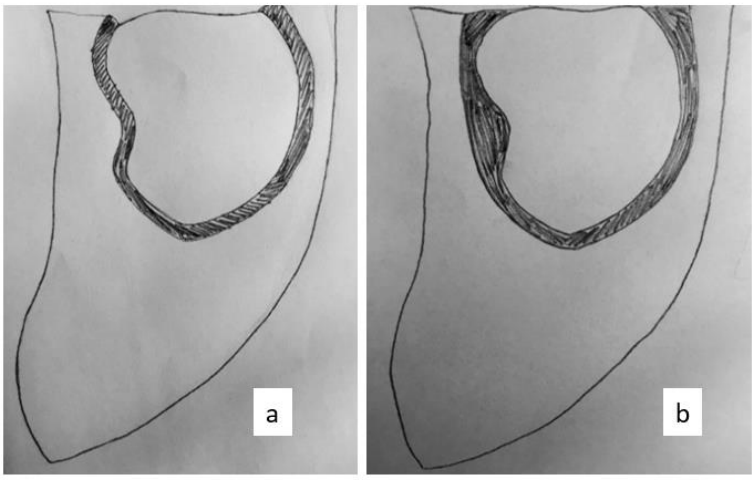

Figure 55: a) Attachment piece with limb contour b) attachment piece with simplified cavity

At the beginning, two main cast designs were considered. The design shown in Figure 55a above would give the turtle more flexibility and freedom of movement within the prosthetic. Figure 55b shows a second option that would create a more uniform, simplified shape for the liner that also completely surrounds the Lola's residual limb. The design in Figure 55b would be more durable and give the patient more support around her residual limb.

To make the cast adjustable, the internal structure of the attachment was organized into multiple layers. Lola's residual limb would first be wrapped with a silicone gel followed by a waterproof polymer canvas layer. This material is flexible and easily deformable, but also durable at the same time for long-term use and comfort. The two inner layers would be built up to a desired volume and shape to fit inside the silicone flipper. Lastly, a neoprene shell would surround the residual limb and the base of the flipper to hold the prosthetic together. This multi-layered design can be achieved with the second cast design in Figure 55b.

Fig. 56 shows pictures of human arm prosthetics manufactured by Hanger Clinic that show a design concept similar to wrapping to customize a secure fit around the contour of the residual limb as well as having an inside liner made of a silicone gel or soft plastic for added support.

Figure 56: Examples of human arm prosthetic fittings from Hanger

A third design idea was to use a thin wetsuit-like jacket to attach over her shell, as used previously in sea turtle prosthetics for Yu, the sea turtle amputee in Japan, but this could restrict movement. Lola's veterinarian advised against this design because sea turtles are not comfortable with harnesses or invasive forms of attachment. The jacket attachment for the flipper prosthetic is an alternative design, but the team will most likely use the second design with multiple layers for a cast that fastens securely around Lola's residual limb.

Figure 57 illustrates the team's multi-layered design for comfort, stability, adjustability, and reusability of the prosthetic. Layer 1, the outermost shell, would be made from neoprene, as used in Allison's wetsuit attachment [13]. Layer 2 would be a soft, waterproof canvas sheet to provide cushioning and make the prosthetic more comfortable for Lola. Layer 3, the innermost, would be made from a silicone gel.

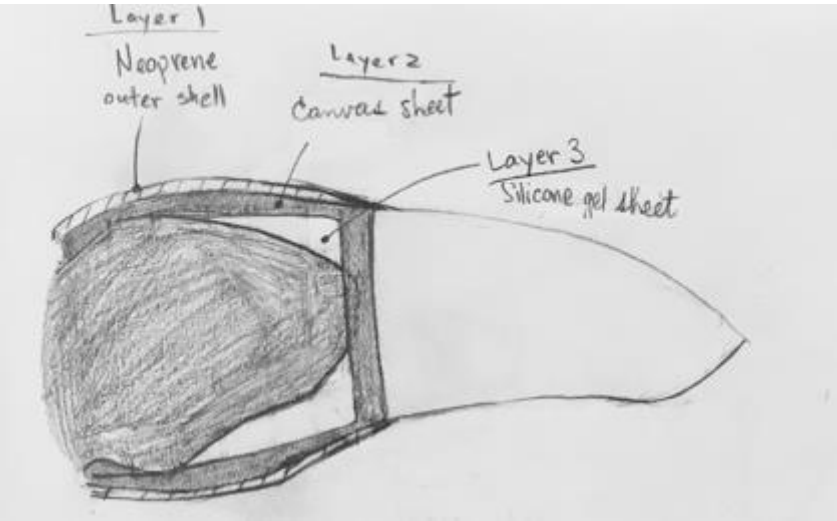

Figure 57: Protective, wrapped component

A side view of the residual limb is shown in Fig. 58. A cut would be made into the flipper blade in the shape of the residual limb using the CAD model from SolidWorks. After the turtle's residual flipper is wrapped in the cast, the layers would be sealed at the distal end it and fit inside the cavity in the silicone flipper blade.

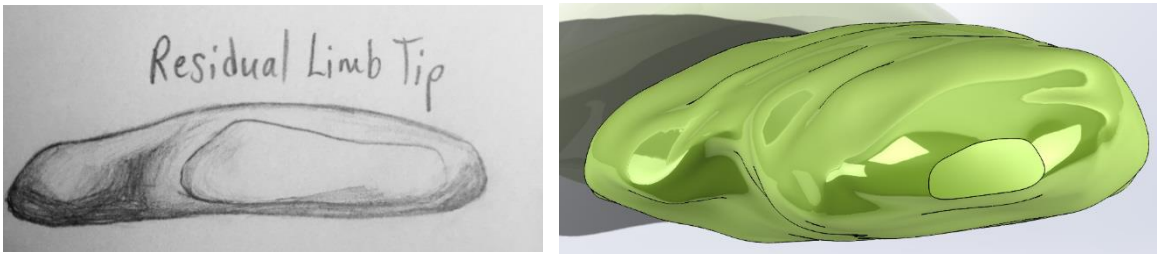

Figure 58: Transverse view of attachment piece

The model of Lola's residual limb was constructed in SolidWorks, using a clay model was as a guide. This model was used to make the cast design in the end. The compilation of pictures and x-ray images were used to make a 3D replica of the residual limb out of clay to compensate

for not having a true mold. The clay model was then cut into slices of 0.25 inch in width. The outline of each slice was traced into SolidWorks, shown in Fig. 59 and Fig. 60.

Figure 59: Clay model of Lola's amputated flipper

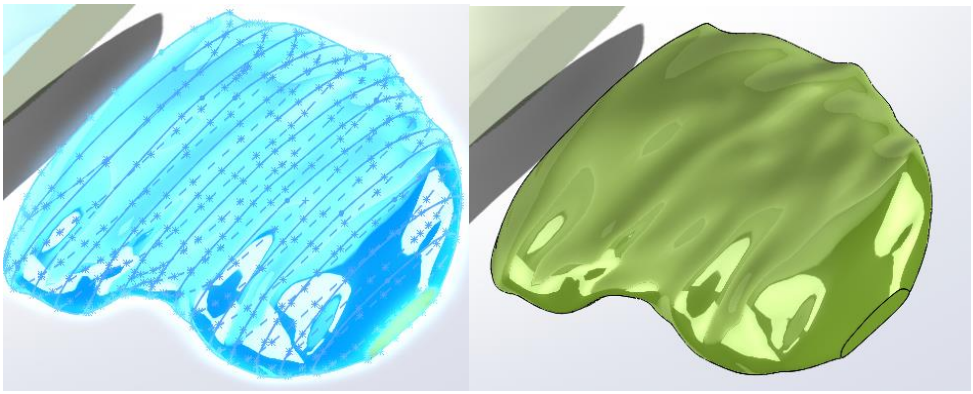

Figure 60: Side view of residual limb profiles

In this section, two attachment system alternative designs were compared. Both conceptual designs were created with Lola's comfort and safety in mind. In addition to the residual limb cast, a mechanism for fixing the final flipper blade to the cast was explored in the following section.

4.6.2 Flipper Fixing Mechanism

A fixing mechanism would integrate the flipper blade with the cast to secure around Lola's residual limb. This would allow Lola to generate forces along the prosthetic to move the flipper blade as desired. In this section, fixing designs used rivets, an integrated clip and Velcro straps are described. The first design to fix the flipper to the attachment piece used rivets. The flipper would be inserted 1.5 cm into the attachment piece and then secured into place with the rivets (Figure 61).

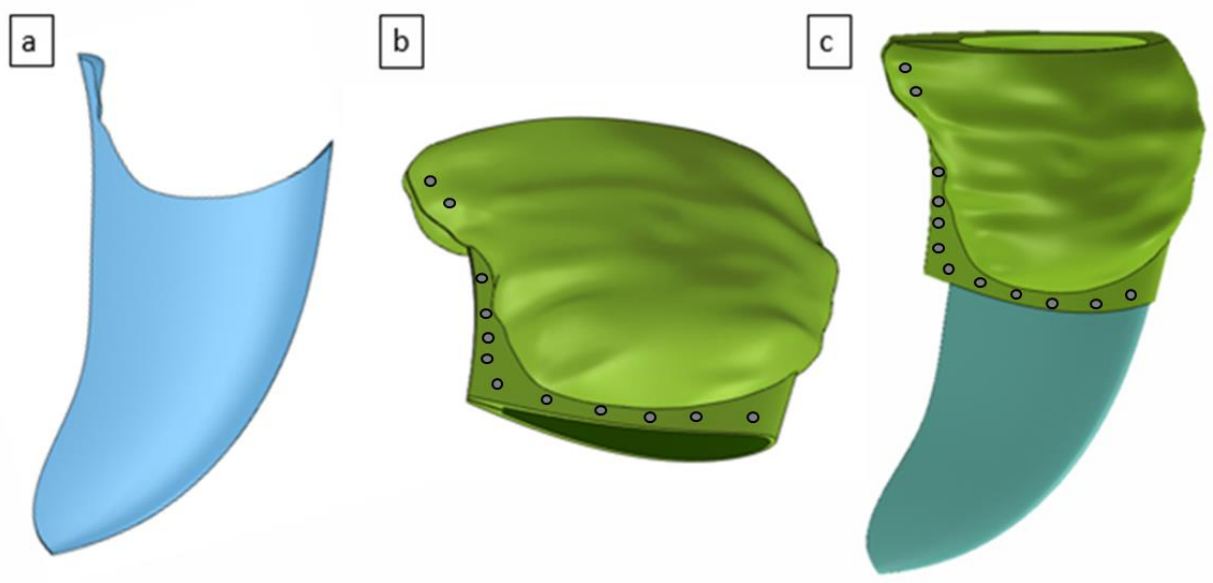

Figure 61: SolidWorks model of Lola's residual limb, individual components of prosthetic include a) Flipper blade and b) Attachment cast c) Assembly

The second design used a metal clip that fit into the silicone flipper. Figure 63 shows the clip location between the flipper blade and cast. One half of the metal clip would be integrated into the flipper blade and the other half into the cast. A similar method of locking prosthetics into place are commonly used in today's commercial prosthetics [96].

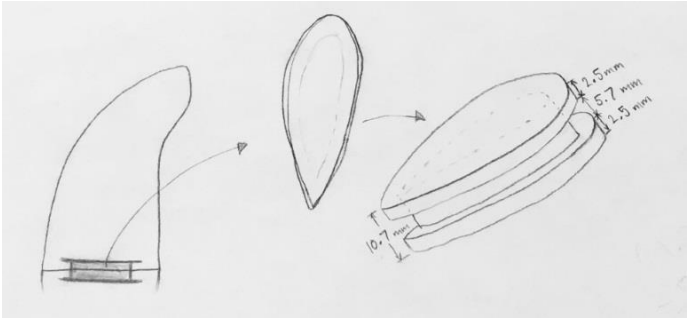

Figure 62: Metal clip

In both the two fixation designs, Velcro straps or buckles would be used around Lola's residual limb adjacent to the trailing edge of the flipper to secure the prosthetic even more. The straps and buckles could be sewn into the neoprene as shown in the Fig. 64 below.

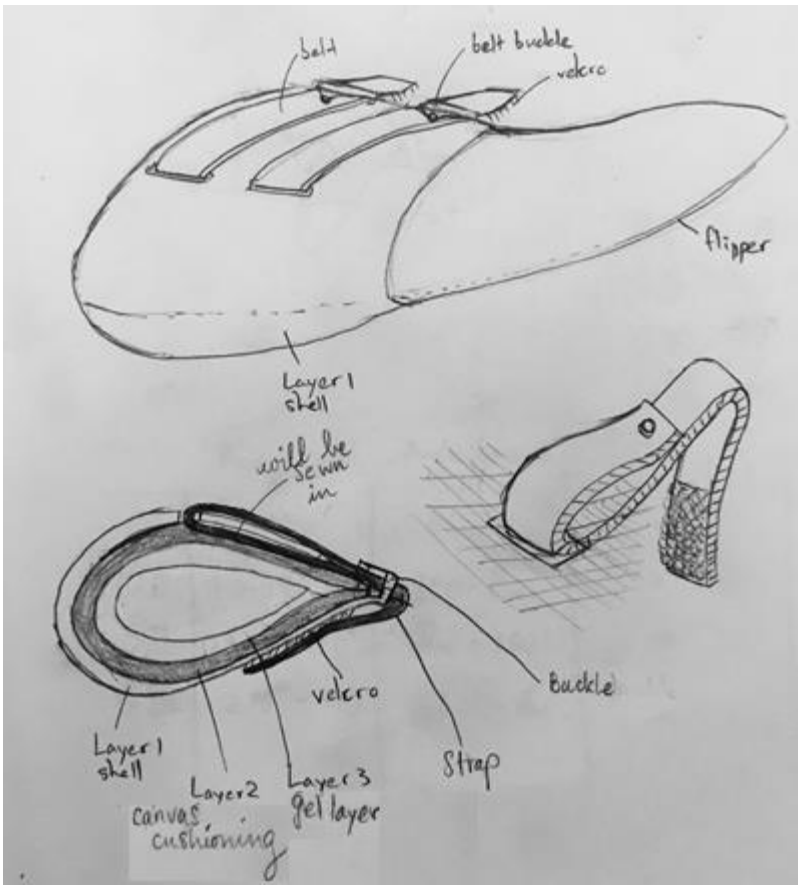

Figure 63: Attachment with Velcro straps and buckles

An attachment system integrating the flipper blade with Lola's residual limb is crucial for a functional prosthetic. Comfort, durability, and safety of Lola's residual limb were the top priorities in the design of the attachment system. Any discomfort or pain caused by the prosthetic would be detrimental. Therefore, further precautions were taken to ensure the prosthetic's safety, as seen in the following sections.

4.7 Prosthetic Predicted Effects and Safety

While the biomimetic properties of the prosthetic flipper are important, safety was one of the top priorities in the design of this prosthetic. The stress concentrations were explored to find the failure point of the prosthetic, as demonstrated in Section 4.7.1. The stress on Lola's shoulder joint and skin were explored as well. In Section 4.7.2, the loadings from the assembled prosthetic were compared with predicted loadings of a healthy flipper to determine the potential impact of stress on the patient.

4.7.1 Stress Analysis

Stresses due to loadings calculated from resultant flipper forces described in Section 4.4.4 were found to ensure the safety of using the prosthetic. Ultimately, the calculated stresses should be lower than the failure stress of the prosthetic. The stresses exerted on Lola should also be minimal for comfort. The shoulder and the residual limb tip would have the maximum stresses in the flipper (if it were modeled as a rigid beam), so those locations were analyzed first to find

normal and shear stresses. The prosthetic flipper and Lola's limb were cumulatively assumed to be a single isotropic, linear elastic cantilever beam. Normal and axial forces were applied at the 1/4MAC to estimate the mechanical effects at the proximal end of the prosthetic and at the residual limb's distal tip. The maximum stresses were caused by rotation in the +z-direction (normal force) or +y-direction (axial force). Equations 33 and 34 were used to calculate maximum normal and shear stresses. All parameters were taken from CAD models and resultant forces.

$$\sigma\_\max = \frac{-Mc}{I\_z} \qquad (33)$$ [78]36

$$\tau\_\max = \frac{V \cdot Q}{I\_z \cdot t} \qquad (34)$$

M = internal bending moment

I_z = moment of inertia about the z-axis

V = internal shear force

Q = y × A'*

t = thickness

An example of the hand calculations for stress due to normal force are explained in the following section.

Example: Stress due to Normal Force at 1/4MAC

Normal force was applied at the 1/4MAC of the flipper blade (Figure 65). Aside from the residual limb, Lola's body was treated as a wall. Cross-sectional cuts were taken at the proximal end of the prosthetic and at the residual limb tip to expose internal moments and shear forces. Normal force was found to equal shear force. The moments were calculated as the product of the force and the perpendicular distance to the cut (d).

a)

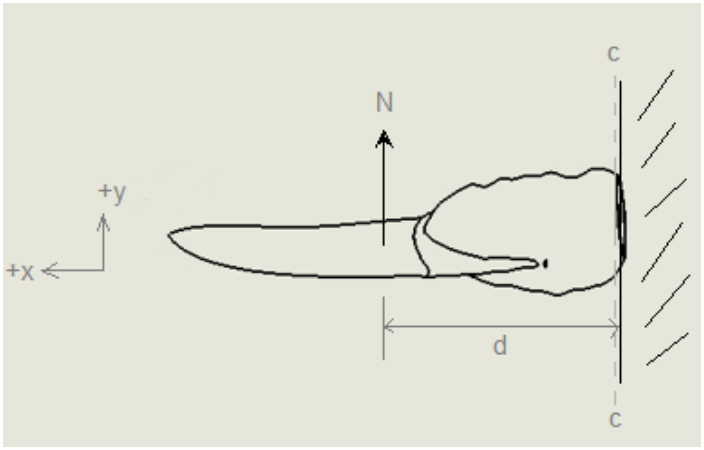

[36] [78] Hibbeler, R.C. (2014). Mechanics of Materials, 9th ed. Prentice Hall.

b)

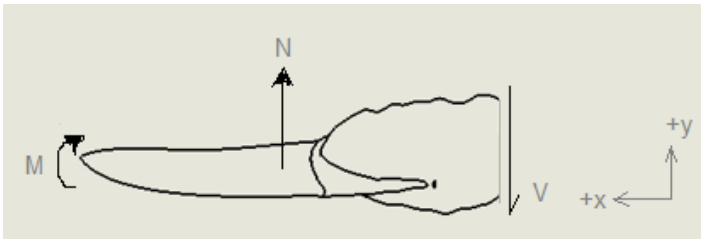

Figure 64: Example of FBD for stress analysis at shoulder a) Normal Force at Distance d b) Moment from Normal Force

Figure 66 illustrates the cross-section of the shoulder reacting to a normal force. The moment bends the flipper upwards clockwise. The parameters shown were used in stress calculations: area above neutral axis (A'), thickness (t), distance from neutral axis to the top of the area (c), and distance from the neutral axis to the centroid (y*). The top half of the model was in compression, while the bottom half was in tension.

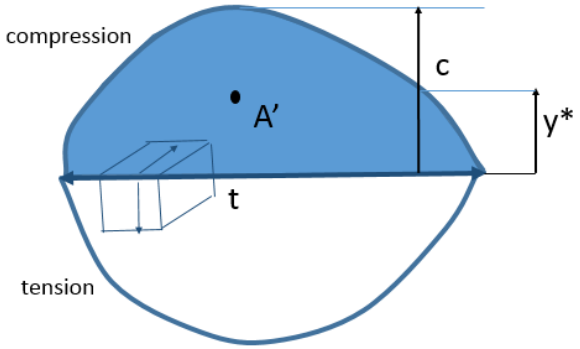

Figure 65: Cross-section of shoulder

The minimum normal stress was also found and assumed to be acting in the center of the prosthetic, modeled as a uniform, rectangular beam as shown in Fig 67.

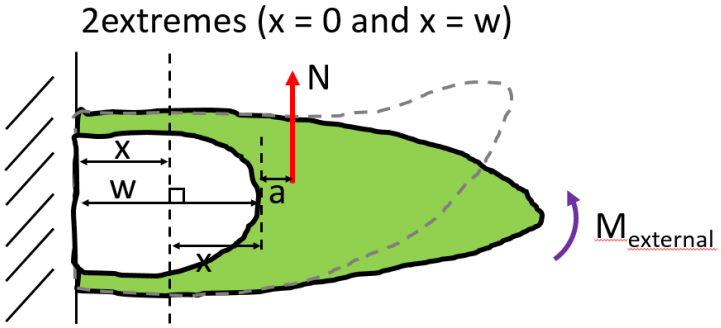

Figure 66: FBD of prosthetic to find minimum normal stress

Shear stresses were ignored for simplicity, assuming no slip inside the prosthetic, and only minimal normal stresses were calculated. The deformation of the prosthetic was dependent on its material

stiffness and external loads, so it would change as Lola moves. Because of this, stress may not be predicted accurately. Eq. 36 was used to generalize stress in the prosthetic as a function of distance from the wall.

$$M_{ext} = (\sigma(x) * x)(w - x) \qquad (35)$$

When x = 0 and x = w the flipper would deform (by changing the value of x) to "adapt" to the external loads, which would try to decrease the stress. The maximum stresses were at these locations. For this reason, it was assumed that the minimum stress would be at x = w/2.

$$M_{ext} = Applied\ Force * \left[\frac{w}{2} + a\right] \qquad (36)$$

In reality, the stresses from this simplification would be in the same order of magnitude as the derived results. The minimum normal stresses were determined using the following equations:

$$If\ x = \frac{w}{2}, then\ \sigma(x) = \sigma_{min} = \frac{M_{ext}}{\frac{w^2}{4}} = \frac{(4 * M_{ext})}{w^2} \qquad (37)$$

w = distance into the prosthetic limb

x = distance across which the stress is distributed

a = distance between tip of residual limb and applied force

Quantifying the stresses within the prosthetic due to Lola's swimming allowed for determining a safety factor of the prosthetic. To further validate the prosthetic design, the loadings at the shoulder from using a healthy limb were compared with loadings due to using the prosthetic. This comparison would allow the team to verify that Lola would be able to use the prosthetic easily to generate the forces required to swim more naturally.

4.7.2 Healthy Flipper Predictions

Predicting the loadings on Lola's shoulder from moving a healthy flipper allows for the direct comparison of loadings generated on the shoulder from using the designed flipper prosthetic. Moments generated at the shoulder from Lola's muscles moving a healthy flipper were found using indirect methodology. The moments generated on Lola's shoulder due to moving the flipper in a powerstroke were also calculated and the magnitudes compared. If Lola's muscles can produce the same loadings required for moving the prosthetic, then she would be able to use the design to swim more effectively. Understanding the torque that a sea turtle's shoulder experiences throughout the powerstroke is essential for estimating the validity of the team's flipper design. The team wanted to estimate the work that Lola would need to produce in order to use the flipper design for a normal powerstroke. Comparing the loadings within the glenohumeral joint (or shoulder) due to using the prosthetic or the healthy flipper would allow for the improvement of the prosthetic.

Finding the moments at the glenohumeral joint (GHJ) produced by the healthy flipper throughout a powerstroke cycle required some indirect methods of analysis. Currently, no literature exists for quantifying muscle forces or moments for an adult sea turtle. Because turtles and human muscle anatomy is somewhat comparable [103], the moments at the GHJ due to human muscles were first found using OpenSim software. OpenSim is a program that models the musculoskeletal system in humans, providing dependable data collected from experiments and

research [104]. Fig. 68 shows an example of the OpenSim interface, with motion controls and a skeletal model with muscles.

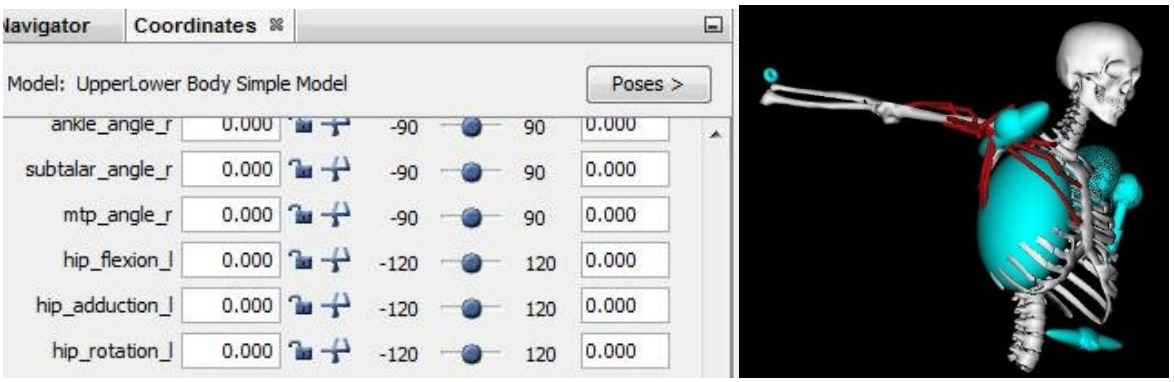

Figure 67: Example of OpenSim software interface with controls and musculoskeletal model

Only five major muscles are used in the powerstroke: the coracobrachialis (CORB), deltoids (DELT), triceps (TRI), pectoralis (PEC), and latissimus dorsi (LAT) [75]. Therefore, only the loadings on the shoulder due to these five muscle groups were explored. For further simplification, not all of the five muscles are used at the same time for a sea turtle's powerstroke, as shown in Fig. 69 (black bars). In this chart, the powerstroke began with the upstroke at 0% and ended with the downstroke at 100%.

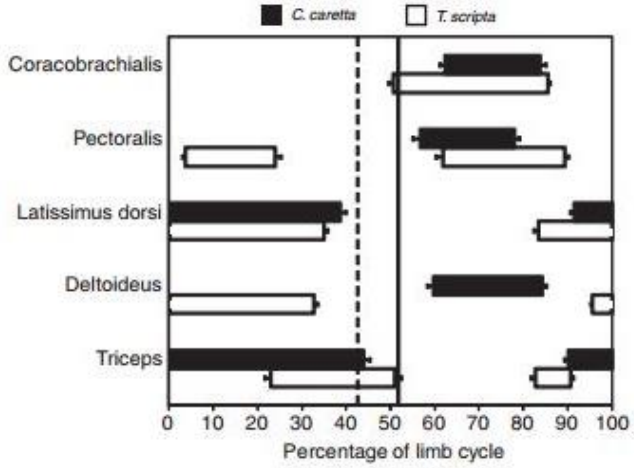

Figure 68: Sea turtle (C. caretta) muscle usage throughout powerstroke cycle [75][37]

From OpenSim, those five muscles in humans were displayed along with the corresponding bones containing the muscle insertion and origin points. The arm was assumed to be a single rigid beam (straight elbow). The muscle lines of action were assumed to be linear from origin to insertion, pulling in the direction of origin. For large fanned-out muscles, such as the latissimus dorsi, multiple lines of action were used to simulate the muscle spread. Muscle constraints existed

[37] [75] Rivera, Angela RV, Jeanette Wyneken, and Richard W. Blob. "Forelimb kinematics and motor patterns of swimming loggerhead sea turtles (Caretta caretta): are motor patterns conserved in the evolution of new locomotor strategies?." The Journal of experimental biology 214.19 (2011): 3314-3323.

only at origin and insertion points, where in reality, there are other tissues and bones that inhibit certain muscle motions. The forces that each muscle exerts were recorded for two degrees of freedom: up-to-down (superiorly-to-inferiorly) and front-to-back (anteriorly-to-posteriorly), or pitch and yaw respectively. The rotational degree of freedom was ignored (rotation within the socket) for simplification. In addition to muscle forces, the muscle fiber lengths were obtained from OpenSim as well.

Human muscle force vs. fiber length data graphs were generated for each muscle, and fiber length for Lola was found using allometric scaling of the muscle fiber force [73]. While allometric scaling of forces across species is still controversial in literature, the scaling of muscle fiber length and cross-sectional area is relatively accepted. Muscle properties are intrinsically the same across all animals. However, different animal locomotion causes muscles in different animals to develop differently, which is why direct muscle force scaling varies so much in literature. Muscle fiber length can be scaled according to body mass [73], and was done so for Lola's case. Lola's muscle force vs. fiber length graphs were found through extrapolation (maintaining the same F-L curve), and data were run through a MATLAB program to obtain forces for each muscle throughout a single powerstroke motion.

Input torque required for a healthy flipper and the prosthetic were compared to ensure that Lola could handle the prosthetic forces. This verification step would support the safety of the overall prosthetic and lend confidence that the design would allow Lola to swim more effectively than her current state.

In Chapter 4, the methodology for designing, fabricating, and validating the initial prototype flipper prosthetic for Lola was presented. Various flipper blade shapes were designed for experimental wind tunnel testing and theoretical software comparison. The flipper blade producing the best aerodynamic tendencies was fabricated in full-size using silicone. Multiple attachment systems were discussed to incorporate the flipper blade with Lola's residual limb. Finally, the strategies for finding stresses and moment comparisons were illustrated. The results and discussion of this section can be found in Chapter 5.

CHAPTER 5 – DESIGN VERIFICATION

Chapter 5 presents the results and discussion of the prosthetic design project. As mentioned previously, the prosthetic was split into two components: the flipper blade and the attachment system. Section 5.1 details the results of experimental wind tunnel testing and theoretical software comparison. The NACA0015 flipper-shape was chosen as the final flipper blade design for its advantageous aerodynamic performance and superior biomimetic qualities. A flexible silicone flipper in this shape would be incorporated into an attachment system design, discussed in Section 5.2. The customized cast encasing with soft silicone lining and rivets was chosen for the attachment piece. Section 5.3 presents results of stress analysis on multiple regions of the total assembly to ensure that the prosthetic would be safe and comfortable for Lola. Finally, Section 5.4 compares the muscle loadings at the shoulder due to a healthy flipper and the prosthetic. The conclusion of these comparisons was that Lola's muscles could easily handle the loadings needed to move the prosthetic in a powerstroke. A minor mass imbalance between Lola's healthy flipper and the prosthetic flipper was discovered, which would cause asymmetrical motion. However, the team plans on correcting this detail prior to sending the prosthetic to Lola's aquarium for live testing scheduled for Summer 2016.

5.1 Flipper Blade Results

Currently, Lola overexerts her residual limb in the attempt to accelerate forward. The flipper prosthetic is meant to improve her ability to generate thrust during level flight. Thus, overall lift and thrust forces needed to be calculated using the powerstroke model (described in Section 4.4). Results from wind tunnel testing and software were compared in order to determine the most viable force coefficients to input into the powerstroke model. In Section 5.1.1, the sensitivity of the wind tunnel force sensor was observed. Compensating for its low sensitivity, 25 m/s wind speed (1.7 m/s in water) was used to test all wings. However, this was slightly higher than the velocities calculated in the powerstroke. It was important to make sure that airfoil performance remained consistent for the higher Reynolds Number. Section 5.1.2 shows that the lift, drag and moment coefficients were consistent, justifying the laminar flow assumption. The next step was to choose the software with the most viable theoretical coefficients to simulate performance. Wind tunnel results could not be used because drag and moments were inaccurate. In Section 5.1.3, wind tunnel data were compared with results from Javafoil and Ansys. Javafoil datasets were chosen to simulate the wings' performance because they correlated with the limited wind tunnel results. The last step was to select the most advantageous wing for the turtle. Section 5.1.4 explains why rectangular wings were omitted. In Section 5.1.5, the remaining custom flippers were compared in terms of total lift and thrust throughout powerstroke. This proved that the NACA0015 flipper was advantageous over the Ryan BQM-34 Firebee flipper. Finally, the process for manufacturing the flexible silicone flipper was described in Section 5.1.6.

5.1.1 Wind Tunnel Experiment: Sting Sensitivity

In order to simulate how the flippers would perform in water, wind speeds were adjusted until the Reynolds numbers of the air and water flow matched (See Section 4.4.2). The force sensor's (the "sting") sensitivity was observed through the performance of the NACA0015 rectangular wing in wind speeds of 11.86, 14.82, 20.75, and 25.20 m/s. Table 5 lists the resultant velocities with their respective wind speeds and Reynolds numbers. At 14.8 m/s (100 cm/s in

water), lift forces were relatively unsteady as shown in Figure 70. Furthermore, the zeroes of the force sensor gradually increased. It was concluded that the results from 80 and 100 cm/s were not as accurate as results from 140 and 170 cm/s. CL from 140 cm/s were comparable to Javafoil values, but oscillated more than results from 170 cm/s. Because the 170 cm/s freestream produced more consistent CL, it was used to evaluate other wings.

Table 5: Resultant Velocity, Wind Tunnel Speed and Reynolds Numbers

80	100	140	170	[cm/s] resultant velocity
11.85957833	14.824473	20.75426208	25.201604	[m/s] WT speed
Re = 30995.356	Re = 38744	Re = 54242	Re = 65865	

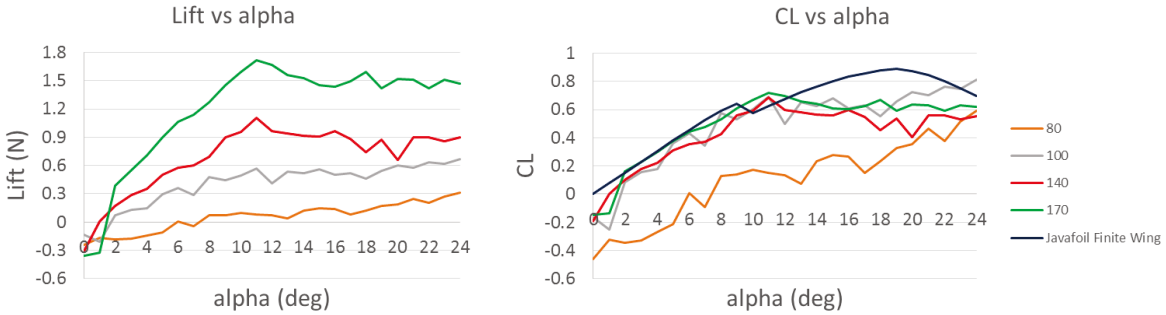

Figure 69: Experimental vs Javafoil Finite Wing: Lift force and coefficients

5.1.2 Theoretical Results

The powerstroke model described in Section 4.4 yielded maximum velocities ranging from 0.9 to 1.4 m/s in water. Because 1.7 m/s water freestream was used instead, it was important to determine if the flow remained laminar and if the aerodynamic coefficients remained consistent at the higher Reynolds number. Recall that Reynolds numbers accounts for the fluid density, dynamic viscosity, freestream velocity, and the wings' MACs. The NACA0015 and Ryan BQM-34 Firebee airfoils were compared at various Reynolds Numbers (RE) to determine the feasibility of using higher RE to predict forces. It was feasible if the coefficients from the lowest RE showed strong correlation with results from the highest RE.

Javafoil was used to evaluate the airfoils in terms of lift, drag and 1/4MAC moment coefficients (Figure 71-73). The two lower RE's corresponded to wind speeds 11.9 and 25.2 m/s that the flipper models would face in the wind tunnel (80 and 170 cm/s in water respectively). The two higher RE's corresponded to 80 and 170 cm/s water freestreams that the actual flippers would face in operation. Because all of the RE's were under 200,000, laminar flow could be assumed for further analysis.

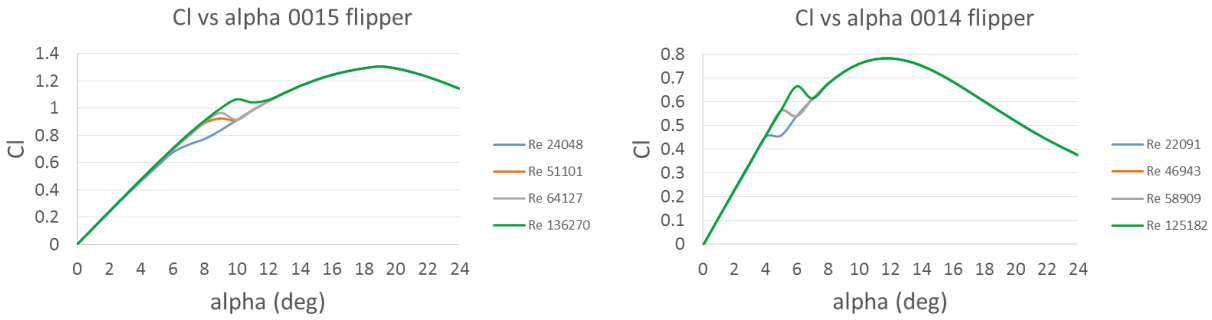

Figure 70: Coefficient of Lift a) 0015 Flipper Airfoil b) Ryan BQM-34 Firebee Flipper Airfoil

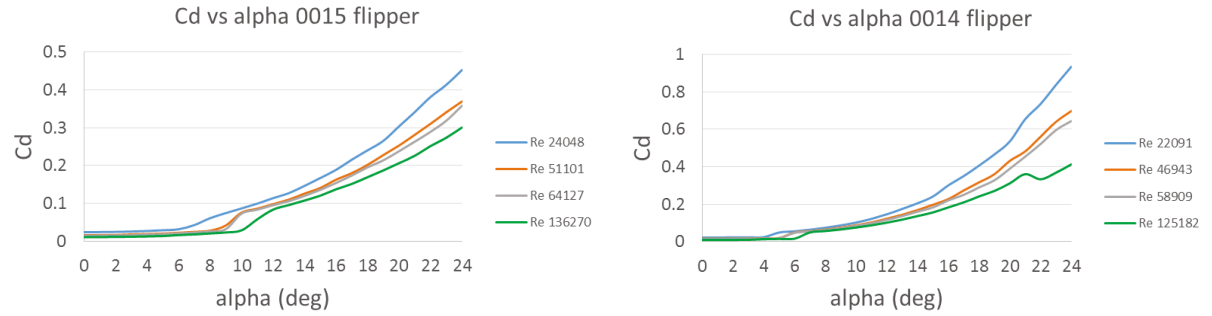

Figure 71: Coefficient of Drag a) 0015 Flipper Airfoil b) Ryan BQM-34 Firebee Flipper Airfoil

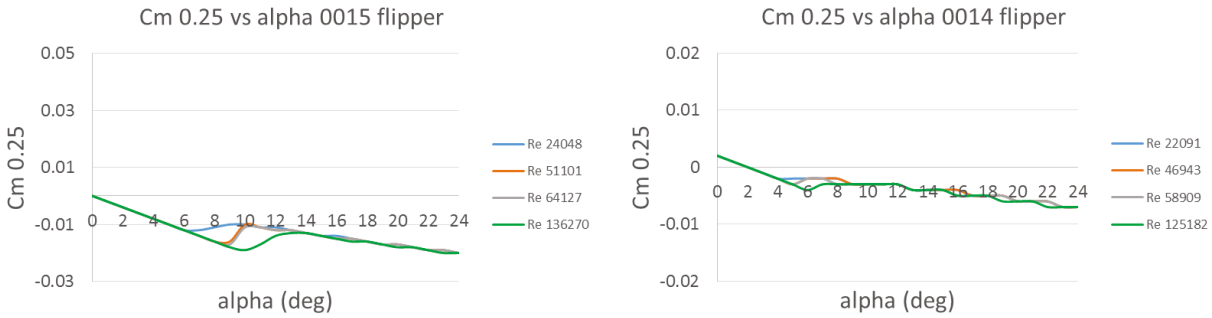

Figure 72: Coefficient of Quarter Chord Moment a) 0015 Flipper Airfoil b) Ryan BQM-34 Firebee Flipper Airfoil

Theoretical results showed that higher Reynolds Numbers produced similar coefficients of lift, drag and quarter chord moments. Figures 71a, 72a and 73a show the NACA0015 flipper's performance. Its lift performance matched closely, except for angles between 6 to 12° where the Cl deviated by values up to 0.2 (Figure 71a). The drag coefficients (Cd) were slightly higher for lower RE (up to 0.15 difference at $\alpha = 24°$) (Figure 72a). Quarter chord moments were minimal, as expected for symmetric airfoils (Figure 73a). Observations were similar for the 0015 rectangular wing. The Ryan BQM-34 Firebee flipper airfoil had comparatively lower performance than 0015. Ryan BQM-34 Firebee shared the same trends with a lower maximum lift coefficient (Clmax), but had higher drag coefficients. Like the 0015, Cl also varied around 0.15 around 4 to 7 degrees

(Figure 71b). Drag slopes were noticeably steeper, with a difference of around 0.5 at α = 24° (Figure 72b). Because the sting's sensitivity was limited and the coefficients remained similar within the range of Reynolds Numbers, it was determined that higher velocities should be used to predict airfoil performance.

5.1.3 Experimental and Software Comparisons

Lift

The NACA0015 airfoil was projected to perform better than the Ryan BQM-34 Firebee (0014) based on its higher maximum lift coefficient and stall angle. Because the rectangular wings had greater planform areas (Swing), they produced higher lift forces. However, their lift coefficients were slightly lower than flipper wings in both Javafoil and experimental results. The NACA0015 rectangular and flipper wings would generate CLmax values up to 0.889 and 0.948 respectively before stalling at 19 degrees. The Ryan BQM-34 Firebee rectangular and flipper wings were projected to produce CLmax values up to 0.546 and 0.567 respectively at 12 degrees. Figure 74 and 75 show lift curves for the rectangular and flipper wings respectively. Ansys correlated with Javafoil and the wind tunnel until flow separations at around 9 to 13 degrees. At higher stall angles, Ansys CL mostly continued to increase to unrealistic values. Since Javafoil was more consistent with the wind tunnel, it was used to predict the performance of the flipper in application. Nevertheless, the limitations of the corrected CL values from Javafoil should be noted. The Ryan BQM-34 Firebee were lower than experimental and the correction method did not increase the stall angle for the swept flippers.

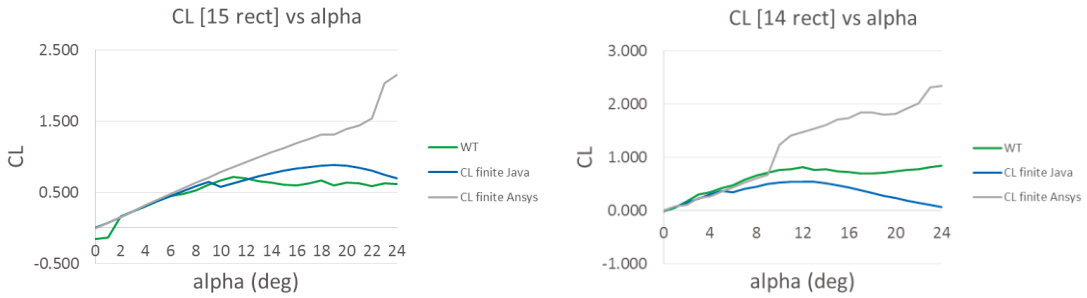

Figure 73: Finite Wing Lift Coefficients a) NACA0015 Rectangle b) Ryan BQM-34 Firebee Rectangle

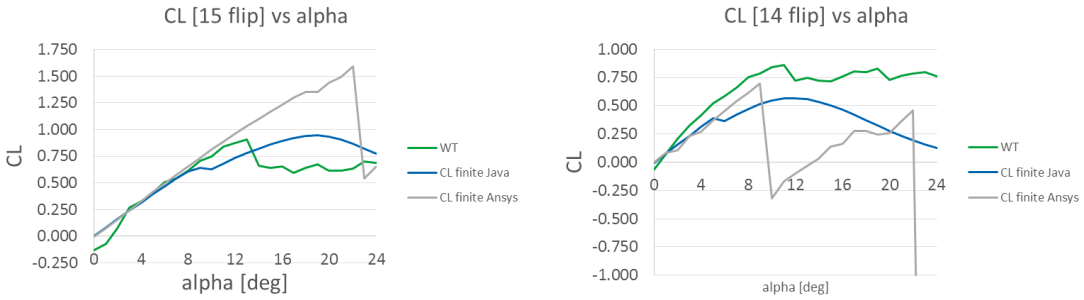

Figure 74: Finite Wing Lift Coefficients a) NACA0015 Flipper b) Ryan BQM-34 Firebee Flipper

Drag

Unfortunately, a limitation of the wind tunnel experiment was the axial force sensor's accuracy. Lift correlated well with theoretical results because it is mainly dependent on normal force, with some contribution from axial force. On the other hand, drag was inaccurate. The dominant axial force was negative because the zero value measured at low power was higher than the value measured at full wind speed as explained in Section 4.5.4. The resultant drag coefficients showed similar trends as theoretical results but at a negative offset (Figure 76 and 77). Ansys results were higher than Javafoil. Based on Javafoil results, the NACA0015 and Ryan BQM-34 Firebee flipper wings had drag coefficients (CD) of 0.394 and 0.405 at 24 degrees. The Ryan BQM-34 Firebee rectangular and flipper wings had drag coefficients (CD) of 0.662 and 0.699. Figure 76 and 77 show lift curves for the rectangular and flipper wings respectively. As predicted in literature, swept wings had higher drag coefficients.

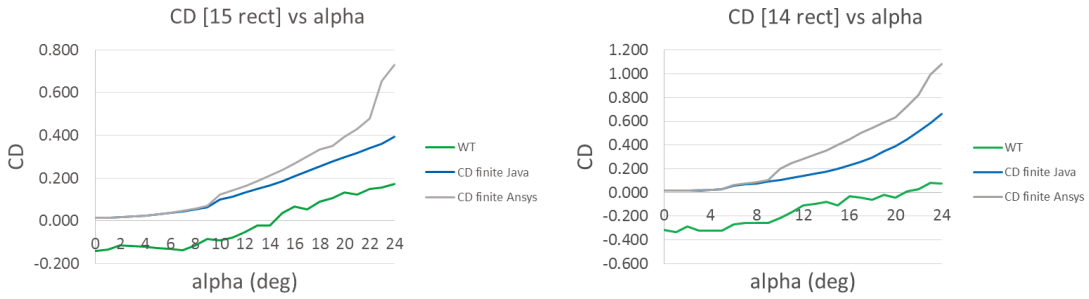

Figure 75: Finite Wing Drag Coefficients a) NACA0015 Rectangle b) Ryan BQM-34 Firebee Rectangle

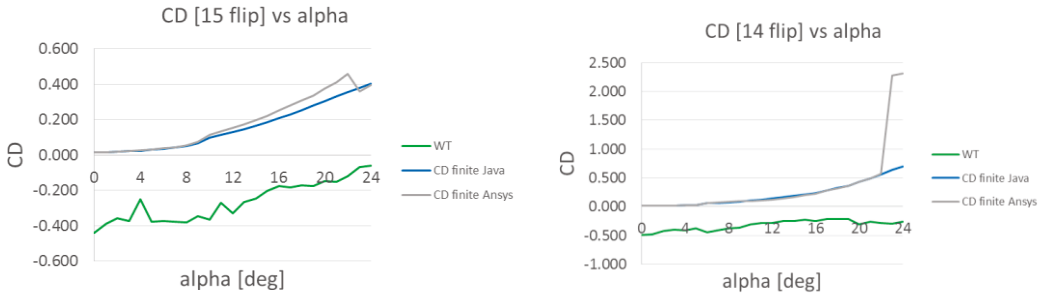

Figure 76: Finite Wing Drag Coefficients a) NACA0015 Flipper b) Ryan BQM-34 Firebee Flipper

Moments

Symmetric airfoils like NACA0015 and Ryan BQM-34 Firebee (0014) should have minimal moments at the quarter chord point, which is approximately at the center of pressure [68]. They are often used for tail fins on aircraft for stability [70]. The wind tunnel yielded high moments that fluctuated above 0.4, but remained consistent for all angles of attack. However, Ansys moments were unrealistic because they only increased with angle of attack. For the purpose of the initial design, negligible moments from Javafoil were used to simulate performance. Figure 78 and 79 show lift curves for the rectangular and flipper wings respectively.

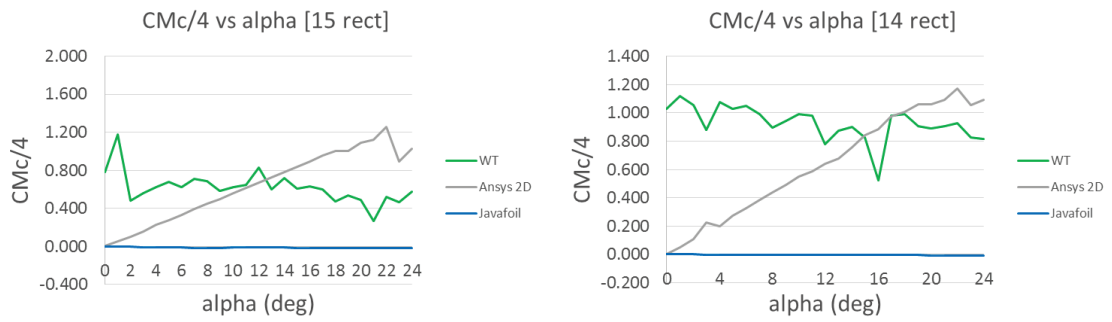

Figure 77: Finite Wing 1/4 Chord Moment Coefficients a) NACA0015 Rectangle b) Ryan BQM-34 Firebee Rectangle

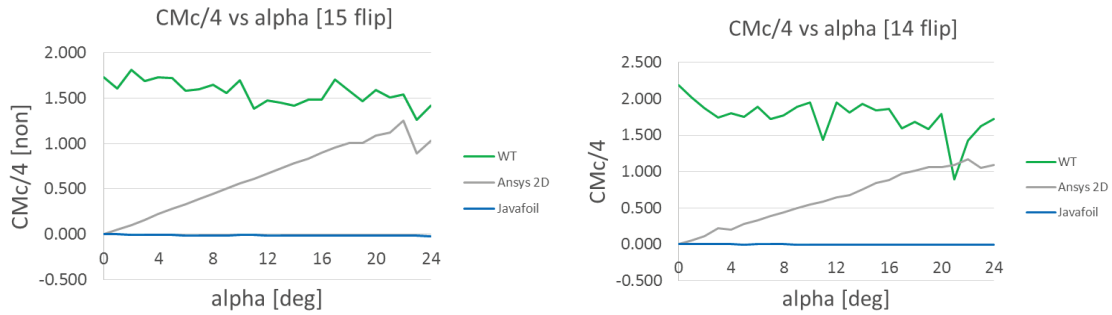

Figure 78: Finite Wing 1/4 Chord Moment Coefficients a) NACA0015 Flipper b) Ryan BQM-34 Firebee Flipper

Observed Stall Characteristics

Aerodynamic stall is a decline in lift that occurs when a critical angle of attack is reached because of a sudden disruption in laminar flow over a wing. The separation of the boundary layer from the airfoil body causes stall [89].

Wind tunnel results showed stall characteristics observed in literature. As shown in Figure 74a, the ideal 0015 wing would generate gradually decreasing CL after stalling at 19° [69]. Experimental results correlated with Javafoil and Ansys values up until 11°, where CL reached a plateau. The CL plateau might be attributed to boundary layer separation. Literature has noted separation starting at 10° for airfoils with thickness ratios higher than 14% [69, 112]. Thus, NACA0015 wings likely experienced stall starting at the trailing edge because it had a thickness ratio of t/c = 14.99% [69].

On the contrary, the Ryan BQM-34 Firebee airfoil was thinner with a thickness ratio (t/c) of 4.95% and seemed to have experienced thin airfoil stall (t/c < 6%) [69]. Javafoil results for the finite wing showed the characteristic CL discontinuity at around 5° (Figure 74b). According to literature, the phenomena correlates with the formation of the boundary layer bubble at the leading edge [69]. Theoretical results were consistent with literature, which stated that CL decreased when the boundary layer bubble detaches from the trailing edge at higher AOA [69]. McCullough and Gault observed the oscillation of CL for a double wedge airfoil (t/c = 4.23%) that was similar to that of the Ryan BQM-34 Firebee rectangular wing (Figure 74b) [70]. McCullough et al. explains

that the bubble transitions into a turbulent boundary layer with negative CL effects at the stall angle [70]. Then, the turbulence reverts to increasing the CL at higher AOA, as observed at 19° in the experimental results [70].

5.1.4 Rectangular Wing Omission

It was decided that the rectangular wings were not a feasible option for a prosthetic, but provided meaningful results that could be compared with the custom flipper. Evolutionarily, the flipper's function is to increase the turtle's mobility in water. The structure of the flipper directly influences its performance [94, 95]. Sea turtle's flippers need the ability to bend easily and maneuver through obstacles in underwater environments. The flipper shape evolved this way for ease of movement and to mitigate hindrances such as swimming through seaweed [95].

5.1.5 Lift and Thrust Values throughout Powerstroke

Lift coefficients calculated from experimental data were verified with results from Javafoil and ANSYS Fluent. Javafoil results were used to simulate the performance of each flipper blade during a powerstroke cycle. The Ryan BQM-34 Firebee and NACA0015 flippers were compared in terms of conventional lift and drag (GCS) and effective lift and thrust (TCS) to determine the most advantageous wing for the prosthetic.

The Global Coordinate System (GCS) describes resultant lift and drag forces with respect to the flipper's angle of attack and effective freestream. Lift and drag forces describe the conventional aerodynamic performance of the wing in air. During the upstroke (50 – 100% of powerstroke cycle), the wings were assumed to be at zero angle of attack ($\alpha = 0°$). The symmetric foils would ideally have minimal Cl and Cd at $\alpha = 0°$. The flippers were expected to generate the most significant lift and drag during the downstroke (0 – 50% of powerstroke cycle) because they are oriented at the peak angles of attack and face the maximum freestream velocity at mid-downstroke. Lift and drag forces generated during the powerstroke are plotted in Figure 80 below.

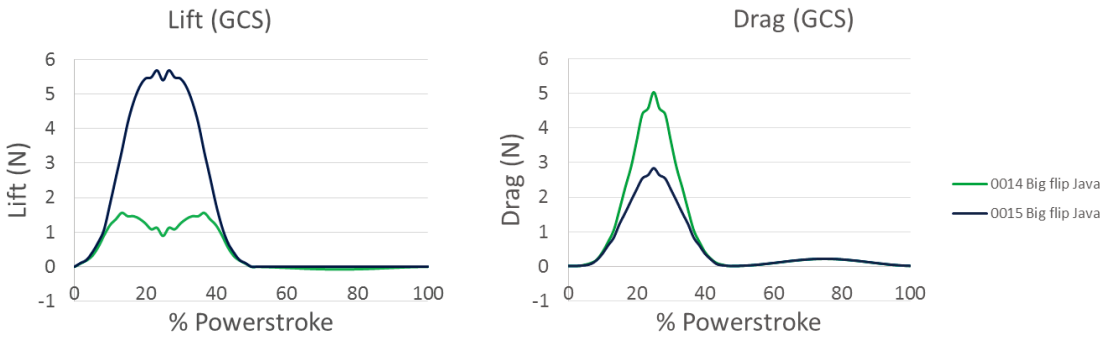

Figure 79: Lift and drag (GCS) during the powerstroke cycle

Average lift and drag values are listed in Table 6. During the downstroke, the NACA0015 flipper produced a higher average lift of 2.916 N, and lower drag of 1.043 N. In comparision, the Ryan BQM-34 Firebee produced 0.961 N of lift and 1.631 N of drag. Despite the slight variations in drag, the flipper wings both produced less drag force during the downstroke than the upstroke. During the downstroke, drag forces increased overall thrust due to the orientation of the flipper

relative to the turtle (TCS). In contrast, drag during the upstroke counteracts thrust. In terms of conventional aerodynamic performance, the NACA0015 flipper performed better than the Ryan BQM-34 Firebee.

Table 6: Average forces generated during the downstroke and upstroke

STROKE	Average Values	Lift [N] (GCS)	Drag [N] (GCS)	Lift Turtle [N] (TCS)	Thrust Turtle [N] (TCS)
DOWN	0014 Big flip	0.961	1.631	1.015	1.158
DOWN	0015 Big flip	2.916	1.043	-0.089	2.788
UP	0014 Big flip	-0.045	0.118	-0.109	-0.062
UP	0015 Big flip	0.000	0.121	-0.075	-0.093

The Turtle Coordinate System (TCS) describes effective lift and thrust forces that propel the turtle upwards and forwards. Effective lift and thrust values account for virtual mass effects from moving in water. Lift and thrust values are plotted in Figure 81 below.

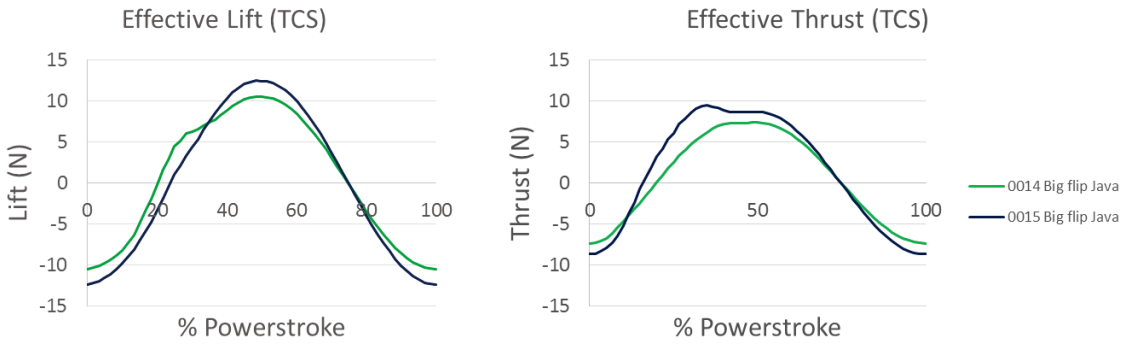

Figure 80: Effective lift and thrust (TCS) during the powerstroke cycle

Virtual mass effects were greater than the effects from lift and drag. Total lift and thrust values are presented in Table 7 below. Assuming the turtle is traveling in a level path, the flipper should produce lift close to zero. The 0015 produced average lift of -0.089 N in the downstroke and -0.075 N in the upstroke. The Ryan BQM-34 Firebee produced 1.015 N and -0.109 N respectively. To improve the efficiency of Lola's powerstroke, higher thrust would be desirable. The NACA0015 produced 2.788 N of thrust and lost 0.093 N to feathering effects during the upstroke. The Ryan BQM-34 Firebee produced 1.158 N and lost 0.062 N. Because the NACA0015 produces a lower magnitude of lift and higher thrust than the Ryan BQM-34 Firebee, the NACA0015 would be advantageous for level flight. Summing the force vectors in each direction, the NACA0015 would generate a total lift of -5.004 N and thrust of 80.741 N during each powerstroke.

Table 7: Total lift and thrust (TCS) generated during the downstroke and upstroke

TOTAL FORCE	DOWN Lift [N] (TCS)	UP Lift [N] (TCS)	TOTAL Lift [N] (TCS)	DOWN Thrust [N] (TCS)	UP Thrust [N] (TCS)	TOTAL Thrust [N] (TCS)
0014 Big flip	30.463	-3.382	27.081	34.731	-1.922	32.809
0015 Big flip	-2.674	-2.330	-5.004	83.639	-2.898	80.741

Therefore, the NACA0015 airfoil with custom planar flipper shape was chosen as the flipper blade for the prosthetic.

5.1.6 Flexible Flipper Blade Fabrication

A full-sized model of the chosen flipper blade was then fabricated using flexible silicone. The SolidWorks drawing of the flipper described previously was used to 3D print a rigid PLA (polylactide or polylactic acid) plastic model of the flipper using a fused deposition 3D printer. Due to the physical size limitations of the printer, the model was printed in two pieces and then manually assembled. A coat of XTC-3D from Reynolds Advanced Material was used to smooth the surface of the assembled flipper. Once the surface of the flipper was smoothed, the rigid model was used to make a silicone mold. To make the master flipper mold, silicone molding material was purchased from Reynolds AM in addition to Plexiglass, clay, acorns, and a releasing agent. Following the instructions provided, a mold of the 3D printed flipper was created with a unique mold key, shown in Fig. 82.

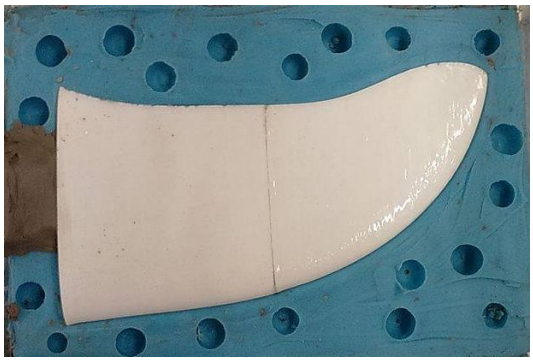

Figure 81: Silicone master mold of flipper with 3D printed part inside

Silicone bases and crosslinkers were purchased from Reynolds Advanced Materials. To cast the flexible flipper, silicone base and crosslinker were mixed according to manufacturer instructions and then degassed in a vacuum. A releasing agent was sprayed on the previously made mold. The mixture was then poured into the mold and allowed to cure overnight. An example resulting flexible flipper of Shore A Hardness 45 can be seen in Fig. 83. Refer to Appendix B for a table of Shore A Hardness values and corresponding stiffnesses.

Figure 82: Shore A Harness 45 silicone flexible flipper

As mentioned previously, a flexible flipper blade was chosen for safety reasons, as it has an enhanced ability to disperse collision energy, as opposed to a rigid flipper. The flexible flipper would be secured to the attachment module using rivets. This attachment cast was form-fitted over Lola's residual limb. Section 5.2 goes over the decisions made for the final attachment design.

5.2 Attachment Design

The multi-layered, adjustable design with rivets was chosen because it protected Lola's residual limb more effectively. This cast was form-fitted over Lola's residual limb and would be reusable to safeguard an amputee whose limb size and shape could change. Using rivets would be easier to manufacture than using a clip, and seemed like a more sensible and safer option. Section 5.2.1 describes the manufacturing process that would be followed when making the final product. Section 5.2.2 describes the reasoning for choosing the multi-layered cast over the plain cast.

5.2.1 Attachment Manufacturing

Due to time limitations, the final design would be manufactured for live testing after the project period was over. Using the CAD model of Lola's residual limb, a 3D model would be printed. The model would then be set into the flipper mold while casting it to create the inner cavity where the residual limb and layers of the cast would fit into. If the clip was used to secure the silicone flipper, then the clip would have to also be placed into the mold during casting so that it would be fused or locked into the base of the flipper. Otherwise, the rivets would be used all around the neoprene sleeve around the base of the flipper blade to fix it into place.

5.2.2 Designs Evaluation

The first alternative design, a simple cast, would require minimal effort to put on. However, this design may be more difficult to remove or more likely to fall off while swimming than the multi-layered design. The simple cast design might not fit the patient perfectly since it was made using 2D images and cannot be adjusted. It would only fit the current size of her residual limb. However, if a softer material is used, it can easily conform to Lola. Using a softer material

could also compromise durability. These reasons lead the team to choose the adjustable, multilayered cast design instead.

The second design is similar to how many prosthetic clinicians create upper extremity prosthetics for their patients, by first wrapping the limb with a durable textile material [96]. In the multilayered design, a protective canvas sheet would wrap around the thin silicone gel layer to more accurately fit around the patient's limb until the outside shape is more regular. This second cast design ultimately allows for a more customizable fit because the prosthetic attachment could be adapted upon every use as the turtle's residual limb changes in size and strength. It would fit snugly around Lola's amputation site. This design would be suitable for daily use, being more reliable and reusable. The next section details the results of stress analysis calculations and shows the safety factors which prove that the prosthetic will be very safe for Lola to use, from the standpoint of stress concentrations.

5.3 Prosthetic Stress Analysis

To identify mechanical failure, theoretical stresses were calculated based on performance simulations. Hand calculations were done to better understand all the components and develop initial results. Finite element analysis could be done in future analyses to pinpoint failure more precisely. Section 5.3.1 explains the greatest stresses that Lola's limb and the prosthetic would encounter during the main stages of the powerstroke. Section 5.3.2 shows the smallest stresses Lola's limb would experience when she wearing the prosthetic and swimming.

5.3.1 Stress at Prosthetic End and Tip of Residual Limb

Maximum normal and shear stresses at the two extremes (mentioned in Section 4.7.1) were calculated using dimensions from the CAD models of the prosthetic. From here, all the values needed to calculate the stresses were determined. The maximum normal and axial forces at three points during the powerstroke were used. The area above the neutral axis was overestimated in every case. The maximum normal and shear forces from the three forces are shown in Table 8. These stresses were compared to the ultimate tensile strength of silicone, which ranges from 2.4 to 5.5 MPa, to determine safety factors. Table 8 below shows the calculated maximum normal and shear stresses at the shoulder and the safety factor range for the prosthetic flipper, assuming silicone material. This safety range is the ratio of the UTS of silicone to the maximum stress [101]. Overall, the largest stresses Lola could experience at her shoulder ranged from approximately 3500 to 9100 Pa, with a safety factor between 90 and 1560.

Table 8: Stresses at the shoulder

	Max. Normal Force [N]	Max. Normal Stress [Pa]	Safety range		Max. Shear Stress [Pa]	Safety range	
Upstroke	10.11	6401	375	859.3	3528	680.3	1559
50%	14.4	9118	263.2	603.2	5025	477.6	1094
Downstroke	-12.42	-7862	-305.3	-699.5	-4334	-553.8	-1269
	Max. Axial Force [N]	Max. Normal Stress [Pa]	Safety range		Max. Shear Stress [Pa]	Safety range	
Upstroke	6.564	13371	149.6	374	20105	119.4	273.6
50%	-4.783	-9744	-246.3	-564.5	-14651	-163.8	-375.4
Downstroke	8.711	17745	135.2	309.9	26682	89.95	206.1

Table 9 shows the calculated maximum normal and shear stresses at the distal end of the residual limb and the safety factor range for the prosthetic flipper, again assuming silicone as the only material to simplify. In summary, the largest stresses Lola could experience at her limb's tip and that the base of the flipper blade would experience ranged from approximately 11600 to 826000 Pa, with a safety factor between 3 and 475.

Table 9: Stresses at distal end of residual limb

	Max. Normal Force [N]	Max. Normal Stress [Pa]	Safety range		Max. Shear Stress [Pa]	Safety range	
Upstroke	10.11	579694	4.14	9.488	11586	207.2	474.7
50%	14.4	825738	2.906	6.661	16503	145.4	333.3
Downstroke	-12.42	-712067	-3.37	-7.724	-14231	-168.6	-386.5

	Max. Axial Force [N]	Max. Normal Stress [Pa]	Safety range		Max. Shear Stress [Pa]	Safety range	
Upstroke	6.564	91254	21.92	54.79	18572	129.2	296.1
50%	-4.783	-66499	-36.09	-82.71	-13534	-177.3	-406.4
Downstroke	8.711	121111	19.82	45.41	24648	97.37	223.1

It is important to note that any number with a negative sign reflected the direction of a force or stress. The absolute values are the magnitudes the flipper and Lola will experience. Even the largest stresses do not exceed 1 MPa [101], and with safety factors above 2, one can be confident that the prosthetic will not cause excessive stress on Lola's limb.

5.3.2 Stresses within Residual Limb

Table 10 shows the estimated minimal average normal stresses Lola's limb would experience.

Table 10: Minimum normal stresses

	Force [N]	M_{ext} [N·m]	Min. σ [Pa]
Max. Normal (Upstroke)	10.11	1.402	520.8
Max. Normal (50 %)	14.4	1.997	741.8
Max. Normal (Downstroke)	-12.42	-1.722	-639.7
Max. Axial (Upstroke)	6.564	0.91	338.1
Max. Axial (50 %)	-4.783	-0.6632	-246.4
Max. Axial (Downstroke)	8.711	1.208	448.7

The magnitudes of all the stress results were much lower than the ultimate yield stress of silicone, so the prosthetic was deemed safe for patient use. Lola's limb, which has a Young's modulus of approximately 60,000 Pa (average estimated for comparison, but soft tissues do not have a real E), assuming human and sea turtle anatomy are comparable, would easily be able to handle the maximum stresses [97,98]. The following section describes how the muscle moments were calculated to ensure that Lola would be able to easily produce the same forces to move the prosthetic.

5.4 Muscle Loadings at Shoulder

Shoulder loadings due to the prosthetic and loadings due to a healthy flipper were compared to verify Lola's capability of using the developed prosthetic. If shoulder moment magnitudes for moving a flipper statically (not accounting for momentum) were much higher than the calculated prosthetic moments, then Lola would be able to handle the prosthetic with ease. Because there is no muscle loading data in literature for sea turtles, the moments were found using an indirect method. In Sections 5.4.1 and 5.4.2, human muscle values were obtained from OpenSim and scaled to reflect Lola's muscle values. Section 5.4.3 uses MATLAB to compile a database of muscle forces throughout the powerstroke motion. The moments due to Lola's predicted muscle forces were calculated in Section 5.4.4 and compared qualitatively to moments calculated using thrust and lift values found previously from Section 5.1.5. An imbalance between the healthy flipper mass and prosthetic mass was found in Section 5.4.5, which can easily be fixed prior to sending the prosthetic for live testing.

5.4.1 Obtaining Human Powerstroke Data

Finding Lola's muscle data required first finding human forces. OpenSim was run to obtain graphs of the forces due to the muscles moving the arm statically with respect to angle for each muscle. Specifically, the pitch data was collected from 0° to 180° (arm straight down as 0° and straight up as 180°), and yaw data was collected from -90° to 90° (straight back to straight forward). Fig. 84 shows the muscle force in Newtons versus the angle for pitch axis. The yaw axis data can be found in the Appendix D.

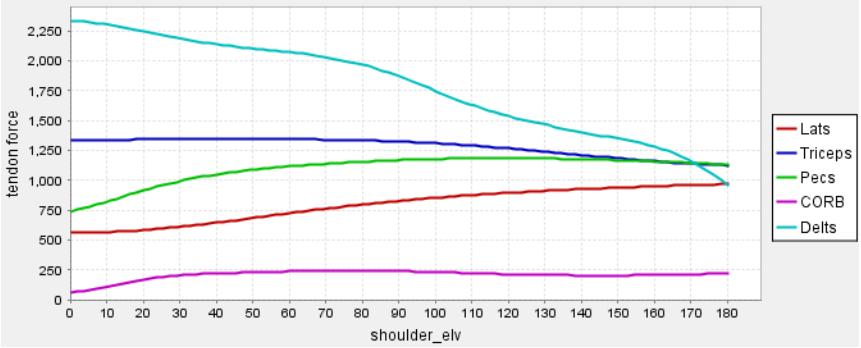

Figure 83: Muscle force (N) vs. angle for selected muscles in pitch axis

DataThief extracted the graph data from OpenSim in numerical matrix form. Pitch and yaw was taken as orthogonal data. A database was created consisting of forces from the yaw and pitch axes (with degrees being the independent variable). These data allowed for the theoretical calculation of the muscle forces for any pitch-and-yaw position combination. Similar to the collection of human muscle force data, the muscle lengths and moment arms for each muscle were obtained for both axes. Fig. 85 shows the muscle fiber lengths in meters with respect to angle for the pitch axis. Yaw axis data can be found in the Appendix D.

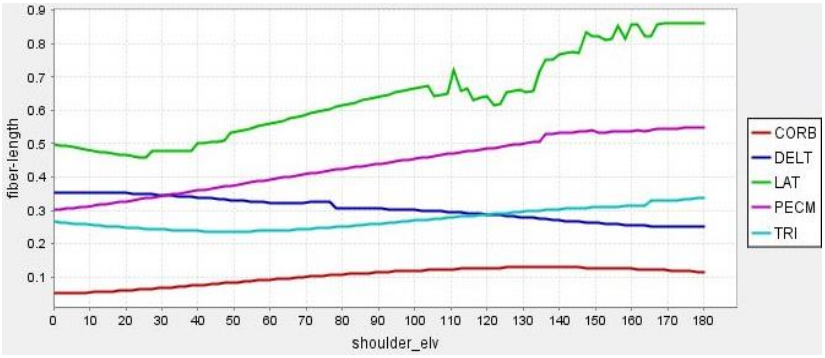

Figure 84: Fiber length (m) vs. angle for selected muscles in pitch axis

Once the muscle forces and fiber lengths were acquired for human data, they were scaled to Lola's body mass to reflect her predicted force values. This would allow for analysis of healthy flipper loadings at the shoulder to compare with loadings due to the prosthetic.

5.4.2 Allometric Scaling

Allometric scaling was used to estimate Lola's muscle data from experimental human values obtained from OpenSim. Direct conversion of forces is debated in literature, as different animals have different forms of locomotion [76]. For example, it is frowned upon to scale human bicep forces to mouse bicep forces directly based on body mass, because mice use all four limbs to move (load bearing) while human biceps are not necessarily loaded as often. However, it has been shown that muscle fiber length can be scaled across species depending on body mass [74]. From the data collected in OpenSim, the muscle force vs. fiber length graphs of each muscle was obtained by plotting in Excel. The force-length curve of a muscle can generally be used as a means of characterization [73]. Fig. 86 shows the experimentally obtained force vs. length graph for a human coracobrachialis in the yaw axis, as well as a generic force-length curve found in literature.

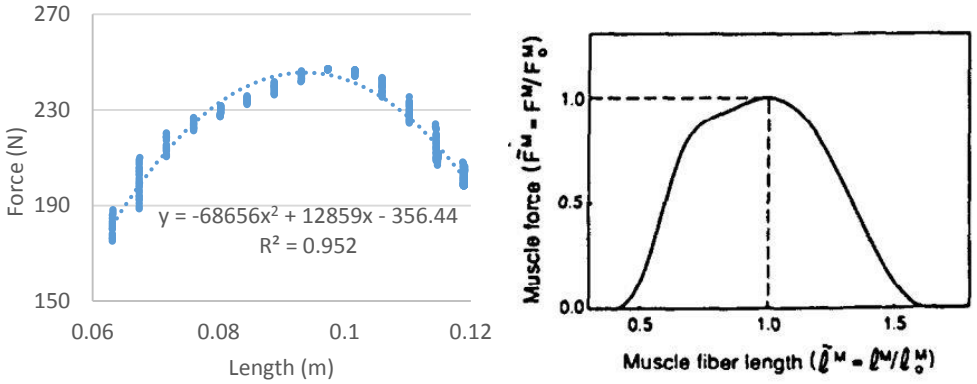

Figure 85: a) Force-length curve of human coracobrachialis in yaw direction b) Example of F-L curve in literature [73][38]

[38] [73] Hoy, Melissa G., Felix E. Zajac, and Michael E. Gordon. "A musculoskeletal model of the human lower extremity: the effect of muscle, tendon, and moment arm on the moment-angle relationship of musculotendon actuators at the hip, knee, and ankle." Journal of biomechanics 23.2 (1990): 157-169.

After the experimental F-L curves for each muscle were obtained in the pitch and yaw axes, the length data were scaled to fit the turtle's body mass. Fig. 87 shows the scaling log plot used for scaling human fiber length data to Lola's predicted fiber length data. Lola's predicted muscle forces were extrapolated to maintain the same F-L muscle curves, also shown in Fig. 87.
The equation for extrapolation can be found in Eq. 38.

$$\frac{L_H}{L_T} = \frac{F_H}{F_T} \qquad (38)$$

where L_H is human muscle fiber length, L_T is turtle muscle fiber length, F_H is human muscle force, and F_T is turtle muscle force.

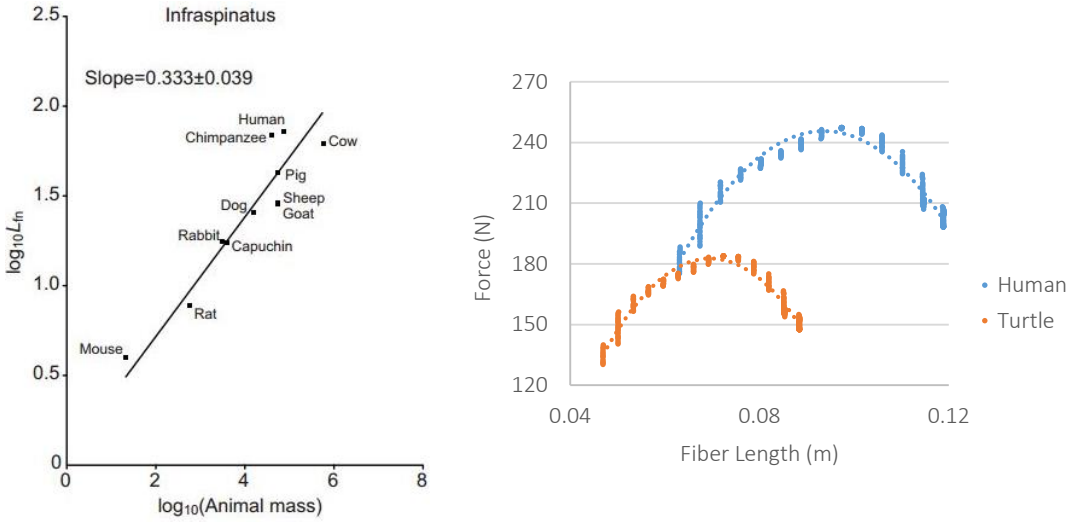

Figure 86: Allometric scaling. a) Scaling of muscle fiber length across species based on mass [74][39] b) Coracobrachialis force-fiber length curves for human data and extrapolated turtle data

The predicted muscle F-L curves for each of Lola's muscles were obtained for the pitch and yaw axis. Lola's muscle forces were then obtained for each degree in pitch and in yaw from the curves. These predicted forces were compiled into a database to automatically calculate Lola's force magnitude throughout the powerstroke, which can be used to find moments at the shoulder.

5.4.3 Powerstroke Loadings Using MATLAB

The forces taken from Section 5.4.2 were compiled into a database. MATLAB was used to create a function that called on the forces at the yaw and pitch axes for an input arm location for the range of an arm (assuming max movement is 0° to 180° in pitch and -90° to 90° in yaw). The force and angle data was input into MATLAB to form a database for each of the five muscles (corb, deltoids, triceps, lats, pecs). The datasets were then normalized to a unit circle consisting of a pitch axis (0° to 180°) and a yaw axis (-90° to 90°), as demonstrated in Fig. 88. The circle

[39] [74] Mathewson, Margie A., et al. "Comparison of rotator cuff muscle architecture between humans and other selected vertebrate species." Journal of Experimental Biology 217.2 (2014): 261-273.

represented the path that the turtle's flipper would trace as it performed the powerstroke. This circular path is a simplification of the turtle's actual coupler curve, and assumed a rigid beam with two degrees of freedom instead of a flexible flipper with many DOF, shown in Fig. 88 (adapted from Fig. 14 from [22]). The MATLAB code can be found in Appendix C.

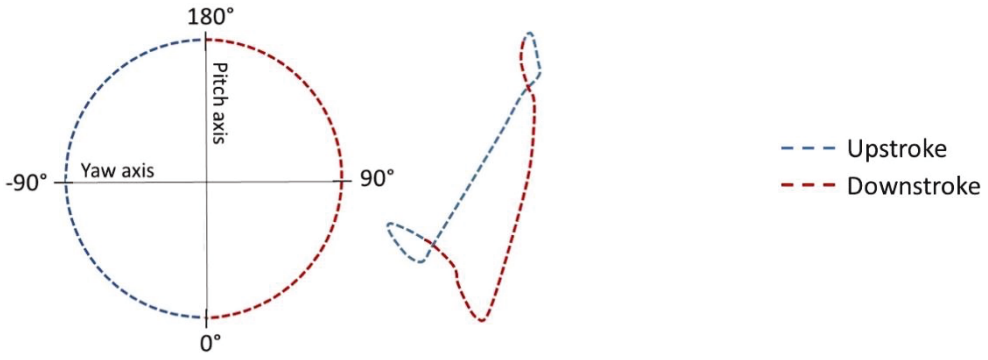

Figure 87: Simplified powerstroke coupler curve with labeled pitch and yaw axes (left) and actual powerstroke coupler curve (right) [22][40]

The MATLAB program provided the force magnitude generated by the muscle at any user-specified point within the coordinate system. This was done assuming that the pitch and yaw axes were orthogonal, and that the force magnitude can be obtained by summing the pitch and yaw vectors with Eq. 39.

$$|F| = \sqrt{{F_P}^2 + {F_Y}^2} \qquad (39)$$

where |F| is the magnitude of the resultant muscle force, F_P is the force in the pitch direction, and F_Y is the force in the yaw direction.

The code automatically calculated and produced a matrix of resultant values throughout a single powerstroke cycle, assuming the coupler curve is a circle. The user defines the muscle and arm angle φ, shown in Fig. 89.

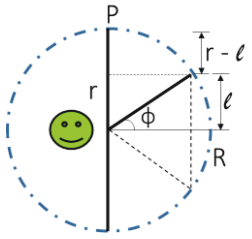

Figure 88: Schematic of spatial hemisphere and arm locations

The angle, φ, dictated the specific path that the coupler curve traced along the hemisphere of all possible points. The spatial hemisphere was dictated by the pitch and yaw axes and the arm bar

[40] [22] Davenport, J., Munks, S. A., Oxford, P. J. (1984). A comparison of the swimming of marine and freshwater turtles. Proceedings of the Royal Society of London B: Biological Sciences 220 (1221): 447-475.

with a length R. The analysis for this project used an amplitude to radius ratio of 0.7 for a rough estimate. Therefore, the force magnitudes generated by each muscle throughout the powerstroke can be found, as seen in Fig. 90. In Fig. 90, the powerstroke began at the beginning of the downstroke (0% of powerstroke cycle), and ended at the end of the upstroke (100% of the powerstroke). Around 50% of the cycle was when the downstroke stopped and upstroke began. Graphs were plotted in Excel.

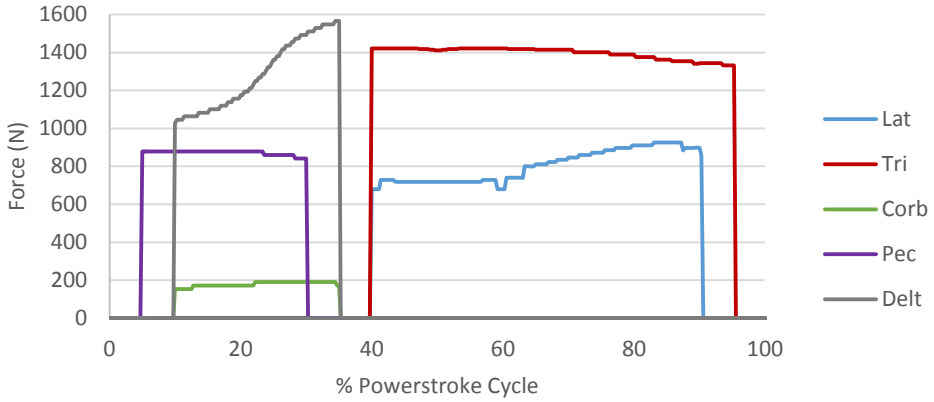

Figure 89: Predicted healthy muscle forces for Lola throughout the powerstroke cycle

Once Lola's predicted force magnitudes throughout the powerstroke were found, the moments at the shoulder due to using a healthy flipper can be calculated. The moments can then be compared with moments exerted on the shoulder due to using the prosthetic in the same simplified powerstroke motion. This analysis would indicate whether Lola could generate the appropriate forces required to use the prosthetic without straining herself.

5.4.4 Shoulder Moment Comparison

This section compares Lola's shoulder moments due to using her healthy flipper and using the prosthetic flipper. The moment arms for each muscle were obtained from OpenSim for human muscle data. The moment arm (perpendicular distance from the line of action to the shoulder) was assumed to be approximately the same across species. The average moment arm for each muscle was found, and multiplied to each muscle force throughout the powerstroke cycle. The average moment arm magnitude for each muscle can be seen in Table 11.

Table 11: Selected muscles with average moment arm length

Muscle	Moment Arm (m)
Coracobrachialis	0.020
Deltoids	0.031
Latissimus dorsi	0.072
Pectoralis	0.044
Triceps	0.013

The moment arms were then multiplied by the forces throughout each point of the powerstroke to obtain the moment magnitude throughout the powerstroke cycle, as seen in Fig. 91.

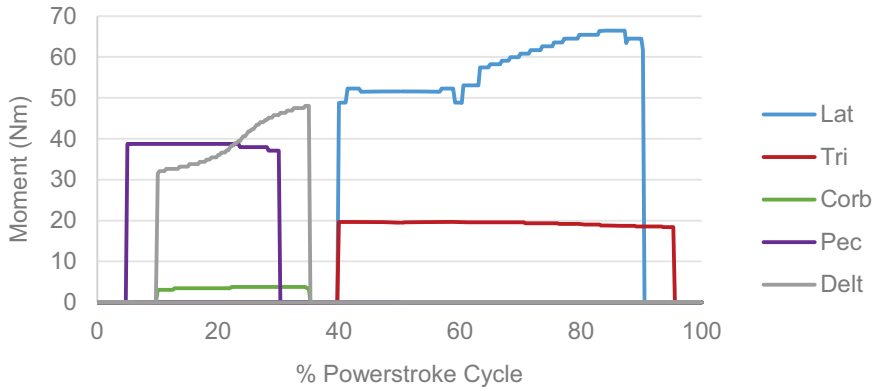

Figure 90: Predicted healthy muscle moments at GHJ for Lola throughout the powerstroke cycle

For comparison, the moments at the GHJ due to Lola's prosthetic were found. In order to use the prosthetic flipper, Lola would need to apply a moment to move her residual limb about her shoulder joint. The moment produces lift and thrust vectors on 1/4MAC at a length *l* from the shoulder joint (Figure 92).

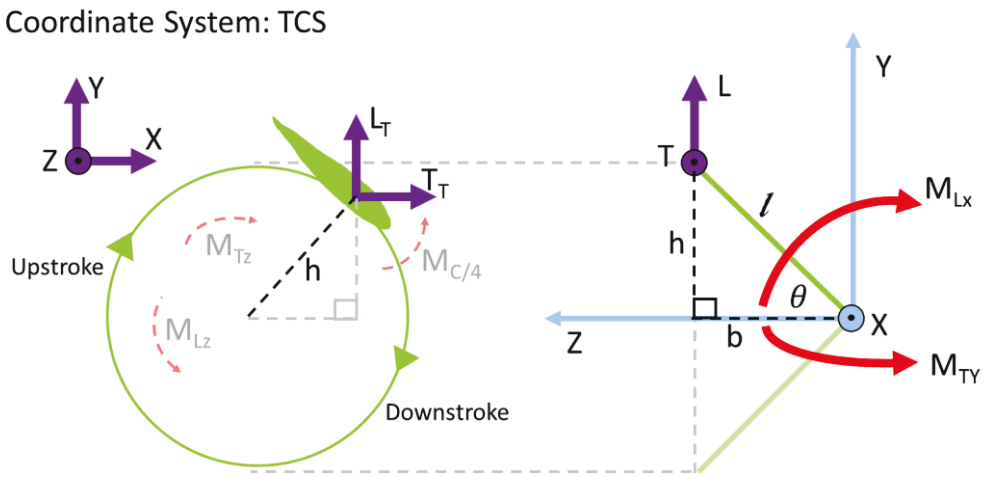

Figure 91: Moment input to generate lift and thrust

The distance between the shoulder and the 1/4MAC was l = 11.8 cm (0015 flipper) and 12.5 cm (Ryan BQM-34 Firebee flipper). Similarly to the healthy muscle calculations, the 1/4MAC was assumed to move in a conical trajectory for simplification. The resultant lift and thrust vectors would act on the moment arm b. The moments were equal to input M_L and M_T on the z-y and z-x planes respectively.

$$M_{Lx} = L_T \times b \qquad (40)$$

$$M_{Ty} = T_T \times b \qquad (41)$$

$$M_R = \sqrt{M_{Lx}^2 + M_{Ly}^2} \qquad (42)$$

M_L and M_T would be experienced at the shoulder. The moment magnitudes of M_L and M_T were calculated and plotted against the percent powerstroke cycle, with 0% being the start of the downstroke and 100% being the end of the upstroke, as seen in Fig. 93. The maximum moment magnitude was found to be approximately 1.3 Nm.

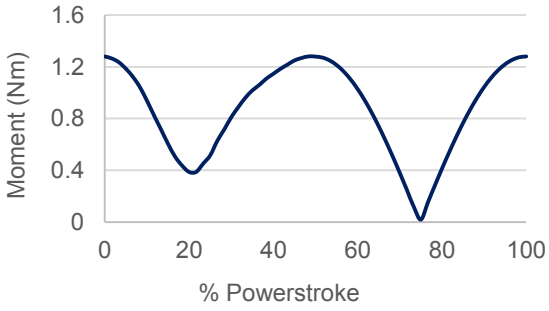

Figure 92: Shoulder moment magnitudes due to NACA0015 flipper blade throughout powerstroke

From Fig. 91, it can be seen that Lola's muscles can handle much greater torques than the predicted moments of the prosthetic flipper blade. However, muscles move in conjunction, which may reduce the overall moment on the shoulder. For example, depending on the line of action, one muscle's moment may counteract another muscle's moment. This physiology allows for muscles to work together to minimize injury. Nonetheless, Lola's muscles produce high enough magnitude values that they would still be able to handle 1.3 Nm to operate the flipper prosthetic. Additionally, Lola is a living and learning being, and can adapt the rate at which her muscles fire to produce desired moments for performing the powerstroke.

5.4.5 Flipper Mass Comparisons

A small difference in masses between Lola's healthy flipper and the fabricated prosthetic was found during analysis. This mass mismatch would cause Lola to use asymmetrical loadings in order to move both her healthy flipper and prosthetic simultaneously, which is non-ideal. However, this issue can be easily resolved prior to live testing. The mass of Lola's healthy flipper was found from x-rays. The surface area of bone and flesh was determined through ImageJ, and an average flipper height of 3.8 cm was used to determine bone and flesh volume. Density of flesh is similar to that of water, 1 g/cm^3 [105]. The density of Lola's bone was found using extrapolation of a sea turtle bone density chart, shown in Fig. 94 [77]. Bone density was chosen as 1.33 g/cm^3.

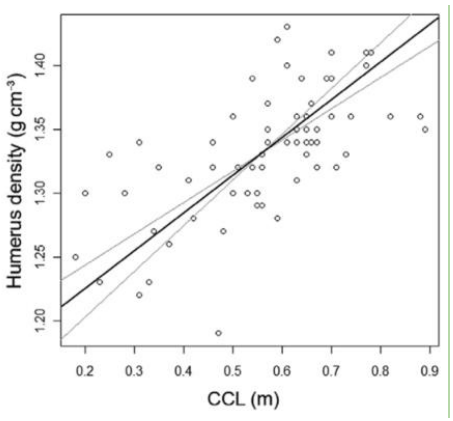

Figure 93: Sea turtle bone density vs. carapace length [77][41]

Mass was then found by multiplying density with volume. Table 12 shows the values of density, volume, and mass for the healthy flipper, from shoulder base to flipper tip.

Table 12: Estimated values of healthy flipper bone and flesh

Material	Density (g/cm^3)	Surface Area (cm^2)	Height (cm)	Volume (cm^3)	Mass (kg)	Flipper Mass (kg)
Bone	1.33	200	3.8	760	1.01	1.77
Flesh	1.00	200	3.8	760	0.76	

The mass of the silicone flipper was found by multiplying silicone density with the flipper volume from SolidWorks. The mass of the flipper (including Lola's residual limb mass calculated similarly as before) was found to be 1.07 kg. This mass difference indicates that Lola would need to apply more muscle input on one flipper than the other in order to produce a symmetrical motion. This mass imbalance can be corrected by embedding the silicone flipper with heavier (but safe) objects during the silicone casting phase. This correction will be completed prior to sending the prosthetic out to Lola's aquarium.

In Chapter 5, the results and discussion of the project were presented. The NACA0015 custom flipper-shape was chosen as the final flipper blade due to its superior lift and thrust capabilities. Rectangular flippers were disqualified due to infeasibility. Stress analysis was performed on key locations of the prosthetic and residual limb to check the safety and comfort of the prosthetic. It was found that the stresses generated throughout the powerstroke were smaller than the UTS of silicone [101,106,107,108], and would have little effect on Lola's limb. For further

[41] [77] Maffucci et. al. (2013). "Bone density in the loggerhead turtle: functional implications for stage specific aquatic habits." The Zoological Society of London. Retrieved from https://www.researchgate.net/publication/257603109_Bone_density_in_the_loggerhead_turtle_functional_implications_for_stage_specific_aquatic_habits_J_Zool.

validation, Lola's healthy muscle loadings were predicted and compared with loadings due to the prosthetic for a powerstroke cycle. It was concluded that Lola's muscles would be able to easily handle the prosthetic for performing the powerstroke. With the analysis completed on the prosthetic flipper (predicted thrust and lift, stress analysis, and healthy flipper muscle comparison), the team is fairly confident that the preliminary flipper prosthetic design will help Lola swim better and make her life a little easier. Future iterations of the design can further improve the control and efficacy of the prosthetic. The next chapter summarizes and explains the final decision in choosing the prosthetic flipper with best performance, reusability, comfort, and practicality.

CHAPTER 6 – Final Design and Validation

The final design for an initial sea turtle prosthetic can be found in Fig. 95. This final design contains the NACA0015 flipper blade with the multi-layered attachment cast. The cast is fixed to the flipper blade with rivets and secured around Lola's residual limb with Velcro straps and buckles (not shown in Figure 95). The final design would be adjustable to fit Lola's limb at any given time. It would not cause excessive stress on her limb either. Furthermore, Lola would could easily handle the moments produced by the prosthetic.

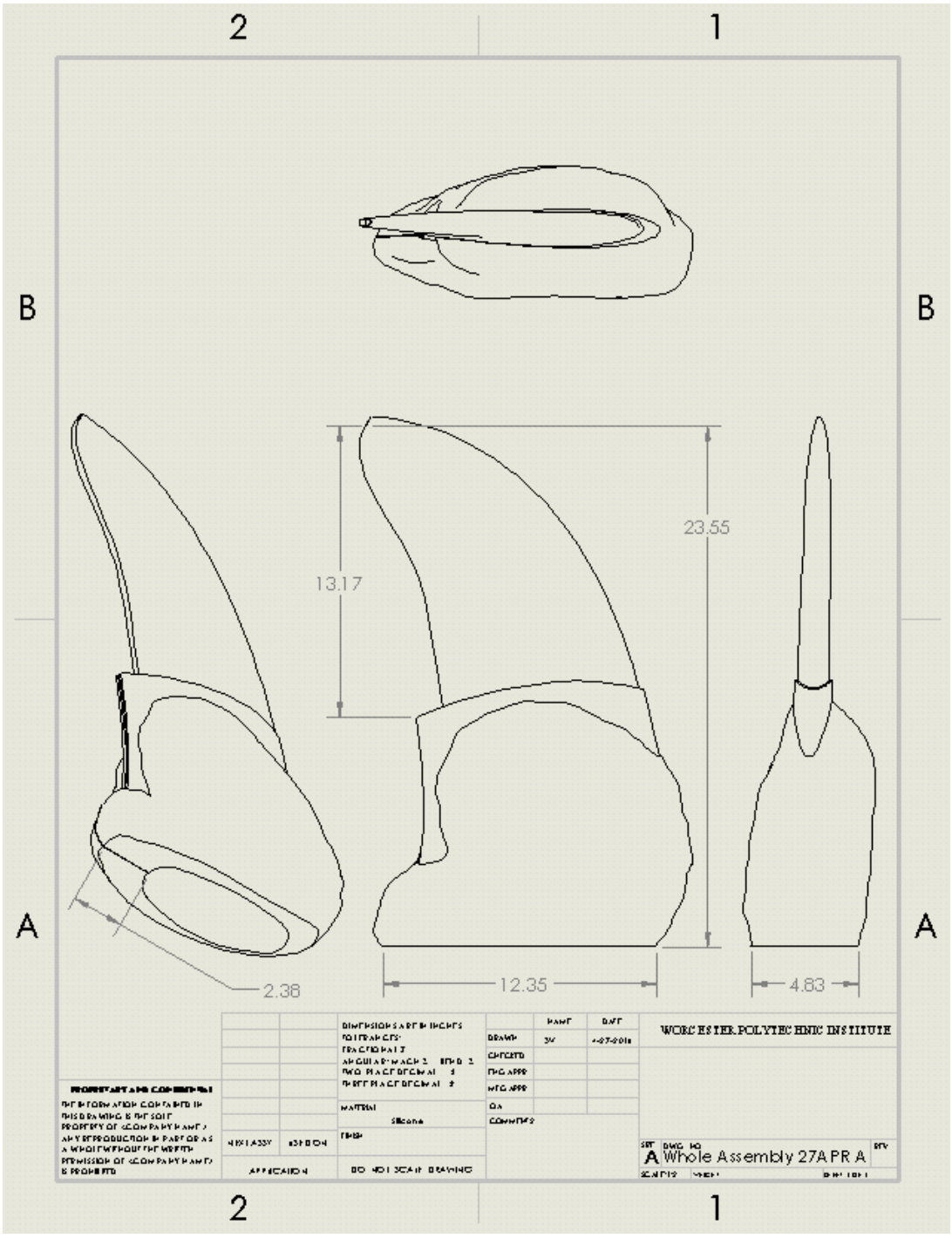

Figure 94: Final Prosthetic Design

Section 6.1 describes the minimal impact the prosthetic design will have on the economy. Section 6.2 explains how Lola's prosthetic will not harm the environment. The influence this project will have on society was outlined in Section 6.3. Section 6.4 explains how the prosthetic will not have any part in the government or the global market. Section 6.5 goes into the ethics concerning the project. Safety and health considerations while designing the prosthetic were expressed in Section 6.6. Finally, Section 6.7 highlights the ease of manufacturability of the design and 6.8 imparts the reusability of the team's design.

6.1 Economics

The design of the prosthetic uses low cost materials for fabrication. It is meant to be a non-profit product for Lola to use to aid her in swimming more efficiently and safely. It should have no major economic impact. However, if multiple design teams decided to create future iterations of this product for their sea turtle amputees and use the same material as our team (silicone from Reynold's Advanced Materials), then there may be a small influx of sales for that particular company.

6.2 Environmental Impact

The prosthetic uses silicone and nondegradable, long lasting parts. It has minimal impact on the environment, as the material is chemically inert and does not produce waste. Proper disposal of silicone waste was executed throughout the manufacturing stage. Lola herself has no major impact on the environment in her enclosure, and thus, Lola and her prosthetic should have no influence on the environment.

6.3 Societal Influence

This product was designed specifically for Lola the sea turtle. The design team has not publicly announced the creation of such a prosthetic, as the staff at Lola's Aquarium wish to disclose this information to the public on their own time (i.e., after live testing is conducted). If the prosthetic is successful in aiding Lola to swim better, then there may be some excitement in news about the design of a flexible sea turtle prosthetic. Hopefully, this would inspire other project teams to continue the development of a more robust prosthetic sea turtle flipper for the future.

6.4 Political Ramifications

This project was created for a non-profit cause, and should not have any major influence on the global market.

6.5 Ethical Concerns

The flipper prosthetic is meant to better Lola's life and the lives of her caretakers. With the prosthetic, Lola should be able to swim more efficiently and be less prone to injury. With further studies, more prosthetics can be developed for sea turtles with missing limbs, which can make their long lives easier and happier as well.

6.6 Health and Safety Issues

This project was designed for the purpose of helping the sea turtle Lola swim more efficiently and to decrease the risk of injury. A more in-depth failure analysis of the material would

be ideal before developing a final design for Lola, but this current prototype is still safe. If the prosthetic were to fail, it would fail at a point that would not cause injury to the turtle or its caretakers.

6.7 Manufacturability

The turtle prosthetic can be developed fairly easily. It consists of two modules: the flipper blade and attachment complex. Both modules were custom-made for Lola. If such a prosthetic was to be created for another turtle, careful measurements of the amputation site would be needed to make a comfortable mold for the attachment piece. The planar surface shape of the turtle's healthy flipper would need to be paired with the NACA0015 airfoil for a model of the healthy flipper, and a custom negative mold can be made. Aside from the customization of the prosthetic, the rest of the manufacturing is standard using materials such as silicone.

6.8 Sustainability

The prosthetic does not use any external forms of energy to run (i.e., motors or batteries), as it is a passive flipper that is meant to be attached to Lola's residual limb. The prosthetic will perform based off Lola's limb inputs. The materials used were meant to be durable and withstand high impacts, making the product-life fairly long. The production of the product uses silicone molding, with the master mold being reusable.

CHAPTER 7 – CONCLUSIONS

This project developed an initial design of a flipper prosthetic for Lola, an amputated turtle. Only one other turtle prosthetic case in the world is similar to this project, where that turtle (Yu) was missing both front flippers. Yu's project team needed to ensure that their flipper prosthetics matched each other, and were able to generate symmetrical forces. In Lola's case, she was missing a single flipper, and our project team needed to design a prosthetic flipper that matched her healthy flipper. This aspect of the design required very thorough research and a high level of understanding of sea turtle locomotion and anatomy.

Even without adult turtle data in literature or access to the patient, the team was still able to develop a preliminary flipper prototype using experimental values from wind tunnel testing and estimated numbers from pictures of the patient. The flipper blade was designed and tested to ensure it was aerodynamic and would be effective in helping Lola swim more efficiently. The attachment design combined several of the most current, practical methods of attachment in the field of prosthetics to create a prosthetic that would fit and be comfortable for Lola. The team engineered the prototype with safety and biomimetics in mind, taking care to keep the prosthetic as similar to Lola's natural flipper as possible.

The shape of the flipper blade traced the contour of Lola's flipper, and the cast was designed using a 3D model of Lola's residual limb. Multiple airfoil shapes were tested in a wind tunnel and compared with theoretical simulations to find the flipper with the highest thrust production. The NACA0015 airfoil with Lola's custom planar shape was chosen as the best flipper blade, and a silicone full-size model was created for the preliminary prototype.

Lola's healthy muscle potential was also studied throughout the powerstroke and estimated to ensure that she would be able to handle the prosthetic generated moments. This provided evidence to show that she could easily handle the loadings. Stress analysis was also conducted to ensure the prosthetic would not fail with a safety factor well over 2.9. This made sure the prosthetic would not add any excessive stress on Lola's limb either. In case of collision with a wall, the silicone flipper would allow energy to disperse safely, reducing chances of material failure or harming Lola. If the flipper prosthetic were to fail, it would fail at the intersection of the flipper blade and the attachment system. This would not harm Lola in any way, and she would simply revert to swimming the way she did before receiving the prosthetic.

To summarize, this capstone project contributed extensive research and an end product to further marine prosthetics and work done on biomimetic, aerodynamic flippers. Previous designs for sea turtle flipper prosthetics had not focused as much on aerodynamics and biomechanics when creating solutions. The team was happy to have the opportunity to learn so much about these two fields while being able to help an amputee at the same time.

7.1 Live Testing

While wind tunnel testing and ANSYS may demonstrate the functionality of a static flipper, they may not fully represent the performance of a dynamic flipper on an animal. The team has requested a live test using Lola for further verification of the flipper. In live animal testing, safety is the most important aspect. The team has taken great care to ensure the flipper attachment

piece is as comfortable as possible. The team will not be handling Lola or putting the prosthetic on her. Instead, the piece will be sent to Lola's caretakers along with detailed instructions. There, the caretakers may attach the flipper to Lola, and if she accepts the flipper, the caretakers will be asked to film Lola swimming with the prosthetic. The team anticipates a learning curve, where Lola may not understand how to use it at first, but given time and practice, she will hopefully be able to use the flipper to restore some of her natural swimming abilities. Live testing has been tentatively scheduled for Summer 2016.

CHAPTER 8 – FUTURE STUDIES

The goal of this project was to develop a passive prosthetic with a flexible flipper blade to increase the turtle's ability to generate thrust. This design could serve as the baseline for future iterations that include a control mechanism, or advanced mechanical features. It was validated through static testing in the wind tunnel and software. Further analysis using dynamic testing and finite element analysis could yield more accurate results to better understand performance.

In the future, the research and work can be extended to improve the prosthetic design. For one, the flipper blade had an overall passive design. There is a lot of room to add flexibility in the flipper. To further increase the flex of the flipper throughout the powerstroke, mechanical attributes could be added to the flipper to make the design more active. Mechanical features could be slots, vents, or geometric cuts in the material.

For example, just like a natural turtle flipper can move because of its complex anatomy, sections of the flipper can be modified to move in different ways. The current design is a single piece prosthetic and motion of the prosthetic is limited even if it is flexible. Sensors could also be used to create a feedback mechanism for the prosthetic. Position, force, and velocity data could be recorded and analyzed to move the flipper according to Lola's needs.

A recent study modeled the torsion of a turtle's flipper rotating through angles of attack in the downstroke. The researchers used ANSYS and ImageJ [48] to map rotation in the flipper. A similar study could be conducted to analyze flipper rotation. A third idea for future studies could be using ANSYS Static Structural to study the stresses and even strains acting on the prosthetic and on Lola given specific material properties. The SolidWorks models of the flipper, Lola's residual limb, and the prosthetic have all been generated and can be the geometry inputs for this study.

Lastly, mechanical testing can be performed to determine fatigue of the prosthetic. The durability of the prosthetic can be better analyzed to find how many loading and unloading cycles the flipper can withstand before mechanical failure. This would be helpful in predicting when exactly the prosthetic could break. Basic hand calculations and stress comparisons were completed to validate the safety of the prosthetic, but further studies would be useful to determine if a stiffer or harder plastic or rubber may be a better material in terms of fatigue resistance.

APPENDICES

APPENDIX A – LOLA'S MEASUREMENTS

The amputated flipper was 12.5 cm in length. Lola's caretakers measured a diameter of 6.36 cm around where the flipper meets the body. The calculated circumference was 20 cm.

Table A: Lola's measurements from the aquarium

Turtle Measurements			
Physical Dimensions	Value	Unit	Source
Flipper length (Max)	28.5	cm	Key West Aquarium
Amputated Flipper length (Max)	12.5	cm	Key West Aquarium
airfoil	NACA 0015 [32] , 0014 [31], 0012[38]		31, 32, 38
Diameter of where the flipper meets the body	6.366197724	cm	Key West Aquarium
Circumference of where the flipper meets the body	20	cm	Key West Aquarium
chord length (Max)	115.15	mm	Key West Aquarium
1/4 Chord point from leading edge	28.7875	mm	Key West Aquarium

Figure A: Lola's x-rays, provided by staff at her aquarium

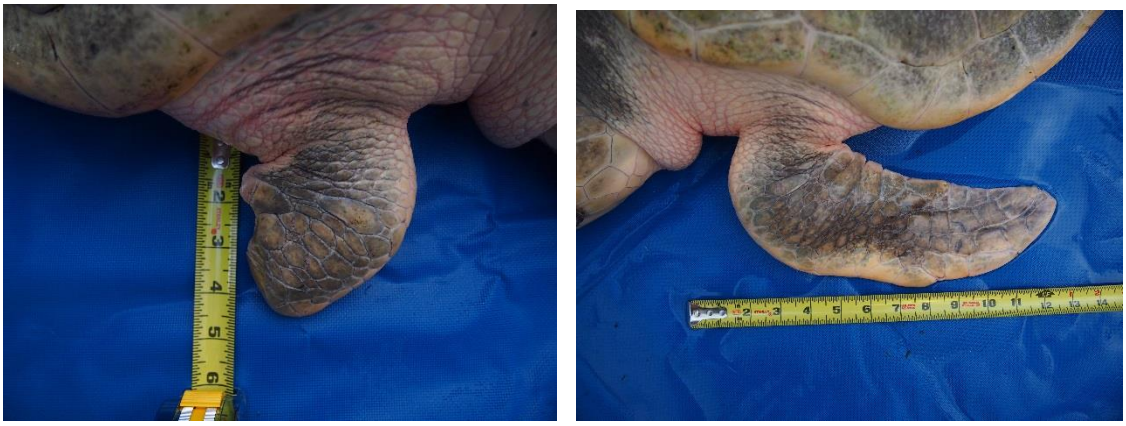

Figure B: Aerial view of Lola's flippers

Figure C: Measurement of Lola's side flipper

Figure D: Lola underwater, provided by staff at her aquarium

APPENDIX B – SHORE A HARDNESS

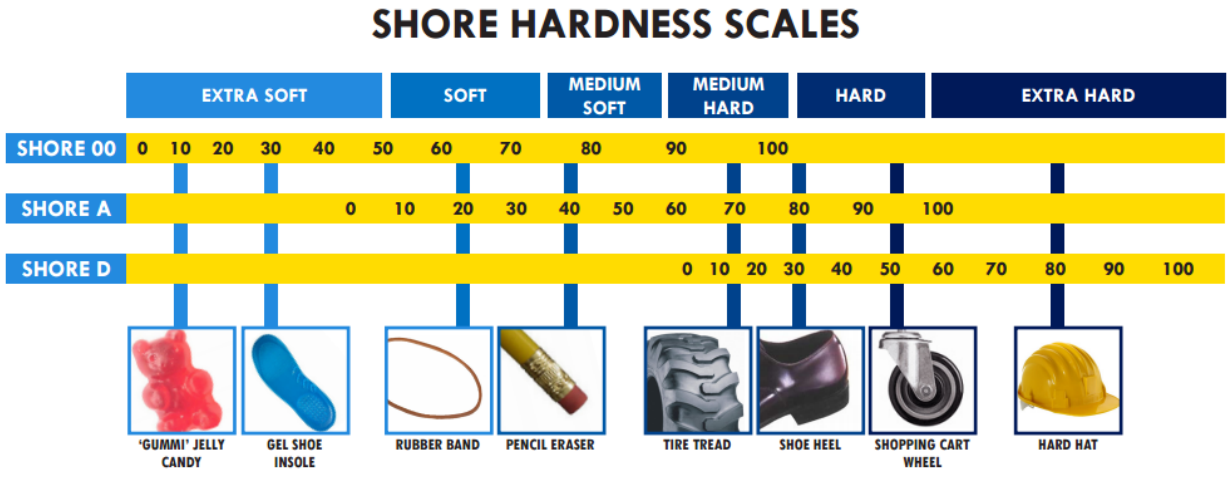

Figure E: Durometer by Smooth-On [10242]

APPENDIX C – MATLAB

Code for healthy muscle predictions

```
%% Import scaled data for turtles
clear all;close all;clc

ShouldPitch=csvread('Turt_force_pitch.csv'); %Shoulder elevation moment data for all muscles
A=ShouldPitch(:,1); %Degrees of shoulder elevation, 0-180
P_corb=ShouldPitch(:,2); %Shoulder elevation force due to coracobrachialis
P_delt=ShouldPitch(:,3); %Shoulder elevation force due to deltoideus
P_lat=ShouldPitch(:,4); %Shoulder elevation force due to latissimus dorsi
P_pec=ShouldPitch(:,5); %Shoulder elevation force due to deltoideus
P_tri=ShouldPitch(:,6); %Shoulder elevation force due to triceps

P_lat_tri=P_lat+P_tri;

ArmYaw=csvread('Turt_force_yaw.csv'); %Elevation angle moment data for all muscles
A2=ArmYaw(:,1); %Degrees of elevation angle -90 to 90
Y_corb=ArmYaw(:,2); %Elevation angle force due to coracobrachialis
Y_delt=ArmYaw(:,3); %Elevation angle force due to deltoideus
Y_lat=ArmYaw(:,4); %Elevation angle force due to latissimus dorsi
Y_pec=ArmYaw(:,5); %Elevation angle force due to deltoideus
Y_tri=ArmYaw(:,6); %Elevation angle force due to triceps

Y_lat_tri=Y_lat+Y_tri;



%% Unit Circle Translation
% Will lose precision, but that's ok

%Input desired parameters
h=0.7; %ratio of amplitude and r, normalizing r=1 (i.e., h=0.75 => amplitude is 75% length of r), h <=1
yaw_musc=Y_delt; %user input, make sure same muscle group as pitch (see above for options)
pitch_musc=P_delt; %user input, make sure same muscle group as yaw (see above for options)

Ys=A2/90;
Ps=(A-90)/90;
P_force(1:361) = 0;
Y_force(1:361) = 0;

   for theta=0:360;
   Ps1=h*sind(theta);
   Ys1=h*cosd(theta);
   indP=find(Ps>=Ps1);
   [Pu,ind]=min(indP);
   P_force(theta+1)=pitch_musc(Pu);
```

[42] [102] Reynolds Advanced Materials. (2016). Technical Overview, Smooth-Sil Series. Retrieved from http://www.reynoldsam.com/product/smooth-sil/.

```
    indY=find(Ys<=Ys1);
    [Yu,ind2]=max(indY);
    Y_force(theta+1)=yaw_musc(Yu);
    end

Pt_force=transpose(P_force);
Yt_force=transpose(Y_force);
Force_mag=sqrt((Pt_force).^2+(Yt_force).^2);
theta1=(0:360);
thetaT=transpose(theta1);
plot(thetaT, Force_mag);
xlabel ('Angle (degrees)'), ylabel ('Force (N)');
title('Forces Throughout Powerstroke'); %Change title as needs to reflect muscle group
```

APPENDIX D – Yaw muscle forces and fiber lengths

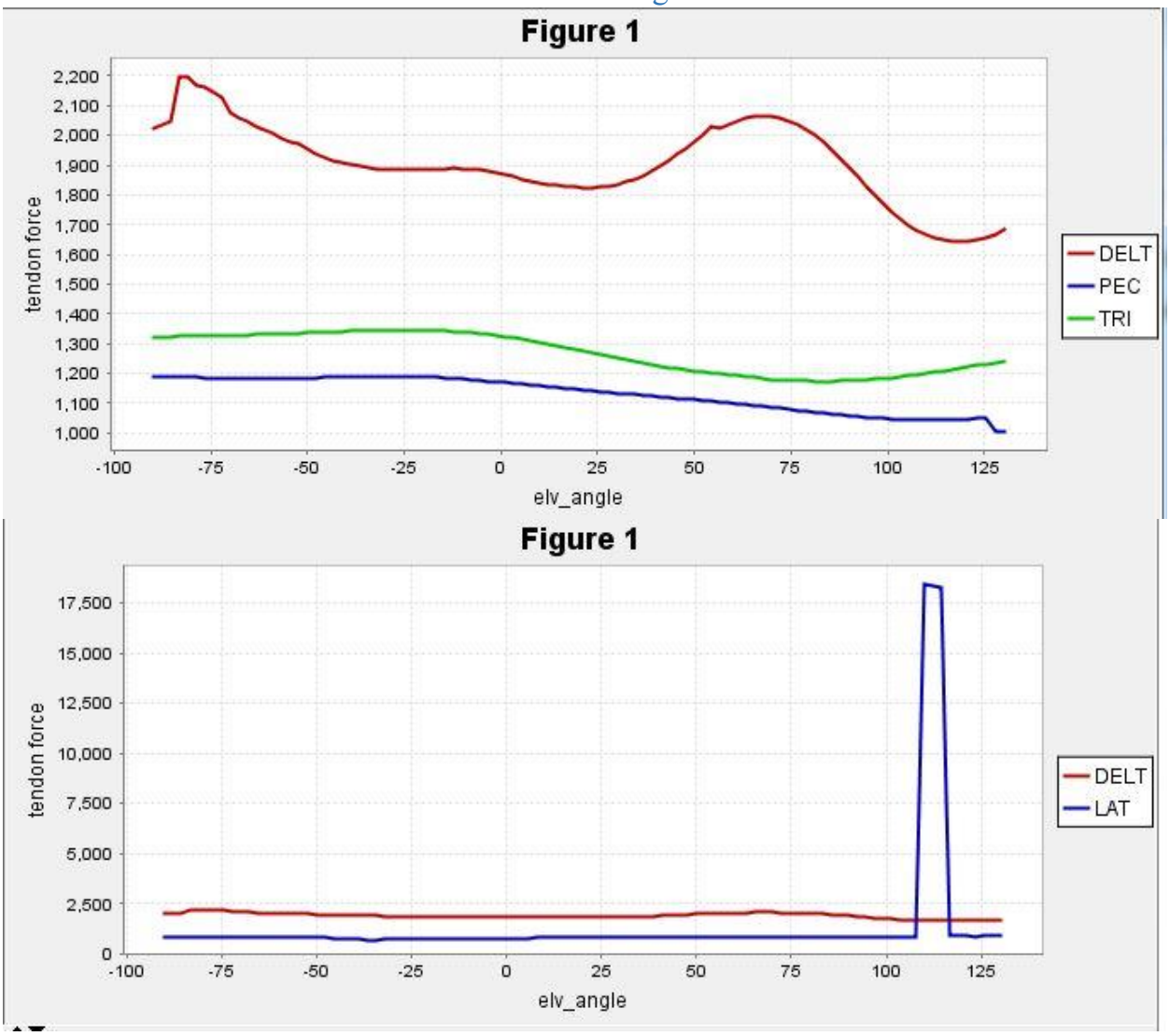

Figure F: Yaw muscle force data obtained from OpenSim

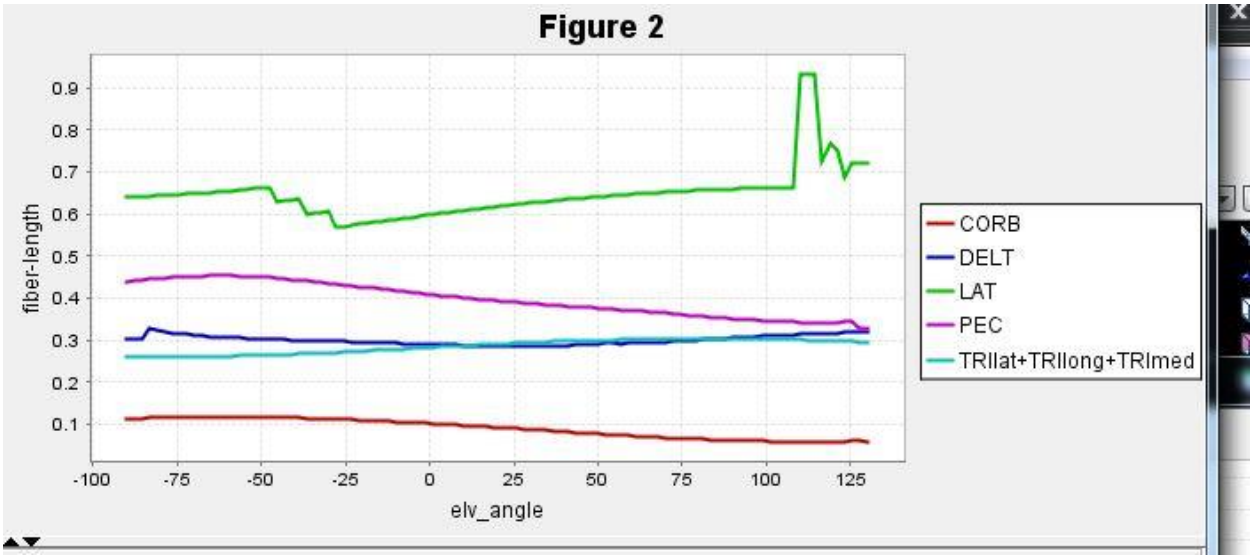

Figure G: Yaw muscle fiber length data obtained from OpenSim

APPENDIX E – 3D ANSYS

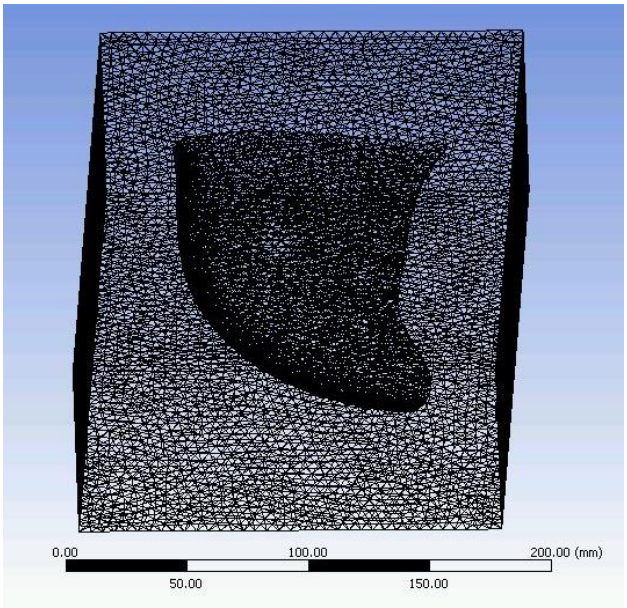

Figure H: Mesh of air channel in 3D ANSYS

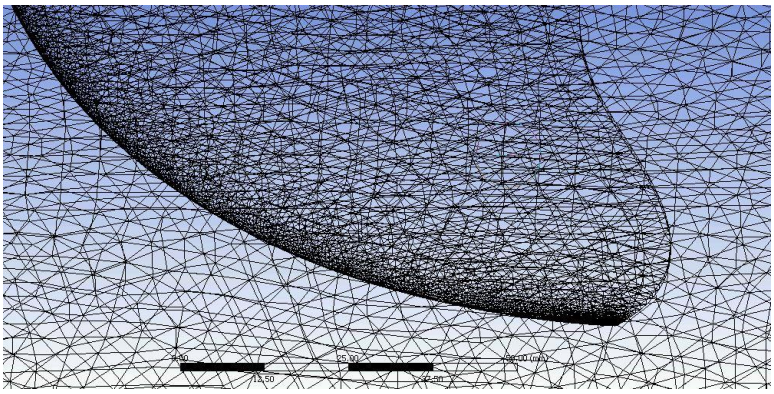

Figure I: Detailed mesh along leading edge, tip, and gradual transition

APPENDIX F – Wing Assembly SolidWorks Drawings

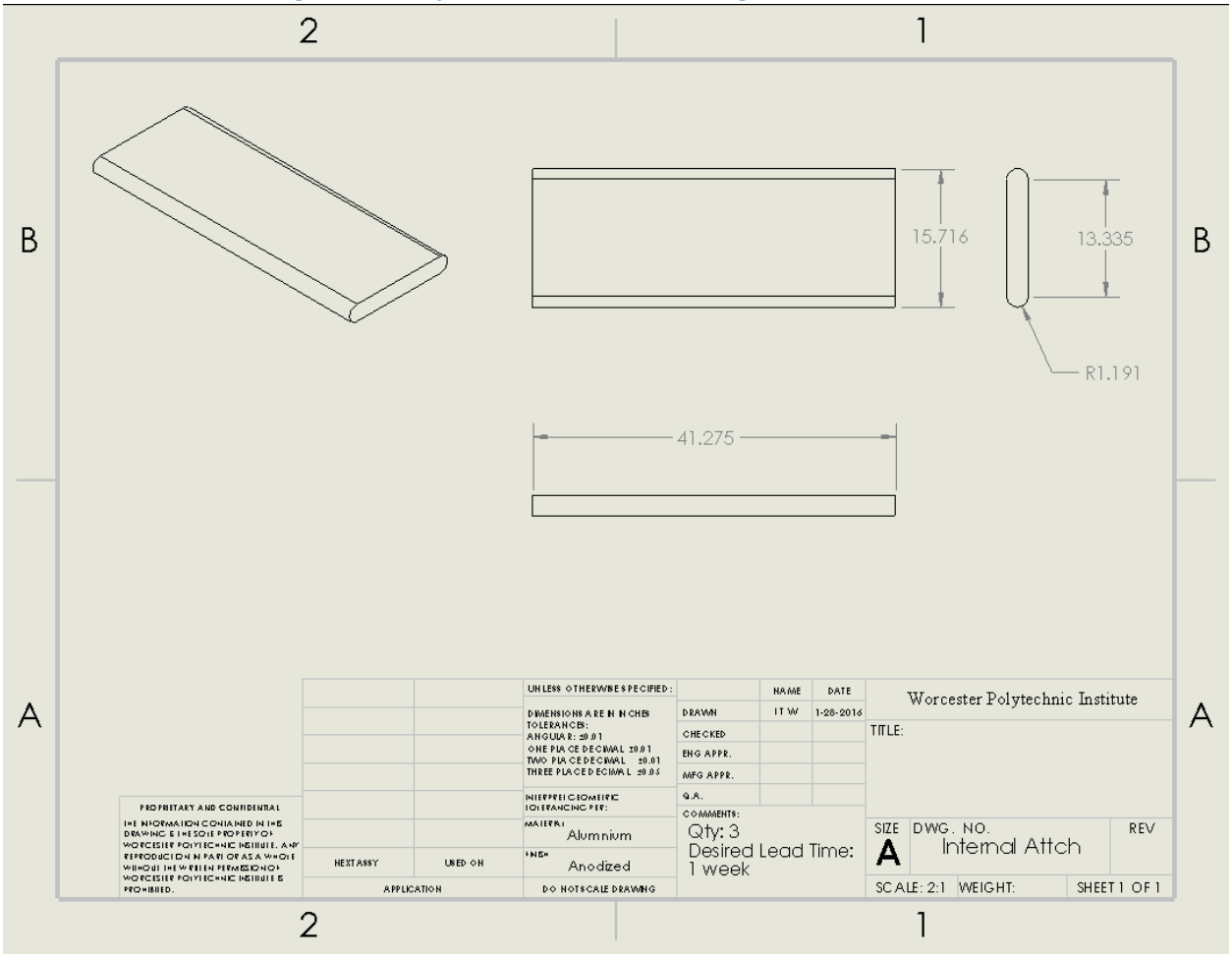

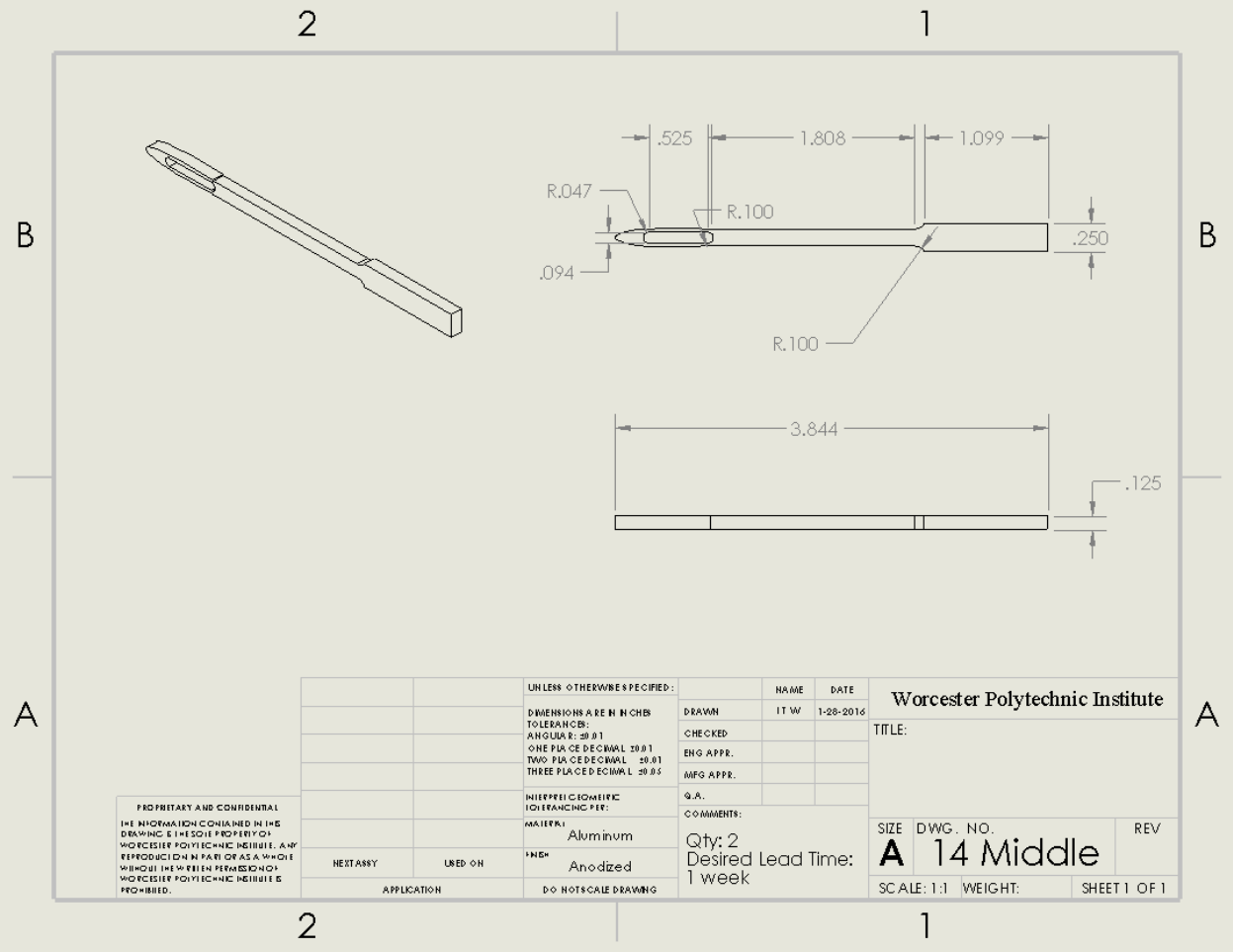
2
1
B
A
.525
1.808
1.099
R.047
R.100
.094
.250
R.100
3.844
.125
UNLESS OTHERWISE SPECIFIED:
DIMENSIONS ARE IN INCHES
TOLERANCES:
ANGULAR: ±0.01
ONE PLACE DECIMAL ±0.01
TWO PLACE DECIMAL ±0.01
THREE PLACE DECIMAL ±0.05
INTERPRET GEOMETRIC TOLERANCING PER:
MATERIAL
Aluminum
FINISH
Anodized
DO NOT SCALE DRAWING
NAME
DATE
DRAWN
IT W
1-28-2016
CHECKED
ENG APPR.
MFG APPR.
Q.A.
COMMENTS:
Qty: 2
Desired Lead Time:
1 week
Worcester Polytechnic Institute
TITLE:
SIZE
A
DWG. NO.
14 Middle
REV
SCALE: 1:1
WEIGHT:
SHEET 1 OF 1
NEXT ASSY
USED ON
APPLICATION
PROPRIETARY AND CONFIDENTIAL
THE INFORMATION CONTAINED IN THIS DRAWING IS THE SOLE PROPERTY OF WORCESTER POLYTECHNIC INSTITUTE. ANY REPRODUCTION IN PART OR AS A WHOLE WITHOUT THE WRITTEN PERMISSION OF WORCESTER POLYTECHNIC INSTITUTE IS PROHIBITED.

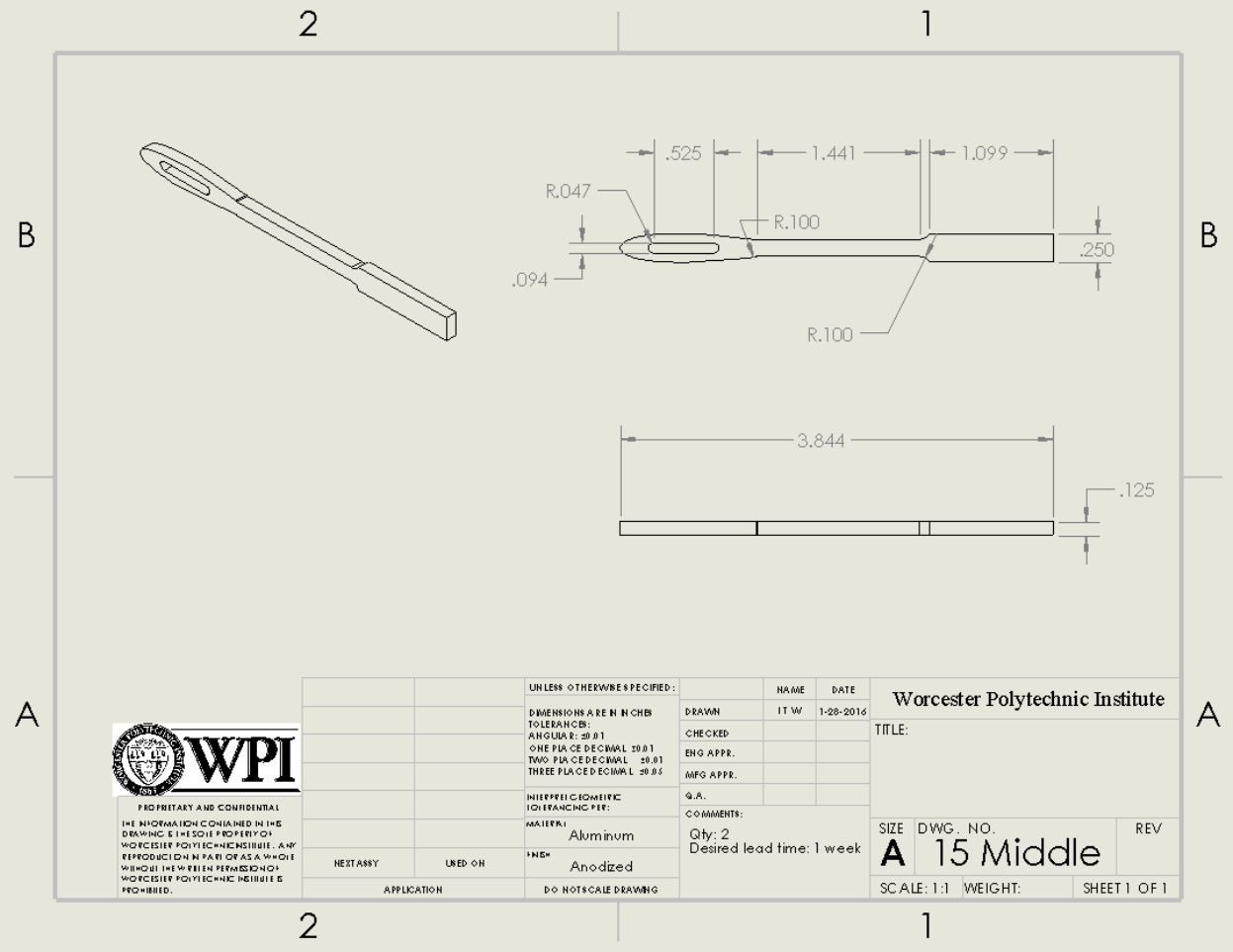
2
1
B
A
.525
1.441
1.099
R.047
R.100
.094
.250
R.100
3.844
.125
WPI
PROPRIETARY AND CONFIDENTIAL
THE INFORMATION CONTAINED IN THIS DRAWING IS THE SOLE PROPERTY OF WORCESTER POLYTECHNIC INSTITUTE. ANY REPRODUCTION IN PART OR AS A WHOLE WITHOUT THE WRITTEN PERMISSION OF WORCESTER POLYTECHNIC INSTITUTE IS PROHIBITED.
UNLESS OTHERWISE SPECIFIED:
DIMENSIONS ARE IN INCHES
TOLERANCES:
ANGULAR: ±0.01
ONE PLACE DECIMAL ±0.1
TWO PLACE DECIMAL ±0.01
THREE PLACE DECIMAL ±0.05
INTERPRET GEOMETRIC TOLERANCING PER:
MATERIAL
Aluminum
FINISH
Anodized
DO NOT SCALE DRAWING
NEXT ASSY
USED ON
APPLICATION
NAME
DATE
DRAWN
I T W
1-28-2016
CHECKED
ENG APPR.
MFG APPR.
Q.A.
COMMENTS:
Qty: 2
Desired lead time: 1 week
Worcester Polytechnic Institute
TITLE:
SIZE
A
DWG. NO.
15 Middle
REV
SCALE: 1:1
WEIGHT:
SHEET 1 OF 1

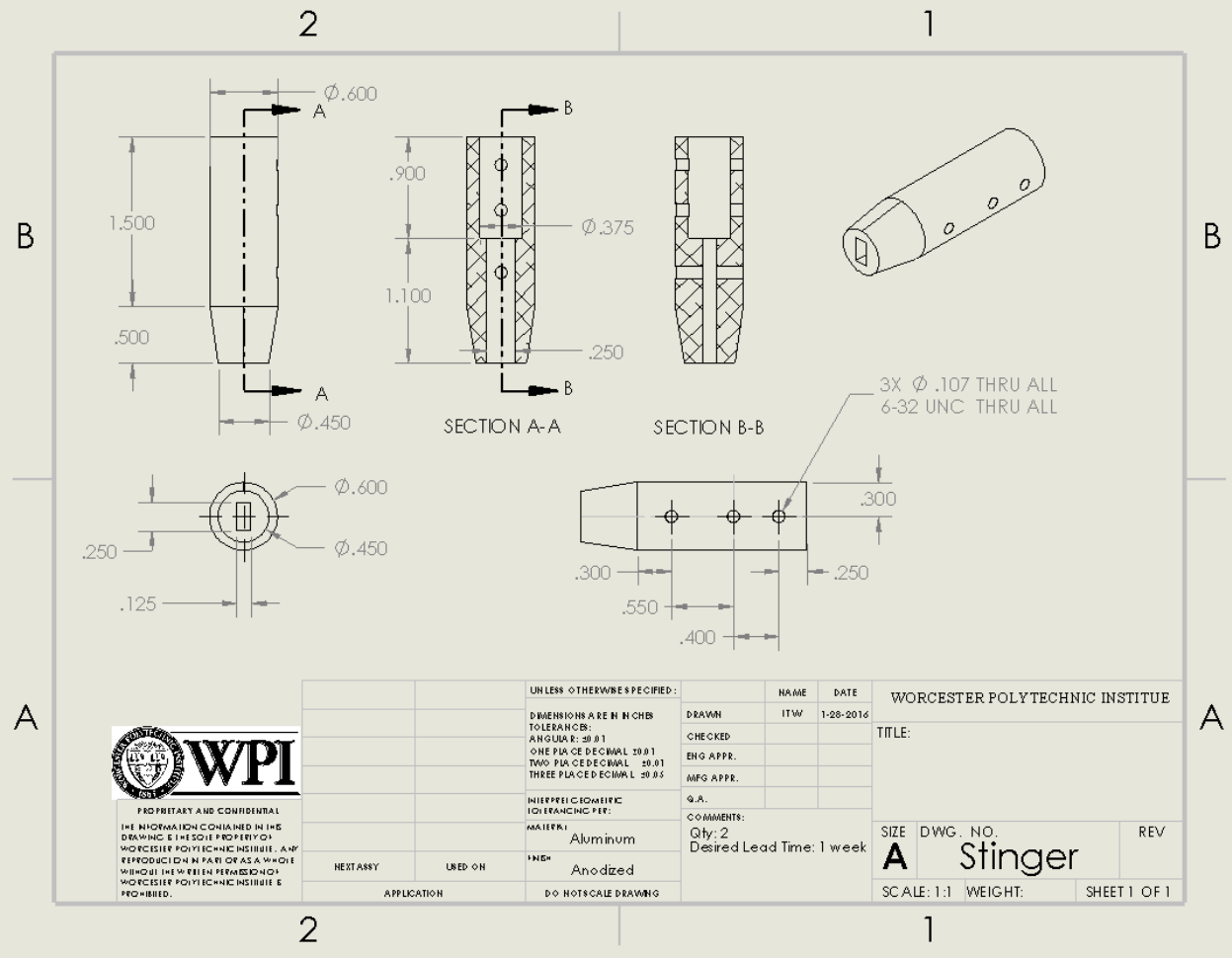

APPENDIX G – 2D ANSYS Airfoils

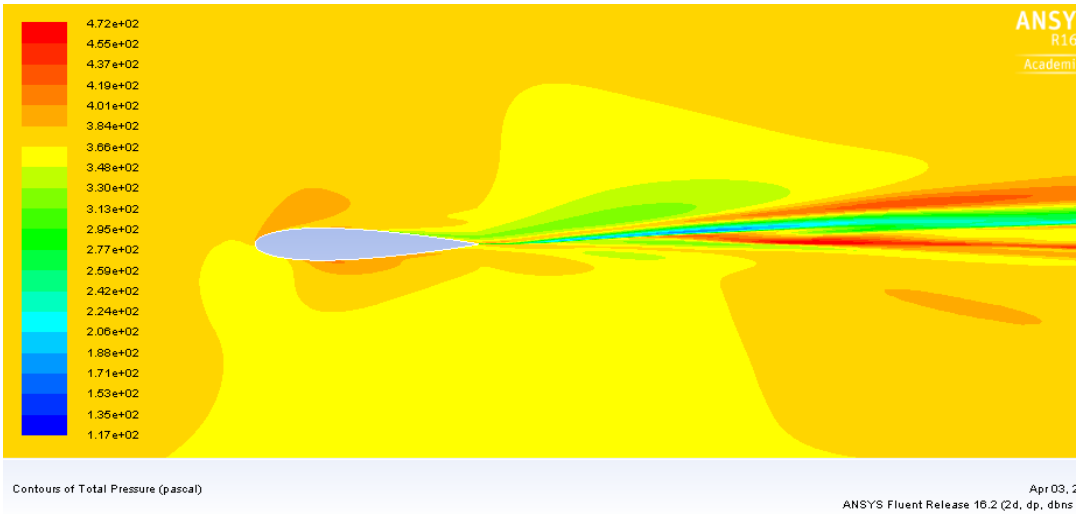

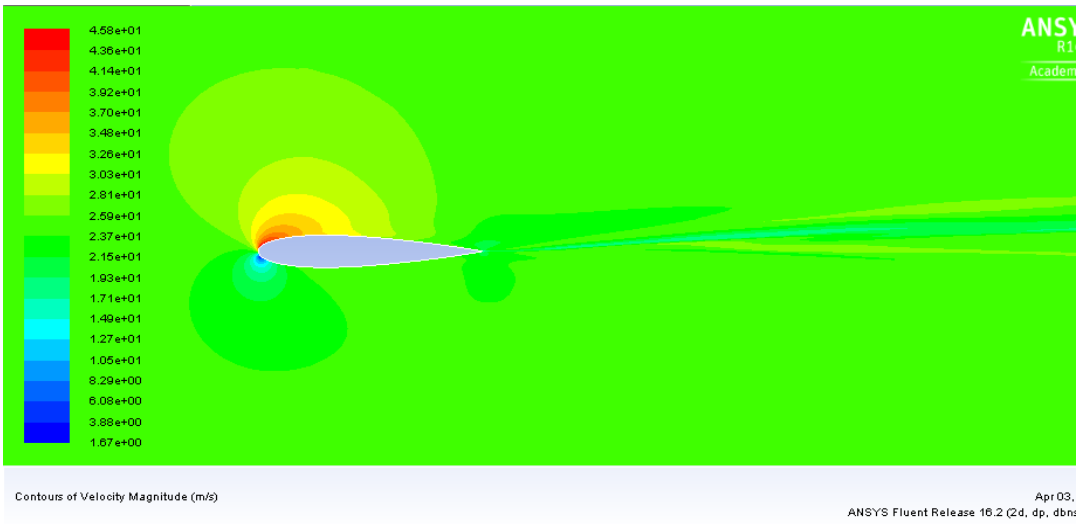
4.58e+01
4.36e+01
4.14e+01
3.92e+01
3.70e+01
3.48e+01
3.26e+01
3.03e+01
2.81e+01
2.59e+01
2.37e+01
2.15e+01
1.93e+01
1.71e+01
1.49e+01
1.27e+01
1.05e+01
8.29e+00
6.08e+00
3.88e+00
1.67e+00
Contours of Velocity Magnitude (m/s)
ANSYS Fluent Release 16.2 (2d, dp, dbns

REFERENCES

[1] Endangered Species Act (7 U.S.C. § 136, 16 U.S.C. § 1531 et seq.)

[2] Thayer, G.W., Bjorndal K.A., Ogden, J.C., et al. (1984). Role of larger herbivores in seagrass communities: Functional ecology of seagrass ecosystems: A perspective on plant-animal interactions. Estuaries 7(4): 351-376.

[3] "Allison's Prosthesis." Allison's Prosthesis. Sea Turtle Inc., Retrieved from http://www.seaturtleinc.org/rehabilitation/allison/.

[4] Jackson, J.B.C., Kirby, M.X., Berger, W.H., et al. (2001). Historical overfishing and the recent collapse of coastal ecosystems. Science 293(5530): 29–637.

[5] McClenachan, L., Jackson, J.B.C., Newman, M.J.H. (2006). Conservation implications of historic sea turtle nesting beach loss. Frontiers in Ecology and the Environment 4(6): 290-296.

[6] Leon, Y.M., Bjorndal, K.A. (2002). Selective feeding in the hawksbill turtle, an important predator in coral reef ecosystems. Marine Ecology Progress Series 245: 249-258.

[7] Houghton, J.D.R., Doyle, T.K., Davenport, J., et al. (2006). Jellyfish aggregations and leatherback turtle foraging patterns in a temperate coastal environment. Ecology 87(8): 1967-1972.

[8] Lynam, C.P., Gibbons, M.J., Axelsen, B.E., et al. (2006). Jellyfish overtake fish in a heavily fished ecosystem. Current Biology 16(13): R492-R493.

[9] Hannan, L.B., Roth, J.D., Ehrhart, L.M., Weishampel, J.F. (2007). Dune vegetation fertilization by nesting sea turtles. Ecology 88(4): 1053-1058.

[10] Ma, C.B., Zieve, D., and Ogilvie, I. (2015). Leg or Foot Amputation. NIH: U.S. National Library of Medicine. Retrieved from http://www.nlm.nih.gov/medlineplus/ency/article/007365.htm.

[11] (2000-2015). Amputation. NorthPoint Domain Inc. Retrieved from http://www.miamivascular.com/handler.cfm?event=practice,template&cpid=23799.

[12] Sea Turtle Conservancy. (1996-2015). *Information About Sea Turtles: Frequently Asked Questions.* Retrieved from http://www.conserveturtles.org/seaturtleinformation.php?page=seaturtle-faq#14.

[13] Hazelton, Liz. (2009, Apr 9). *Saved from Swimming in Circles: Allison the One-finned Turtle Gets a New Prosthetic.* Daily Mail. Retrieved from http://www.dailymail.co.uk/news/article-1168707/Saved-swimming-circles-Allison-finned-turtle-gets-new-prosthetic.html.

[14] Clearwater Marine Aquarium. (2015). *Winter.* Retrieved from http://www.seewinter.com/winter.

[15] Paulus, S.C. (2008). *Palliative Care: An Ethical Obligation.* Santa Clara University. Retrieved from http://www.scu.edu/ethics/practicing/focusareas/medical/palliative.html.

[16] Khudson, Duane. (2007). Fundamentals of Biomechanics. Springer: 1-250. Retrieved from http://www.profedf.ufpr.br/rodackibiomecanica_arquivos/Books/Duane%20Knudson-%20Fundamentals%20of%20Biomechanics%202ed.pdf.

[17] St. Joseph Hospital (2015). *Rehabilitation Center (Inpatient).* St. Joseph Hospital. Retrieved from http://www.stjosephhospital.com/Rehabilitation-Center.

[18] Wyneken, Jeanette. Personal Interview. 18 Aug. 2015.

[19] Mader, DVM, Doug. Personal interview. 20 May 2015.

[20] Hirth, H. F. (1980). *Some aspects of the nesting behavior and reproductive biology of sea turtles.* American Zoologist 20 (3): 507-523.

[21] Wyneken, J., Labarbera, M. (1987). Locomotor strategies of hatchling sea turtles. American Zoologist. 27(4): 63A.

[22] Davenport, J., Munks, S. A., Oxford, P. J. (1984). A comparison of the swimming of marine and freshwater turtles. Proceedings of the Royal Society of London B: Biological Sciences 220 (1221): 447-475.

[23] Wyneken, J. (1997). Sea turtle locomotion: mechanisms, behavior, and energetics. The biology of sea turtles Vol. 1. CRC Press.

[24] Hernandez, R.J. & Kravitz, L. (2003). The mystery of skeletal muscle hypertrophy. ACSM's Health and Fitness Journal, 7, 18-22. Retrieved from http://www.unm.edu/~lkravitz/Article%20folder/hypertrophy.html.

[25] Donatelli, R. (2010-2015). Muscle Imbalance and Common Overuse Injuries. sportsmd.com. Retrieved from http://www.sportsmd.com/performance/muscle-imbalance-common-overuse-injuries/.

[26] Hall, B. (2007). Fins into Limbs: Evolution, Development, and Transformation. Available from https://books.google.com/books?id=Z0YWn5F9sWkC&pg=PA321&lpg=PA321&dq=sea+turtles+center+of+mass+while+swimming&source=bl&ots=5IrDmP34U5&sig=aNdNdB7ZS24XBM2llTl076NpNqI&hl=en&sa=X&ei=z1aXVaXaDYiWyQTEnYHYCg&ved=0CDEQ6AEwAw#v=onepage&q=sea%20turtles%20center%20of%20mass%20while%20swimming&f=false.

[27] Wyneken, J. (2001). Muscle Anatomy. The Anatomy of Sea Turtles: 59-67.

[28] Wyneken, J. (2001). Skeletal Anatomy. The Anatomy of Sea Turtles: 51-54.

[29] Lutz, P. L., Musick, J. A., Wyneken, J. (2002). The Biology of Sea Turtles Vol. 2. CRC press.

[30] Wyneken, J. (1988). Comparative and functional considerations of locomotion in turtles. Dissertation. University of Illinois at Urbana-Champaign.

[31] Font, D., Tresanchez, M., Siegentahler, C., Palleja, T., Teixido, M., Pradalier, C., & Palacin, J. (2011). Design and Implementation of a Biomimetic Turtle Hydrofoil for an

Autonomous Underwater Vehicle. Sensors, volume number 11, Issue 12. Retrieved from http://www.mdpi.com/1424-8220/11/12/11168/htm.

[32] Siegenthaler, C. (2012). System Integration and Fin-Trajectory Optimization for a Robotic Turtle (Master Thesis). Retrieved from Swiss Federal Institute of Technology Zurich. (386) http://students.asl.ethz.ch/upl_pdf/386-report.pdf.

[33] Index of /ads/afplots. Retrieved from http://m-selig.ae.illinois.edu/ads/afplots/.

[34] Liz Hazelton. (2009, Apr 9). "Saved from Swimming in Circles: Allison the One-finned Turtle Gets a New Prosthetic." Daily Mail. Retrieved from http://www.dailymail.co.uk/news/article-1168707/Saved-swimming-circles-Allison-finned-turtle-gets-new-prosthetic.html.

[35] Iacurci, Jenna. (2014, May 17). "Sea Turtle Amputee Swims Again with Jet-Like Prosthetic Fin." Nature World News. Retrieved from http://www.natureworldnews.com/articles/7110/20140517/sea-turtle-amputee-swims-again-with-jet-like-prosthetic-fin.htm.

[36] [puuh37]. (2014, Apr 12). US Aerospace Design Helps Save 'Freedom' The Turtle. [VideoFile]. Retrieved from https://www.youtube.com/watch?v=6V8RmImn0Jk.

[37] Wang, Yue. (2013). Disabled Sea Turtle Gets 27th Pair of Artificial Fins. Time. Retrieved from http://newsfeed.time.com/2013/02/22/disabled-sea-turtle-gets-27th-pair-of-artificial-fins/.

[38] Licht, S. C., Wibawa, M. S., Hover, F. S., & Triantafyllou, M. S. (2010). In-line motion causes high thrust and efficiency in flapping foils that use power downstroke. The Journal of experimental biology, 213(1), 63-71.

[39] Sharqawy, M. H., Lienhard V, J. H., Zubair, S.M. (2010). Thermophysical Properties of Sea Water: A Review of Existing Correlations and Data. Desalination and Water Treatment, 16, 354-380.

[40] Edwards, K. (2015). LMNO Engineering, Research, and Software, Ltd.: Gas Viscosity Calculator [Software]. Available at http://www.lmnoeng.com/Flow/GasViscosity.php.

[41] The Engineering Toolbox. (n/a). Air Density and Specific Weight [Data file]. Retrieved from http://www.engineeringtoolbox.com/air-density-specific-weight-d_600.html.

[42] Hays, G. C., Marshall, G. J., Seminoff, J. A. (2007). “Flipper beat frequency and amplitude changes in diving green turtles, Chelonia mydas.” Marine Biology, 150:1003–1009.

[43] Hays, G. C., Metcalfe, J. D., Walne, A. W., Wilson, R. P. (2004). “First records of flipper beat frequency during sea turtle diving.” Journal of Experimental Marine Biology and Ecology, 303(2): 243 - 260.

[44] Zhou, K., Liu, J., Chen, W. (2015). Proceedings from 2015 IEEE: International Conference on Information and Automation. Lijiang, China.

[45] University of Illinois at Urbana-Champaign Applied Aerodynamics Group. (n/a). UIUC Airfoil Coordinates Database [Data file]. Retrieved from http://m-selig.ae.illinois.edu/ads/coord_database.html.

[46] Yamaguchi, H., Bose, N. (1994). "Oscillating Foils for Marine Propulsion." International Society of Offshore and Polar Engineers. 3: 539-544.

[47] Fryer, C. "Upper-Limb Prosthetics: Harnessing and Controls for Body-Powered Devices." Digital Resource Foundation for the Orthotics and Prosthetics Community, Atlas of Limb Prosthetics: Surgical, Prosthetic, and Rehabilitation Principles, Ch. 6B. Retrieved from http://www.oandplibrary.org/alp/chap06-02.asp.

[48] Dudley, P., et al. (2014, Oct 29). Leatherbacks Swimming In Silico: Modeling and Verifying Their Momentum and Heat Balance Using Computational Fluid Dynamics. Plos One. Retrieved from http://journals.plos.org/plosone/article?id=10.1371/journal.pone.0110701.

[49] National Association of Scale Aeromodelers. (2016). Online Mean Aerodynamic Cord Calculator. Retrieved from http://www.nasascale.org/howtos/mac-calculator.htm.

[50] Lift coefficient atlas. Retrieved from http://baike.baidu.com/pic/%E5%8D%87%E5%8A%9B%E7%B3%BB%E6%95%B0/6221003/0/faf2b2119313b07efc8a4a630dd7912397dd8ca1?fr=newalbum#aid=0&pic=faf2b2119313b07efc8a4a630dd7912397dd8ca1.

[51] ANSI B4.1-1967, R1987. Retrieved from

http://mach.jlu.edu.cn/jxcx/standars/AGMA-ANSI/ANSI%20B4.1-1967%20Preferred%20Limits%20and%20Fits%20for%20Cylindrical%20Parts.pdf.

[52] [Image] Retrieved from http://baike.baidu.com/pic/%E5%8D%87%E5%8A%9B%E7%B3%BB%E6%95%B0/6221003/0/faf2b2119313b07efc8a4a630dd7912397dd8ca1?fr=newalbum#aid=0&pic=faf2b2119313b07efc8a4a630dd7912397dd8ca1.

[53] ASTM D3182. (2016, Apr 27). Smithers Rapra. Retrieved from http://www.smithersrapra.com/testing-services/resources/standard-test-protocols/astm/astm-d3182.

[54] Simiu, Emil et. al. (2012, Mar 13). "An Assessment of ASCE 7-10 Standard Methods for Determining Wind Loads." Journal of Structural Engineering. Retrieved from http://www.itl.nist.gov/div898/winds/pdf_files/asce_7_tn_simiu_et_al_2013.pdf.

[55] Simiu, Emil. (2009, Dec). Towards a Standard on the Wind Tunnel Method. National Institute of Standards and Technology (NIST). Retrieved from http://www.itl.nist.gov/div898/winds/pdf_files/NISTTN1655.pdf.

[56] Technical Communications Packages. (2016). Dassault Systemes. Retrieved from https://www.solidworks.com/sw/products/technical-communication/packages.htm

[57] Wasserman, Shawn. (2015, Jan 13). *ANSYS' Model-Based System Engineering Software Meets Automotive ISO Standards.* Retrieved from

http://www.engineering.com/DesignerEdge/DesignerEdgeArticles/ArticleID/9331/ANSYS-Model-Based-System-Engineering-Software-Meets-Automotive-ISO-Standards.aspx.

[58] U.S. Environmental Protection Agency. (2016, Apr 21). *Hazardous Waste Data.* RCRA. Retrieved from https://www3.epa.gov/wastes/inforesources/data/index.htm.

[59] Norton, Robert L. Design of Machinery: An Introduction to the Synthesis and Analysis of Mechanisms and Machines, 5th ed. Worcester, MA: McGraw-Hill.

[60] Wing Geometry Definitions. Retrieved from http://adg.stanford.edu/aa241/wingdesign/winggeometry.html.

[61] Dawkins, Paul. (2016). Approximating Definite Integrals. Retrieved from http://tutorial.math.lamar.edu/Classes/CalcII/ApproximatingDefIntegrals.aspx.

[62] Gallaway, Benny J. and Caillouet, Jr., Charles W. (2013, Jun). Kemp's Ridley Stock Assessment Project. Retrieved from http://www.gsmfc.org/publications/Miscellaneous/Kemp%20Ridley%20Stock%20Assessment%20Report%20Final%20June%2027%202013.pdf.

[63] Renaud, Maurice L. and Williams, Jo A. (2005). "Kemp's Ridley Sea Turtle Movements and Migrations." Chelonian Conservation and Biology, Chelonian Research Foundation, 4(4): 808-816. Retrieved from http://www.sefsc.noaa.gov/turtles/PR_Renaud_Williams_2005_CCB.pdf.

[64] Fossette, Sabrina et. al. (2010). Behaviour and buoyancy regulation in the deepest-diving reptile: the leatherback turtle. Journal of Experimental Biology, 213: 4074-4083. Retrieved from http://jeb.biologists.org/content/213/23/4074.

[65] Maniaci, David C., Li, Ye. (2012). "Investigating the Influence of the Added Mass Effect to Marine Hydrokinetic Horizontal-Axis Turbines Using a General Dynamic Wake Wind Turbine Code." NREL. Journal Article-5000-54403. Retrieved from http://www.nrel.gov/docs/fy12osti/54403.pdf.

[66] White, Frank M. (2011). Fluid Mechanics, 7th ed. New York, NY: McGraw-Hill.

[67] Hepperle, Martin. (2007, Jan 27). JavaFoil- Analysis of Airfoils. Retrieved from http://www.mh-aerotools.de/airfoils/javafoil.htm.

[68] Anderson, Jr., John D. (2011). Fundamentals of Aerodynamics, 5th ed. New York, NY: McGraw-Hill.

[69] McCullough, George B. and Gault, Donald E. (1951, Sept). "Examples of Three Representative Types of Airfoil-Section Stall at Low Speed." National Advisory Committee for Aeronautics. Retrieved from http://naca.central.cranfield.ac.uk/reports/1951/naca-tn-2502.pdf.

[70] Raymer, Daniel P. (2012). Aircraft Design: A Conceptual Approach, 5th ed. Reston, VA: American Institute of Aeronautics and Astronautics, Inc.

[71] Hager, Grant. High Aspect Ratio Wings. Retrieved from http://cosmos.ucdavis.edu/archives/2010/cluster3/HAGER_Grant.pdf.

[72] Lift for a Finite Wing. Retrieved from http://www.srmuniv.ac.in/sites/default/files/downloads/class4-2012.pdf.

[73] Hoy, Melissa G., Felix E. Zajac, and Michael E. Gordon. "A musculoskeletal model of the human lower extremity: the effect of muscle, tendon, and moment arm on the moment-angle relationship of musculotendon actuators at the hip, knee, and ankle." Journal of biomechanics 23.2 (1990): 157-169.

[74] Mathewson, Margie A., et al. "Comparison of rotator cuff muscle architecture between humans and other selected vertebrate species." Journal of Experimental Biology 217.2 (2014): 261-273.

[75] Rivera, Angela RV, Jeanette Wyneken, and Richard W. Blob. "Forelimb kinematics and motor patterns of swimming loggerhead sea turtles (Caretta caretta): are motor patterns conserved in the evolution of new locomotor strategies?." The Journal of experimental biology 214.19 (2011): 3314-3323.

[76] Biewener, Andrew A. "Scaling body support in mammals: limb posture and muscle mechanics." Science 245.4913 (1989): 45-48.

[77] Maffucci et. al. (2013). “Bone density in the loggerhead turtle: functional implications for stage specific aquatic habits.” The Zoological Society of London. Retrieved from https://www.researchgate.net/publication/257603109_Bone_density_in_the_loggerhead_turtle_functional_implications_for_stage_specific_aquatic_habits_J_Zool.

[78] Hibbeler, R.C. (2014). Mechanics of Materials, 9th ed. Prentice Hall.

[79] Absolute, Dynamic, and Kinematic Viscosity. Retrieved from http://www.engineeringtoolbox.com/dynamic-absolute-kinematic-viscosity-d_412.html.

[80] Air Properties. Retrieved from http://www.engineeringtoolbox.com/air-properties-d_156.html.

[81] Speed of Sound in Air. Retrieved from http://www.engineeringtoolbox.com/air-speed-sound-d_603.html.

[82] LMNO Engineering, Research, and Software, Ltd. (2015, Aug 25). Gas Viscosity Calculator. Retrieved from http://www.lmnoeng.com/Flow/GasViscosity.php.

[83] CASIO. (2016).Velocity of sound in sea-water calculator. CASIO COMPUTER CO., LTD. Retrieved from http://keisan.casio.com/exec/system/1258122391.

[84] 1976 Standard Atmosphere Calculator. Retrieved from http://www.digitaldutch.com/atmoscalc/index.htm.

[85] Mullen, Benjamin. (2014, Feb 9). FLUENT- Flow over an Airfoil. Retrieved from https://confluence.cornell.edu/display/SIMULATION/FLUENT+-+Flow+over+an+Airfoil.

[86] Mehta, Pavan. [Pavan Mehta]. (2013, Nov 9). Flow over an airfoil - part 1 - Ansys Fluent 14 tutorial. [Video File]. Retrieved from https://www.youtube.com/watch?v=LAIB7qK-9pE.

[87] Mehta, Pavan. [Pavan Mehta]. (2013, Nov 9). Flow over an airfoil - part 2 - Ansys Fluent 14 tutorial. [Video File]. Retrieved from https://www.youtube.com/watch?v=FQK51-cb-78.

[88] Taira, Kunihiko, Dickson, William B, Colonius, Tim, Dickinson, Michael H., and Rowley, Clarence W. (n.d.). Unsteadiness in Flow over a Flat Plate at Angle-of-Attack at Low Reynold's Numbers. Retrieved from https://pdfs.semanticscholar.org/4b0f/11e10779d82f4835fee00604d344373a084e.pdf.

[89] NASA. (2015, May 5). Inclination Effects on Lift. Retrieved from https://www.grc.nasa.gov/www/k-12/airplane/incline.html.

[90] Finite Wings. Retrieved from http://people.clarkson.edu/~pmarzocc/AE429/AE-429-4.pdf.

[91] Spedding, G.R. and McArthur, J. (2010). Span Efficiencies of Wings at Low Reynolds Numbers. Journal of Aircraft, Vol. 47, No. 1. Retrieved from http://drydenwt.usc.edu/documents/LowReAero/SMac_JA_10.pdf.

[92] Hall, Nancy. (2015, May 5). Downwash Effects on Lift. NASA. Retrieved from https://www.grc.nasa.gov/www/k-12/airplane/downwash.html.

[93] SP-367 Introduction to the Aerodynamics of Flight, VI. SUPERSONIC FLOW. Retrieved from http://history.nasa.gov/SP-367/chapt6.htm.

[94] Weber, Paul W., Howle, Laurens E., Murray, Mark M., and Fish, Frank E. (2009, Apr 11). Lift and Drag Performance of Odontocete Cetacean Flippers. Retrieved from http://jeb.biologists.org/content/212/14/2149.

[95] Koehl, M. A. R. (1996). When Does Morphology Matter? Retrieved from https://ib.berkeley.edu/labs/koehl/pdfs/WhenDoesMorphologyMatter_1996.pdf.

[96] thetruth365film]. (2016, Jan 11). "Live Your Dreams and Never Give Up" featuring Gabi Shull. [Video file]. Retrieved from https://www.youtube.com/watch?v=aZG3hxITTP0.

[97] Ozkaya and Nordin. (1999). Fundamentals of Biomechanics. Springer.

[98] Choi, Alex P. C. (2008, Aug). "Estimation of Young's Modulus and Poisson's Ratio of Soft Tissue using Indentation." The Hong Kong Polytechnic University. Retrieved from http://ira.lib.polyu.edu.hk/bitstream/10397/2777/2/b2321420x_ir.pdf.

[99] Silicone Rubber. Retrieved from http://www.matbase.com/material-categories/natural-and-synthetic-polymers/elastomers/material-properties-of-silicone-rubber.html#properties.

[100] Kunz, Johannes and Studer, Mario. (2006). Determining the Modulus of Elasticity in Compression via the Shore A Hardness. Retrieved from www.kunststoffe-international.com.

[101] Silicone Rubber. (2016). Retrieved from http://www.azom.com/properties.aspx?ArticleID=920.

[102] Reynolds Advanced Materials. (2016). Technical Overview, Smooth-Sil Series. Retrieved from http://www.reynoldsam.com/product/smooth-sil/.

[103] The Green Team. Retrieved from http://thegreenteamfoundation.weebly.com/anatomy.html.

[104] OpenSim Project Overview. Retrieved from https://simtk.org/home/opensim.

[105] Vanlngen-Dunn, Caroline, Todd R. Hurley, and Gershon Yaniv. (1993). "Development of a humanlike flesh material for prosthetic limbs." Engineering in Medicine and Biology Society, 1993. Proceedings of the 15th Annual International Conference of the IEEE.

[106] Mechanical Behavior, Testing, and Manufacturing Properties of Materials. Retrieved from https://www.pearsonhighered.com/samplechapter/0136081681.pdf

[107] American Chemistry Society. (2016). Plastics Properties. Retrieved from https://plastics-car.com/FAQs/Plastics-Properties.html.

[108] Selig, Michael S., Deters, Robert W., and Williamson, Gregory A. (2011, Jan). Wind Tunnel Testing Airfoils at Low Reynolds Numbers. American Institute of Aeronautics and Astronautics, Inc. Retrieved from http://m-selig.ae.illinois.edu/pubs/SeligDetersWilliamson-2011-AIAA-2011-875-LRN-AirfoilWindTunnelTesting.pdf.

[109] [thetruth365film]. (2016, Jan 11). "Live Your Dreams and Never Give Up" featuring Gabi Shull. [Video file]. Retrieved from https://www.youtube.com/watch?v=aZG3hxITTP0.

[110] (2015). Winter the Dolphin. Hanger, Inc. Retrieved from http://www.hangerclinic.com/success-stories/winter-the-dolphin/Pages/prosthesis.aspx.

[111] (2016) Winter. Clearwater Marine Aquarium. Retrieved from http://www.seewinter.com/winter.

[112] n.a. (2010, Mar 12). The ‘Prosthetic Tale’ of a Dolphin Tail. WB Engineering. Retrieved from http://www.seewinter.com/web-cam-angle-3.

[113] n.a. (2007, Aug 26). Dolphin’s new tail can help human amputees. NBC News. Retrieved from http://www.nbcnews.com/id/20415964/ns/health-health_care/t/dolphins-new-tail-can-help-human-amputees/#.VyHFzvkrLIV.

[114] Morris, Don. (2011, Oct 13). Don Morris meets Winter, the star of Dolphin Tale. Retrieved from http://alexanderpollard.typepad.com/the_pimento_files/2011/10/don-morris-meets-winter-the-star-of-a-dolphin-tale.html.